AD_____

Award Number: DAMD17-98-1-8186

TITLE: Measurements of Breast Tissue Optical Properties

PRINCIPAL INVESTIGATOR: Albert Cerussi, Ph.D.
Bruce Tromberg, Ph.D.

CONTRACTING ORGANIZATION: University of California
Irvine, California 92697-1875

REPORT DATE: October 2000

TYPE OF REPORT: Annual Summary

PREPARED FOR: U.S. Army Medical Research and Materiel Command
Fort Detrick, Maryland 21702-5012

NOTICE

USING GOVERNMENT DRAWINGS, SPECIFICATIONS, OR OTHER DATA INCLUDED IN THIS DOCUMENT FOR ANY PURPOSE OTHER THAN GOVERNMENT PROCUREMENT DOES NOT IN ANY WAY OBLIGATE THE U.S. GOVERNMENT. THE FACT THAT THE GOVERNMENT FORMULATED OR SUPPLIED THE DRAWINGS, SPECIFICATIONS, OR OTHER DATA DOES NOT LICENSE THE HOLDER OR ANY OTHER PERSON OR CORPORATION; OR CONVEY ANY RIGHTS OR PERMISSION TO MANUFACTURE, USE, OR SELL ANY PATENTED INVENTION THAT MAY RELATE TO THEM.

LIMITED RIGHTS LEGEND

Award Number: DAMD17-98-1-8186
Organization: University of California
Location of Limited Rights Data (Pages):

Those portions of the technical data contained in this report marked as limited rights data shall not, without the written permission of the above contractor, be (a) released or disclosed outside the government, (b) used by the Government for manufacture or, in the case of computer software documentation, for preparing the same or similar computer software, or (c) used by a party other than the Government, except that the Government may release or disclose technical data to persons outside the Government, or permit the use of technical data by such persons, if (i) such release, disclosure, or use is necessary for emergency repair or overhaul or (ii) is a release or disclosure of technical data (other than detailed manufacturing or process data) to, or use of such data by, a foreign government that is in the interest of the Government and is required for evaluational or informational purposes, provided in either case that such release, disclosure or use is made subject to a prohibition that the person to whom the data is released or disclosed may not further use, release or disclose such data, and the contractor or subcontractor or subcontractor asserting the restriction is notified of such release, disclosure or use. This legend, together with the indications of the portions of this data which are subject to such limitations, shall be included on any reproduction hereof which includes any part of the portions subject to such limitations.

THIS TECHNICAL REPORT HAS BEEN REVIEWED AND IS APPROVED FOR PUBLICATION.

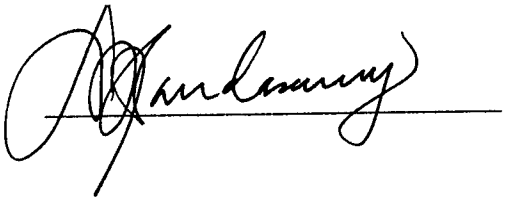

03/26/01

REPORT DOCUMENTATION PAGE

Form Approved
OMB No. 074-0188

1. AGENCY USE ONLY (Leave blank)	2. REPORT DATE	3. REPORT TYPE AND DATES COVERED
	October 2000	Annual Summary (30 Sep 99 - 29 Sep 00)

4. TITLE AND SUBTITLE
Measurements of Breast Tissue Optical Properties

5. FUNDING NUMBERS
DAMD17-98-1-8186

6. AUTHOR(S)
Albert Cerussi, Ph.D.
Bruce Tromberg, Ph.D.

7. PERFORMING ORGANIZATION NAME(S) AND ADDRESS(ES)
Beckman Laser Institute
University of California
Irvine, California 92697-1875

E-MAIL:
acerussi@bli.uci.edu

8. PERFORMING ORGANIZATION REPORT NUMBER

9. SPONSORING / MONITORING AGENCY NAME(S) AND ADDRESS(ES)
U.S. Army Medical Research and Materiel Command
Fort Detrick, Maryland 21702-5012

10. SPONSORING / MONITORING AGENCY REPORT NUMBER

11. SUPPLEMENTARY NOTES
This report contains colored photos

12a. DISTRIBUTION / AVAILABILITY STATEMENT
DISTRIBUTION STATEMENT: Distribution authorized to U.S. Government agencies only (proprietary information, Oct 00). Other requests for this document shall be referred to U.S. Army Medical Research and Materiel Command, 504 Scott Street, Fort Detrick, Maryland 21702-5012.

12b. DISTRIBUTION CODE

13. ABSTRACT ***(Maximum 200 Words)***

Near-infrared (NIR) optical spectroscopy demonstrates unique possibilities for non-invasively monitoring tissue physiology. A bedside-capable instrument, using low levels of non-ionizing NIR light delivered by a hand-held probe, measures both absorption and scattering properties of tissues. A diffusive model for photons traveling through large tissue volumes quantifies oxygenated and deoxygenated hemoglobin, water, and lipid by their absorption signatures. Cellular density, fat, and collagen content are evaluated from the measured light-scattering spectra. This quantitative functional information cannot be obtained with other non-invasive radiological techniques.

The prototype instrument revealed physiological changes in breast consistent with age-dependent histological alterations in 28 healthy female volunteers. A preliminary in vivo measurement of the therapeutic efficacy of two chemotherapy agents on a tumor in a human subject is also presented. Instrument performance was not adversely affected by subject age or menopausal status. Potential applications based upon these findings include monitoring the effectiveness of treatments that affect breast composition (i.e., hormone replacement and chemotherapy), characterizing tumors, and evaluating physiologic changes that affect breast cancer risk. The prototype instrument is comparable in cost to commercialized ultrasound.

14. SUBJECT TERMS
Breast Cancer

15. NUMBER OF PAGES
130

16. PRICE CODE

17. SECURITY CLASSIFICATION OF REPORT	18. SECURITY CLASSIFICATION OF THIS PAGE	19. SECURITY CLASSIFICATION OF ABSTRACT	20. LIMITATION OF ABSTRACT
Unclassified	Unclassified	Unclassified	Unlimited

Table of Contents

Cover.....

SF 298.....2

Introduction.....4

Body.....5

Key Research Accomplishments.....9

Reportable Outcomes.....9

Conclusions.....10

INTRODUCTION

Near-infrared light offers unique possibilities for revealing physiological information from within biological tissues without injections, surgery, dangerous radiation, or great expense. Although it has been known for some time that non-ionizing near-infrared light penetrates a few centimeters into biological tissues, only recently have scientists been able to take advantage of this penetration by taking into account tissue scattering. Near-infrared light provides a way to quantify the concentration and the oxygenation state of hemoglobin and also the scattering properties of the tissue and thus provide criteria to characterize breast lesions *in vivo* without surgery. This optical information will provide clinicians with entirely new criteria for deciding if lesions are benign or malignant, which may help reduce some of the ambiguities and false-negatives currently encountered in conventional breast examinations.

Optically monitoring physiological changes in breast tissue also provides a new way to look at both disease progression and prevention. Using near-infrared light from an instrument we have developed, we have observed changes in hemodynamics and structure that are characteristic of tumors. In addition, we have also observed changes in breast tissue physiology resulting from hormone replacement therapy, menopausal status, and estrous cycle stage. Because our technique is safe, non-invasive and comparable in cost to ultrasound, patients can be studied as often as necessary without risk. Currently, we are in the process of performing clinical measurements on women with breast tumors and on normal volunteers receiving hormone replacement therapy with selective estrogen receptor modulator drugs (such as tamoxifen).

ITEMS IN THE ORIGINAL SPECIFIC AIMS

For convenience, I will list below summaries of the specific aims of the original proposal, "Measurement of Breast Optical Properties":

(1) *Optimize* the instrumentation and theory currently used to extract the absolute optical absorption and reduced scattering parameters.

(2) *Perform clinical measurements* of breast tissue optical properties in order to determine exact absorption and scattering factors in different tissue regions.

(3) *Compare* optical property measurements to gross pathology, histopathology, ultrasound, and mammography results in order to determine absorption and scattering factors characteristic of tumor and normal tissue.

SUMMARY OF PROGRESS

Important leaps in my training have led me to make significant progress on two of the three specific aims. Enough testing and optimization have gone into place that has enabled me to make significant improvements to the instrumentation such that a second instrument will be ready this year for permanent clinical use. I have also performed over 40 clinical measurements that have led to two publications and two more submitted publications. These measurements are of vital importance since the provide information as to the scattering and absorption contrast of near-infrared optical methods in the breast.

RESULTS OF CLINICAL MEASUREMENTS

Clinical Summary: Normals

I have been able to quantify via absorption the concentrations of blood, water, and fat in the breasts of over 35 healthy volunteers. The addition of fat has provided some unique insights into breast physiology that were not available to us only a year ago. In addition, I now have evidence that suggests that the scattering properties of the breast are highly influenced by the amounts of fat and connective tissue, and thus provide complementary information about breast composition. This newly introduced spectroscopic information has provided a more complete picture of the breast, the first of its kind.

Current data have demonstrated several things:

(1) Increased blood and water in pre-menopausal versus post-menopausal breasts.

(2) General increase in lipids in the post-menopausal breast.

(3) Increased scattering in the pre-menopausal breast, which is likely due to increased connective tissue density and decreased amounts of fat.

(4) Tissue saturation measurements of pre-menopausal women are statistically lower than those of post-menopausal women. In addition, post-menopausal women on hormone replacement therapy (HRT) show tissue saturation values closer to the pre-menopausal breast than the post-menopausal breast. (This saturation is a measure of the hemoglobin saturation in the tissue with both arterial and venous contributions).

All of the findings are not surprising, but until now, none of these compositional properties of the tissue could be measured non-invasively in a safe manner.

This information is important for several reasons:

(1) These are the first data anywhere that help establish a baseline of "normal" optical properties for use in cancer detection and diagnosis. Such data will help by providing background optical properties to investigators perusing optical mammography.

(2) Knowledge of "normal" optical properties also provides potential for monitoring any treatments (i.e., HRT, neo-adjuvant) that will affect the composition of breast tissue. In addition, we have demonstrated metabolic changes in the breast that are due to both endogenous and exogenous hormonal influence (i.e. estrogen and progesterone).

(3) For the first time we might possibly quantify the origins of radiological mammographic density, which is thought to correlate with breast cancer risk. To date, the physiology behind mammographic density is speculated. This technique could provide the answers.

These findings have become the subject of two research papers which have been recently been submitted for publication.

Clinical Summary: Cancer

I also managed to perform an interesting measurement that showed significant changes in the breasts of a patient receiving chemotherapy: cytoxan (20 mg/mL) and doxorubiein (2 mg/mL). Prior to therapy, the tissue saturation of the tumor was very low, about 44%. (Errors are difficult to estimate for this subject, but certainly an absolute error of 8% is a conservative estimate).

Although 44% is somewhat low, low tissue saturation is representative of high metabolic demand, particularly that of tumors. After the first bolus of chemotherapy agents, the saturation ballooned to 73%, a highly significant change. This large change in tissue saturation is evidence that the cells are relaxing their demand for oxygen, implying that these cells are dying. Normal saturation values for the breast fall into the 70-80% range. A measurement 3 weeks later revealed that the tissue saturation remained at 72%. Interestingly, the normal breast showed a 61% saturation before treatment and a 75% after. Another measurement 3 weeks later showed that the tissue saturations of both breasts were equal at 75%, which is a perfectly normal value. It is important to state that the term "perfectly normal value" would not be possible without the data I have obtained in our study of normal subjects.

These measurements are very preliminary and of great value to the community of therapeutic intervention. Our technique monitored the changes in tumor oxygen metabolism. Given that the effect of metabolic decrease was very high after the initial treatment and then leveled off indicates that subsequent treatments may have been ineffective. Perhaps we have witnessed resistance of the tumor to the chemotherapy. These questions are of critical importance in battling cancer and modulating treatment that is specific for individual tumor response.

INSTRUMENT IMPROVEMENTS

Two technical improvements promise to forward the achievement of the initial specific aims. We have incorporated a steady-state spectrometer into the FDPM instrument. The application of a simple model then transforms a seven-wavelength instrument to a hundreds of wavelengths instrument. The topic of introducing the spectrometer into the system was the subject of a recently accepted paper. Adding the spectrometer should provide previously unimaginable precision in determining the physiological makeup of tissues.

I am also on the verge of completing a second FDPM instrument that will reside permanently in the Breast Center at the Chao Comprehensive Cancer Center. This instrument represents some significant technical advances, including a completely fiber-based probe and faster measurement times. Completion of the instrument is expected in the fourth quarter of 2000. Personally, I am very excited by this instrument since it should become a means from which to collect vast amounts of data, most particularly on cancer patients.

PROTOCOL DESIGN, CONSTRUCTION, AND IMPLEMENTATION

I have continued to manage two research protocols here at UCI (#95-563 & #99-2183). I have added some modifications to these protocols that should help us gain further insight into the optics of breast tissue. One example is a measurement we have started that will take place over the entire menstrual cycle of a 27 year old volunteer. No difficulties or complications have occurred during the courses of these trials.

CLINICIAN INTERACTION

I have continued to work with clinicians here at UCI. A recent addition to the research team is Dr. David Hsiang, a clinical breast cancer surgeon. He and Dr. Butler will be instrumental in orchestrating breast cancer measurements at the Chao Comprehensive Cancer Center in the upcoming year. I have had the opportunity to see breast cancer in a more clinical light after consultations with these physicians. Their interest in research has proven invaluable to my development as a breast cancer researcher.

WORKING WITH STUDENTS

I am also continuing to work with Dr. Tromberg's students. Dr. Tromberg now has four students working in FDPM, and I am responsible for training and guiding them in their collective study of biomedical optics. Ryan Lanning and I have begun looking at optical measurements of human

tumors in mice in order to better understand this key link between the microscopic tumor characteristics (i.e., vessel counts, collagen disruption) and the macroscopic optical properties that we measure *in vivo*. Natasha Shah and Dorota Jakubowski and I have continued to look at optical measurements of both healthy and diseased breast. Finally, David Cuccia and I have begun some work that will correlate optical signals in tumors with high-resolution MRI images.

PROLIFERATION OF RESULTS

Over the last year I have presented my results at several meetings and have published/submitted four manuscripts. These are listed in the reportable outcomes section. In addition to these, I will be attending the SPIE Optics meeting In January (San Jose, CA).

ATTENDANCE AT CLASSES

I have also begun to observe a class at UCI entitled "Clinical Cancer for Basic Scientists." It is a graduate-level course that introduces cancer researchers to how clinical practice is performed.

TARGETS FOR NEXT YEAR

There are still many more normals to observe. Just now, we are entering into a position where we can seriously address issues involved with cancer diagnosis and treatment. For example, we are beginning to look into correlations between our compositional findings and breast cancer risk. For this part of the study, we will require many normal as well as cancer patients. . The results of our neo-adjuvant study are highly preliminary, but warrant more careful study. Continuation of this protocol allows us to verify our findings, especially with a second instrument at UCIMC. We therefore request another year of study to help mature the FDPM technique into a useful clinical tool.

APPENDIX

RESEARCH-RELATED ACCOMPLISHMENTS

- successful measurements on 40 subjects (mostly normals)
- shown that compositional and functional differences can be observed in the breast using non-invasive optical techniques
- demonstrated a preliminary link between a non-invasive measurement of metabolism (oxygen saturation) and hormonal influence
- performed one of the first measurements on the monitoring of the efficacy of chemotherapy agents *in vivo*
- second generation instrument completion expected by end of calendar year

REPORTABLE OUTCOMES: CONFERENCES

[1] A. E. Cerussi, A. J. Berger, F. Bevilacqua, D. Jakubowski, N. Shah, and B. J. Tromberg, "Non-Invasive quantification of breast tissue physiology; Optical measurements of blood, water, and lipids," Biomedical Engineering Society 2000 Meeting, Seattle, WA, Presentation 14794, (October 2000).

[2] A. E. Cerussi, A. J. Berger, F. Bevilacqua, N. Shah, D. Jakubowski, J. Butler, R. F. Holcombe, and B. J. Tromberg, "Quantitative non-invasive optical spectroscopy of breast tissue physiology," Optical Imaging Workshop: From Bench to Bedside at the NIH, Bethesda, MD, P-23, (September 2000).

[3] A. E. Cerussi, N. Shah, A. J. Berger, D. Jakubowski, J. B. Fishkin, J. Butler, and B. J. Tromberg, "Quantitative near-infrared spectroscopy of normal and cancerous breast tissue: uses in detection and prevention," DOD Breast Cancer Research Program: Era of Hope, Atlanta, GA, E-14 (June 2000).

REPORTABLE OUTCOMES: PEER-REVIEWED PUBLICATIONS

[1] A. E. Cerussi, A. J. Berger, F. Bevilacqua, N. Shah, D. Jakubowski, J. Butler, R. F. Holcombe, and B. J. Tromberg' "Sources of absorption and scattering contrast for non-invasive optical mammography," (*submitted*).

[2] N. Shah, A. Cerussi, C. Eker J. Espinoza, J. Butler, J. Fishkin, R. Hornung, B. Tromberg, "Non-Invasive functional optical spectroscopy of human breast tissue " (*submitted*).

[3] F. Bevilacqua, A. Berger, A. Cerussi, D. Jakubowski, and B. Tromberg, "Broadband absorption spectroscopy in turbid media by combining frequency-domain and steady-state methods," (*accepted for publication, Appl. Opt.*).

[4] B. J. Tromberg, N. Shah, R. Lanning, A. Cerussi, J. Espinoza, T. Pham, L. Svaasand, J. Butler, 'Non-Invasive in vivo characterization of breast tumors using photon migration spectroscopy,' *Neoplasia* **2**, 1-15 (2000).

REPORTABLE OUTCOMES: ADDITIONAL FUNDING

We have received funding based upon this work from the California Breast Cancer Research Program, a 3 year, $500,000 collaborative effort with Dr. Laura Esserman at University of California at San Francisco.

The Chao Comprehensive Cancer Center has also received a gift from Avon for being a cancer center for excellence. From this gift, $250,000 was appropriated to the optical breast cancer detection program because of our contributions to the field.

CONCLUSIONS

In the past year, we have made some significant contributions to the field of biomedical optics that may ultimately play a role in the prevention, detection, and treatment of breast cancer. Our work provides information as to the contrast available in near-infrared spectroscopy of the breast. Our results on normal volunteers demonstrate adequate physiologic sensitivity to long-term hormone-induced changes in the breast. We have just begun to use this data to interpret cancer measurements.

QUANTITATIVE NEAR-INFRARED SPECTROSCOPY OF NORMAL AND CANCEROUS BREAST TISSUE: USES IN DETECTION AND PREVENTION

A. E. Cerussi[1], N. Shah[1], A. J. Berger[1], D. Jakubowski[1], J. B. Fishkin, J. Butler[2], and B. J. Tromberg[1,2]

[1]Beckman Laser Institute, University of California at Irvine, Irvine, CA 92612
[2]Department of Surgery, University of California at Irvine

acerussi@bli.uci.edu

Near-infrared light offers unique possibilities for revealing physiological information from within biological tissues without injections, surgery, dangerous radiation, or great expense. Although it has been known for some time that non-ionizing near-infrared light penetrates a few centimeters into biological tissues, only recently have scientists been able to take advantage of this by taking into account tissue scattering. Near-infrared light provides a way to quantify the concentration and the oxygenation state of hemoglobin and thus characterize breast lesions without surgery. This information will provide clinicians with entirely new criteria for deciding if lesions are benign or malignant, which may help reduce some of the ambiguities and false-negatives currently encountered in conventional breast examinations.

Optically monitoring physiological changes in breast tissue also provides a new way to look at both disease progression and prevention. Using near-infrared light from an instrument we have developed, we have observed changes in hemodynamics and structure that are characteristic of tumors. In addition, we have also observed changes in breast tissue physiology resulting from hormone replacement therapy, menopausal status, and estrous cycle stage. The technique may also be extended to monitoring the effects of drugs that affect breast tissue (such as estrogen or tamoxifen) in order to enhance efficacy and minimize side effects. Because our technique is safe, non-invasive and comparable in cost to ultrasound, patients can be studied as often as necessary without risk. Currently, we are performing clinical measurements on women with breast tumors and on normal volunteers receiving breast cancer prevention drugs such as tamoxifen and raloxifene.

The U. S. Army Medical Research and Material Command under DAMD17-98-1-8186 helped support this work.

Non-invasive quantification of breast tissue physiology: Optical measurements of blood, water, and lipids.

Albert Cerussi[1], Andrew Berger[1], Frederic Bevilacqua[1], Natasha Shah[1], Dorota Jakubowski[1], and Bruce Tromberg[2]
[1]University of California, Irvine, Beckman Laser Institute and Medical Clinic, Irvine, CA
[2]University of California, Irvine, Surgery, College of Medicine, Irvine, CA

Near-infrared (NIR) optical spectroscopy demonstrates unique possibilities as a non-invasive tool for monitoring biological tissue physiology. We have developed a bedside-capable instrument that uses safe levels of non-ionizing NIR light. The instrument measures the absorption and the scattering properties of tissues by applying a diffusive model of light transport to photons that have traveled through a large volume of tissue. Hemoglobin, water, and lipids may be quantified by their absorption properties, and scattering information is sensitive to items such as cellular density and collagen.

We have used a prototype instrument uncovered physiological changes in breast that are consistent with known changes in breast parenchyma as a result of age and menopausal status in a sample of 21 healthy female volunteers (ages 18 to 60). Combining the scattering and the absorption information together reveals functional information in the breast. Such information could be used to monitor the effectiveness of treatments that affect the composition of the breast, such as hormone replacement therapy and neo-adjuvant therapy. All of this was done with an instrument that in its prototype form is comparable in cost to commercialized ultrasound technology.

Quantitative non-invasive optical spectroscopy of breast tissue physiology

A. E. Cerussi[1], A. J. Berger[1], F. Bevilacqua[1], N. Shah[1], D. Jakubowski[1], J. Butler[2], R. F. Holcombe[3], and B. J. Tromberg[1]

[1]Beckman Laser Institute and Medical Clinic
University of California, Irvine
(949)824-4713

[2]Department of General Surgery
University of California, Irvine Medical Center
(714)456-8030

[3]Department of Hematology/Oncology
University of California, Irvine
(714)456-5153

Near-infrared (NIR) optical spectroscopy demonstrates unique possibilities as a non-invasive monitor of tissue physiology. We have developed a bedside-capable instrument that uses safe levels of non-ionizing NIR light. Our instrument measures both absorption and scattering properties of tissues by applying a diffusive model of light transport to photons that have traveled through a large volume of tissue. Oxygenated and deoxygenated hemoglobins, water, and lipids were quantified by their absorption signature. Additional information was obtained from tissue scattering, which is sensitive to items such as cellular density and collagen content.

This prototype instrument uncovered physiological changes in breast that are consistent with known changes in breast parenchyma as a result of age and menopausal status in a sample of 21 healthy female volunteers (ages 18 to 60). Combining scattering and absorption information together reveals age-dependent functional information in the breast. This physiological information is not obtainable with any other method to date. Such information could be used to monitor the effectiveness of treatments that affect breast composition, such as hormone replacement therapy and neo-adjuvant therapy, as well as evaluate individual breast cancer risk. The prototype instrument in its present form is comparable in cost to commercialized ultrasound technology.

REVIEW ARTICLE

Neoplasia • Vol. 2, Nos. 1–2, January-April 2000, pp. 26–40 26

www.nature.com/neo

Non-Invasive *In Vivo* Characterization of Breast Tumors Using Photon Migration Spectroscopy[1]

Bruce J. Tromberg, Natasha Shah*, Ryan Lanning*, Albert Cerussi*, Jennifer Espinoza*, Tuan Pham*, Lars Svaasand† and John Butler‡*

*Laser Microbeam and Medical Program (LAMMP), Beckman Laser Institute and Medical Clinic, University of California, Irvine, CA; †NTNU, Norwegian Technological University, Trondheim, Norway; ‡Department of Surgery, University of California, Irvine, CA

Abstract

Frequency-domain photon migration (FDPM) is a non-invasive optical technique that utilizes intensity-modulated, near-infrared (NIR) light to quantitatively measure optical properties in thick tissues. Optical properties (absorption, μ_a, and scattering, μ_s', parameters) derived from FDPM measurements can be used to construct low-resolution (0.5 to 1 cm) functional images of tissue hemoglobin (total, oxy-, and deoxy-forms), oxygen saturation, blood volume fraction, water content, fat content and cellular structure. Unlike conventional NIR transillumination, FDPM enables quantitative analysis of tissue absorption and scattering parameters in a single non-invasive measurement. The unique functional information provided by FDPM makes it well-suited to characterizing tumors in thick tissues. In order to test the sensitivity of FDPM for cancer diagnosis, we have initiated clinical studies to quantitatively determine normal and malignant breast tissue optical and physiological properties in human subjects. Measurements are performed using a non-invasive, multi-wavelength, diode-laser FDPM device optimized for clinical studies. Results show that ductal carcinomas (invasive and *in situ*) and benign fibroadenomas exhibit 1.25 to 3-fold higher absorption than normal breast tissue. Within this group, absorption is greatest for measurements obtained from sites of invasive cancer. Optical scattering is approximately 20% greater in pre-menopausal versus post-menopausal subjects due to differences in gland/cell proliferation and collagen/fat content. Spatial variations in tissue scattering reveal the loss of differentiation associated with breast disease progression. Overall, the metabolic demands of hormonal stimulation and tumor growth are detectable using photon migration techniques. Measurements provide quantitative optical property values that reflect changes in tissue perfusion, oxygen consumption, and cell/matrix development. *Neoplasia* (2000) **2,** 26–40.

Keywords: tissue optical properties, absorption, scattering, diffuse optical imaging, near-infrared spectroscopy, hemoglobin, tumor vasculature, extracellular matrix.

Introduction

Pathologists routinely examine thin sections of surgically removed tissue in order to diagnose cancer. If similar information could be provided by techniques that allow us to see internal structure, physicians would be able to find and characterize tumors non-invasively. Historically, this reasoning lead to the development of "diaphanography", a near-infrared (NIR) light imaging method introduced nearly 70 years ago to locate and identify breast cancer [1]. NIR imaging is a simple, low-cost, risk-free procedure that, unlike X-ray mammography, does not employ ionizing radiation. Unfortunately, the initial promise of NIR diaphanography was never realized, primarily due to intense light scattering.

Distinguishing between absorption and scattering is generally recognized as one of the principal limitations to detecting cancer with light. This problem has challenged scientists who study how light interacts with turbid materials for many years. Recent developments in theory and instrumentation, collectively referred to as "photon migration" (PM), now enable us to probe and analyze multiply-scattered light signals on an ultra-fast time scale (e.g., picoseconds). These technological advances provide a simple framework for measuring the exact magnitude of absorption and scattering (i.e., optical properties) in turbid materials. Optical properties can, in turn, be used to locate and identify physiological changes characteristic of tumors, hormonal stimulation, pharmacologic agents, and age-related tissue remodeling.

Research by our group and many others in the Biomedical Optics community has helped rejuvenate interest in optical methods for detecting and characterizing solid tumors [2]. The use of ultra-fast light provides new information with the

Address all correspondence to: Dr. Bruce J. Tromberg, Laser Microbeam and Medical Program, Beckman Laser Institute and Medical Clinic, 1002 Health Sciences Road, East, University of California, Irvine, CA 92612-1475. E-mail: tromberg@bli.uci.edu

[1]This work was made possible, in part, through access to the Laser Microbeam and Medical Program (LAMMP) and the Chao Family Cancer Center at the University of California, Irvine. These facilities are supported by the National Institutes of Health under grants RR-01192 and CA-62203, respectively. Support was also provided by the NIH Institute of General Medical Sciences (GM-50958), the Department of Energy (DOE #DE-FG03-91ER61227), the U.S. Army Breast Cancer Research Program, and the Beckman Foundation.

Received 14 December 1999; Accepted 20 December 1999.

same advantages as conventional NIR diaphanography (e.g., low cost, zero risk, compact devices). However, in order to demonstrate whether normal and malignant structures can actually be resolved using light, reliable measurements of both normal and tumor tissue optical properties must be performed in human subjects.

Few studies have been completed that accurately measure human tissue optical properties *in vivo*. This can be a particularly difficult hurdle to overcome because photon migration, as a fundamentally new method, is not widely accessible. PM technology development requires interdisciplinary expertise in diverse fields while measurements require strong clinical collaborations. Clinical studies are now underway here (about 70 human subjects have been enrolled in breast, brain, and cervical protocols to date) and in other laboratories that will provide critical information for determining whether non-invasive photon migration measurements are useful for characterizing, imaging, and detecting solid tumors. Early results show that unique tumor optical signatures are, in fact, measurable. Organs of greatest initial promise appear to be breast and brain. Changes in blood flow, oxygen consumption, and tissue architecture (cellular and matrix) can be measured in these structures quantitatively using NIR photon migration. Most importantly, these signals appear to reflect fundamental physiological processes associated with malignancy, disease progression, and response to therapy.

In this work, we review basic principles of photon migration [3] in thick tissues and highlight how light–tissue interaction mechanisms provide unique opportunities for solid tumor diagnostics. Details of instrumentation and theory development in photon migration spectroscopy are presented along with results of clinical studies in human breast tumor patients. Because many attributes related to the origin, progression, and therapeutic response of breast cancers are common to other types of tumors, these data should provide insight into how continued optical technology development will impact cancer diagnosis and screening.

Light Propagation in Thick Tissues

Spectral Dependence

Light propagation in biological tissues is a complex function of scattering and absorption, which, in turn, are dependent on cellular structure and molecular composition.

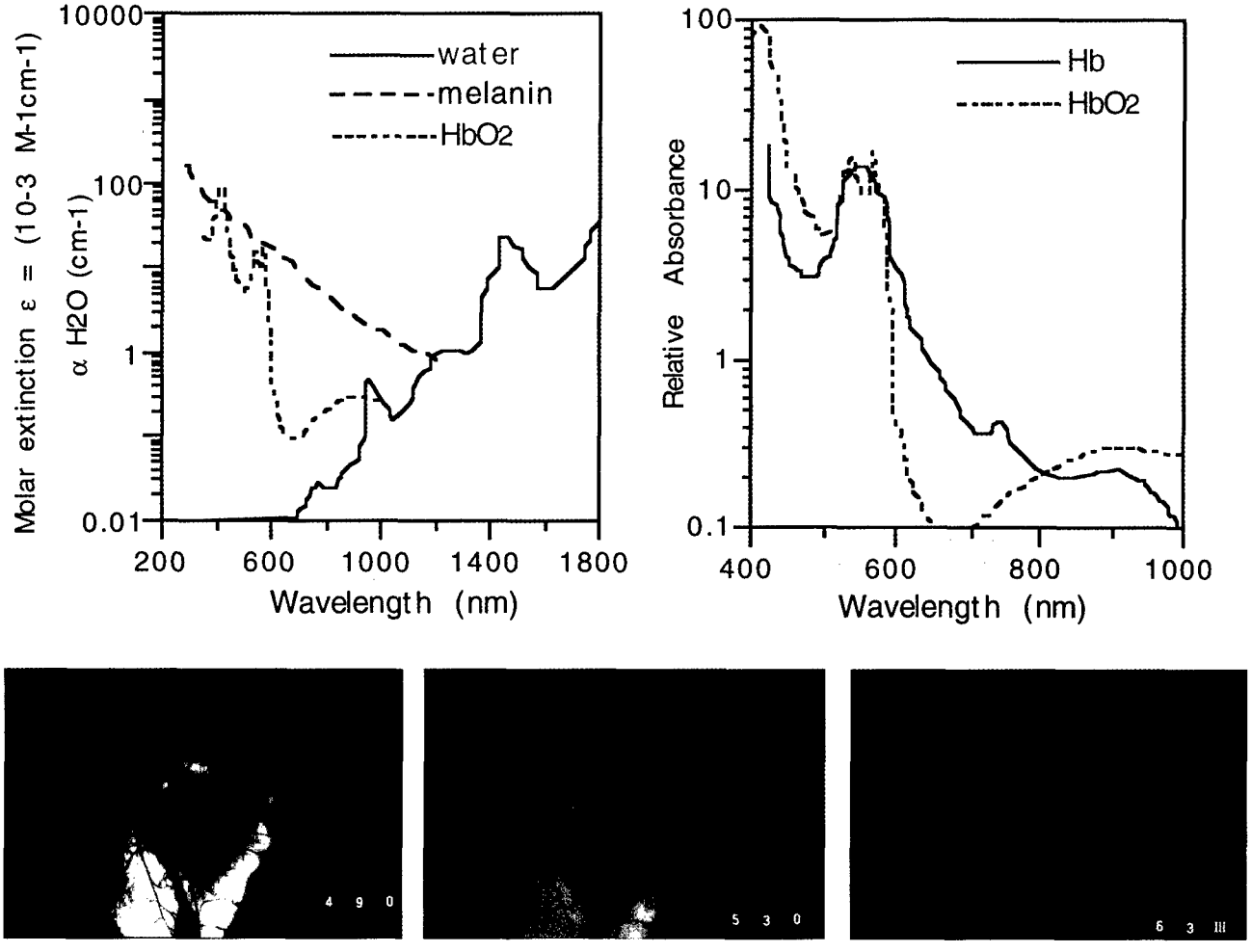

Figure 1. *Upper panels: Spectral dependence of tissue chromophore absorption. A tissue optical "window" exists in the red/NIR between 600 and 1300 nm (from J.L. Boulnois, Lasers in Medical Science, 1986: 1: 47–66). Lower panels: Spectral dependence of light transmission through rabbit ear with implanted tumor model.*

Figure 1 illustrates that within the visible (300 to 700 nm) water window, hemoglobin and melanin are the dominant endogenous absorbers [4].

Although melanin absorption coefficients are, on average, greater than those of hemoglobin, the overall influence of melanin on light propagation in thick tissues is generally less substantial. This is due to the fact that melanin is typically confined to a thin, superficial skin layer. In contrast, hemoglobin is widely distributed throughout most tissues at a volume fraction that ranges from 1% to 5%. Exceptions to this include avascular structures and tissues with abnormally high melanin content, such as melanotic melanomas.

Scattering originates from inhomogeneities in tissue structure, which, in turn, are determined by refractive index discontinuities occurring both between and within cells. In the spectral region of 600 to 700 nm, hemoglobin absorptivity is attenuated by approximately 20 dB (nearly 100-fold) and scattering eclipses absorption. This condition persists until water absorption resumes as the primary attenuation mechanism at approximately 1.3 μm. Thus, the spectral region between 600 and 1300 nm is considered to be the tissue optical "window" since both absorption and scattering losses are minimal throughout this interval. This concept is illustrated in the series of three photographs shown at the bottom of Figure 1. Here, a rabbit ear implanted with a tumor model is transilluminated using blue (490 nm), green (530 nm) and red (630 nm) light. In the blue and green photographs, excellent contrast is observed between light-absorbing blood vessels and the surrounding ear cartilage. This is due to strong hemoglobin absorption in these spectral regions and relatively high attenuation of light from scattering. Because the tumor has substantial blood vessel/hemoglobin content, it appears as a large light-absorbing shadow. In the red light case, however, the image appears quite diffuse and the small vessel structures have disappeared. This is a consequence of the substantially reduced hemoglobin absorption at 630 nm, making these vessels appear to be "transparent". In addition, red light is scattered less than blue/green. As a result, many of the scattered photons contribute to the image as "multiply scattered light," further degrading spatial resolution and contrast while improving transparency. The net result is a "cloudy" tumor that appears to be different than its actual physical dimension.

The wavelength-dependent intensity of light penetrance into biological tissues can be used to characterize structures of different composition. Table 1 provides several practical examples of wavelength-dependent "optical penetration depths", δ, a value that corresponds to the distance at which the optical fluence rate (i.e., mW/cm^2) is reduced to $1/e$=0.37 of the initial value [5]. These data highlight the dynamic interplay between absorption and scattering. For example, since human retinoblastomas contain no melanin, low levels of hemoglobin, and are only minimally scattering, penetration depths are relatively large; ranging from 2.9 mm at 600 nm to 5.1 mm at 1.06 μm. Light penetrance is commensurately reduced in brain and hand tissue due to their high-scattering/low-absorption and moderate-scattering/moderate-absorption properties, respectively. In contrast, the high melanin content of melanotic melanomas strongly attenuates light throughout the visible region and maximum light penetrance is only 1.4 mm at 1.064 μm.

These examples indicate that, in general, δ for non-melanotic tissues follows hemoglobin absorption. Thus, from 480 to 590 nm, δ ranges from 0.5 to 1.5 mm. A substantial penetration depth increase from about 1 to 3 mm occurs between 600 and 650 nm, and a more gradual increase is observed from 650 to 750 nm (δ=2 to 4 mm). Between 750 and 900 nm, values tend to plateau, and maximum light penetrance of 3 to 6 mm generally occurs in the 1000 to 1100 nm region.

Multiple Scattering

On a cellular level, there are clear, visible differences between normal and malignant tissues. These changes may include, among others, multinucleation, structural distortion, hyperpigmentation, and membrane and mitochondrial variations. On a bulk tissue level, there are distinct variations in tumor vasculature, extracellular matrix and biochemical milieu. Pathologists utilize visible, microscopic anomalies in cell/tissue architecture to formulate diagnoses. Thus, variations in bulk tissue optical penetration depths are expected, given the large body of supporting histologic evidence [6]. These fundamental optical property differences can, in principle, provide novel diagnostic criteria for thick-tissue photon migration methods.

However, our ability to employ thick-tissue optical methods for cancer detection is limited by a form of light-scattering behavior known as "multiple scattering". Light launched into tissue is efficiently scattered out of an incident collimated beam into an almost isotropic distribution within a few millimeters from the source. This "multiple scattering" behavior degrades the information content of light that propagates through thick tissues. In practical terms, optical imaging methods that cannot distinguish between scattering

Table 1. Optical Penetration Depth (mm) as a Function of Wavelength (From Ref. [5]).

Tissue	Wavelength (nm)							
	600	650	700	750	800	850	900	1064
Human retinoblastoma (*in vitro*)	2.9	3.8	4.0	4.0	4.1	4.2	4.3	5.1
Porcine brain (*in vitro*)	1.8	2.4	2.9	3.0	3.3	3.5	3.7	4.0
Human hand (*in vivo*)	1.4	2.0	2.6	2.7	3.0	3.0	3.0	–
Melanotic melanoma in athymic mice	–	0.28	0.34	0.41	0.50	0.56	0.64	1.4

and absorption are incapable of providing a complete diagnostic picture. This concept is illustrated schematically in Figure 2.

In homogeneous, non-scattering media, light propagation is simply a function of the absorption coefficient, μ_a, and distance, z:

$$I = I_0 e^{-\mu_a z} \quad (1)$$

where $\mu_a = 1/l_{ab}$ and l_{ab} is the absorption length, or average distance between absorption events. The absorption coefficient can be expressed in terms of molecular concentration via the Lambert-Beer law (i.e., $A = \log I/I_0 = \varepsilon bC$, where A, ε, b, are C are absorbance units, molar extinction coefficient, pathlength, and molar concentration, respectively):

$$\mu_a = 2.3\varepsilon C \quad (2)$$

Thus, measurements of light penetrance in tissues can, in principle, provide quantitative information regarding the concentration of physiologically relevant absorbers.

However, in non-transparent, turbid media, both scattering and absorption contribute to the distance-dependent light attenuation. The total attenuation coefficient, μ_t, is the sum of absorption and scattering parameters ($\mu_t = \mu_a + \mu_s$). Here, μ_s is the scattering parameter, or the reciprocal of the scattering length (l_{sc}). In the special case of "multiple scattering", the incident light intensity diminishes according to:

$$I = I_0 e^{-\mu_{eff} z} \quad (3)$$

where the effective attenuation coefficient, $\mu_{eff} = 1/\delta = [3\mu_a(\mu_a + \mu_s')]^{1/2}$ is the reciprocal of the mean penetration depth (δ). In order to account for multiple scattering, the reduced scattering parameter, $\mu_s' = \mu_s(1-g)$ is defined in terms of μ_s and the angular dependence of scattering, g, where $g = \langle \cos\ theta \rangle$, (i.e., the average cosine of the scattering angle). In most tissues, scattering is highly forward-directed and g values range from 0.7 to 0.9 [6]. In practical terms, large g values delay the distance photons must travel before optical energy is isotropically distributed. Generally, this "transport mean free path" (tmfp) is on the order of 1 mm in most tissues and can be defined as the reciprocal of the transport scattering coefficient, $\mu_{tr} = \mu_a + \mu_s'$.

The Diffusion Approximation

In order to probe large volumes of tissues with acceptable signal-to-noise levels, measurements are generally conducted in spectral regions of greatest transparency, i.e., the tissue optical window (600 to 1300 nml see Figure 1). Under these conditions, scattering dominates absorption and light propagation can be described by a diffusion approximation [12,21]. Since scatterers and absorbers are distributed in

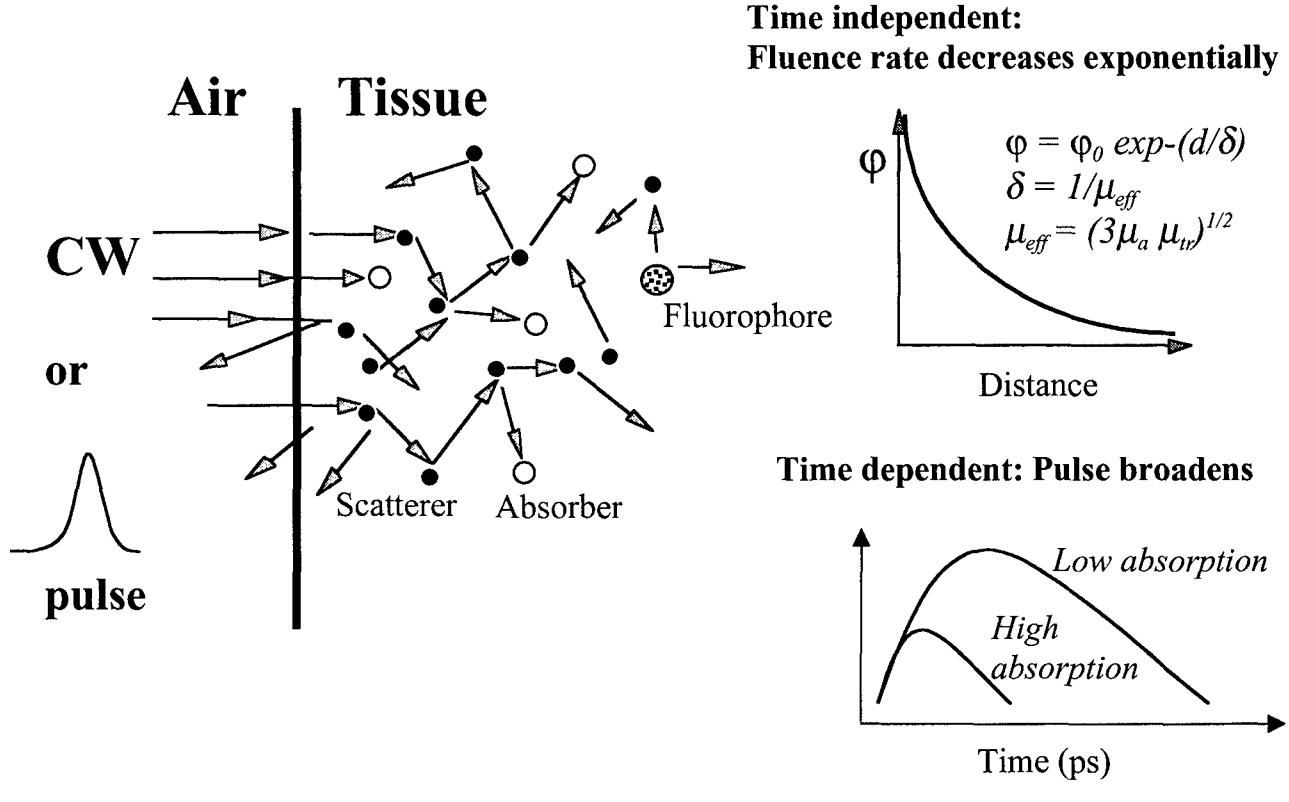

Figure 2. *Red/NIR light launched into tissue propagates with directional changes (scattering) until captured by an absorber (molecule). Multiple scattering increases the mean photon path length. A short, e.g., picosecond, light pulse launched into tissue spreads out in proportion to the number of available photon paths. Absorption is a loss mechanism that reduces the number of available photon paths and hence limits the temporal dispersion of the pulse. Under low absorption conditions, a light pulse will experience maximal dispersion. The photon density, or fluence rate (φ) decays exponentially with distance from the source. The 1/e exponential decay constant, or optical penetration depth (δ) is a function of the absorption, μ_a, and scattering, μ_s', properties of the medium.*

tissues on dramatically different spatial scales (i.e., $\mu_s'z.Gt\mu_a$), the transport scattering length can be approximated by $1/\mu_{tr} \approx 1/\mu_s'$. Under these conditions, an additional descriptive domain, i.e., time or frequency, is required to resolve light scattering from absorption.

As shown in Figure 2, launching light into tissue results in multiple scattering events that can dramatically increase the mean path length beyond the linear distance from source to detector. If the light source continuously illuminates the sample (i.e., it is time-independent), the fluence rate (in mW/cm^2) or number density of photons measured in the sample from all directions decays exponentially with distance from the source. The decay rate is a function of the penetration depth, δ, which in turn can be given by the absorption and scattering properties. When a time-dependent light source is used such as a picosecond (psec) laser pulse or a sinusoidally intensity-modulated laser, the large number of photon paths available due to multiple light scattering processes causes broadening of the source temporal profile. Thus, measurements of the time-dependent propagation characteristics of short light pulses or intensity-modulated waves in tissues can be used to separate the contributions of absorption from scattering. When combined with an appropriate mathematical framework, this allows precise calculation of tissue optical properties, namely tissue absorption, μ_a, and reduced scattering, μ_s', properties.

Temporal Resolution

Over the past few years, remarkable gains in our understanding of tissue optical properties have been realized by interrogating tissues with the unique temporal (i.e., short pulse) properties of lasers [7–11]. Pulse propagation methods provide information about the distribution of scatterers and absorbers in a single measurement [12,13]. These optical properties may be used in a variety of therapeutic and diagnostic techniques, including: imaging tissue structure [14–16] and cortical activity [17,18]; monitoring physiology [19–23] and drug concentration [24]; dysplastic transformation [25], and predicting optical dosimetry for laser-based procedures [26].

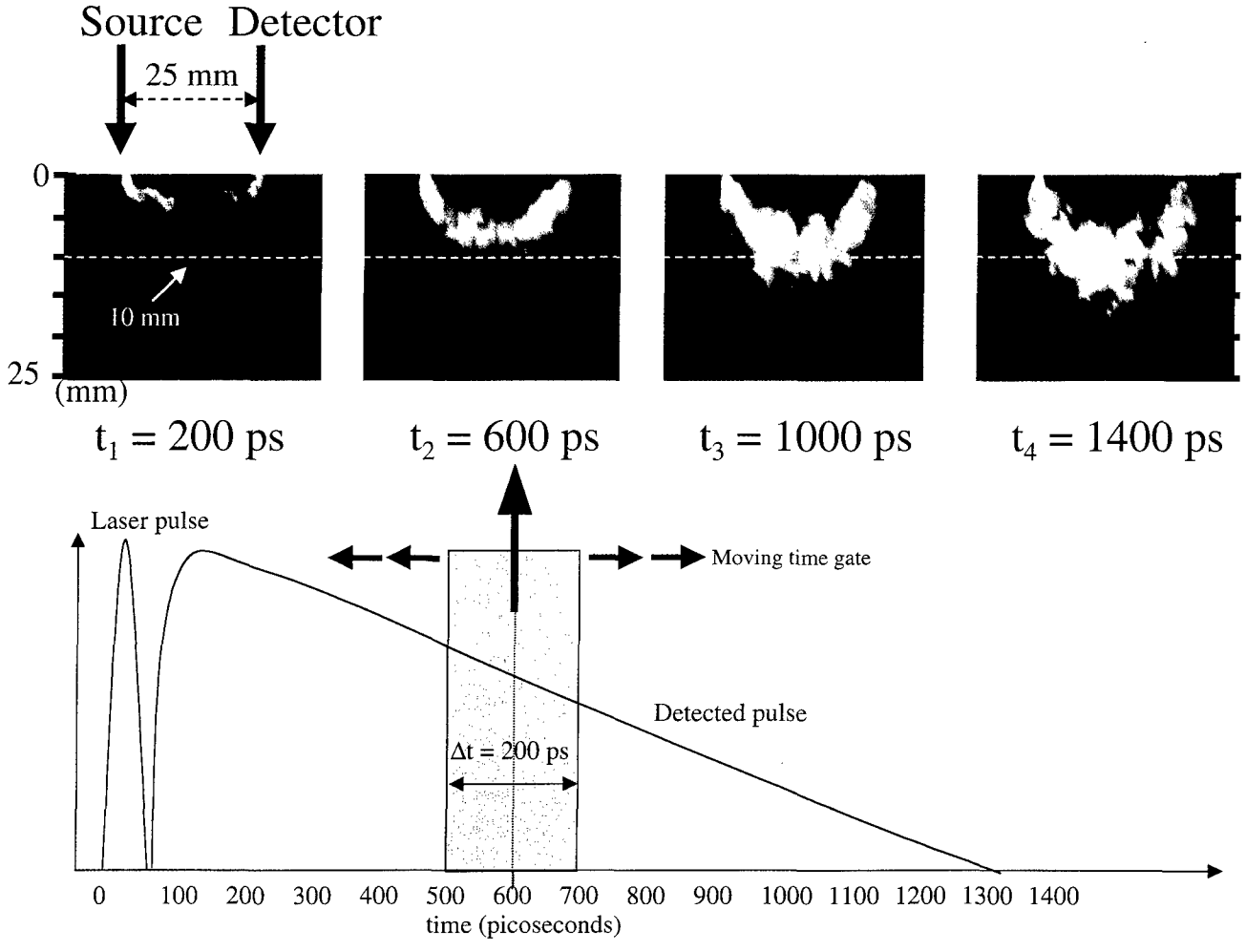

Figure 3. *Numerical simulation showing time-dependent propagation of ultrashort light pulse in tissue with optical properties similar to human breast (μ_a=0.1 cm^{-1}, μ_s'=10 cm^{-1}). Two-dimensional x–z views (40×25 mm^2) of detected photon density are shown. Time-gating of the detector provides control over depth and volume of tissue probed.*

The conceptual basis for the time-domain approach generally involves solutions to the radiative transfer equation [27,28] using Monte Carlo simulation [29–31] and diffusion theory approximations [7,32]. Diffusion-based methods provide relatively straightforward analytical expressions that describe the shape of a diffusely reflected or transmitted pulse in terms of the optical properties of the medium [10]. Thus, the observed temporal broadening of ultra short pulses can be mathematically related to the large number of optical paths available in multiple-scattering media. Since the introduction of losses (absorbers) reduces the average path length, absorber-dependent changes in pulse propagation time can be used to calculate absorption coefficients [10]. This concept is illustrated in Figure 3. Here, a picosecond light pulse is launched into a tissue-like medium with optical coefficients similar to human breast tissue (μ_a=0.1 cm^{-1}, μ_s'=10 cm^{-1}). The transport characteristics of the source are simulated numerically using a Monte Carlo technique [33]. The figure shows how the detected pulse spreads out in time and space, due to the large number of photon paths available. By time-gating the detector, one can adjust the "viewing volume" in the tissue. For example, at early times after the pulse is launched, shorter photon paths are detected. This is demonstrated by the 200 psec time point that samples tissue volumes above the 1 cm depth line. When the 200 psec observation "gate" is shifted to t=600 psec, the mean interrogation depth and volume are substantially greater. This is due to the fact that at longer times, photons have traveled tens of centimeters, substantially further than the 2.5 cm linear distance between source and detector. By moving the observation window through the time course of the detected signal, the spatial distribution of absorbers and scatterers in the tissue can be reconstructed, and sensitivity to deep tissue structures, such as tumors, can be optimized.

Frequency-domain optical methods can be adapted to diffusion theory models in a similar manner. Fishkin and Gratton [34] first suggested that amplitude-modulated light propagates through homogeneous multiple-scattering media as diffuse waves with a coherent front. These photon density waves can be characterized by a phase velocity (V_p) and modulation wavelength (λ_m) that are primarily functions of media optical properties. Measurements are performed by launching intensity-modulated light into tissue and recording the phase delay (*phi*) and demodulation amplitude (*m*) (with respect to the source) at a fixed distance from the launch site. Optical properties (the absorption coefficient, μ_a, and the reduced scattering coefficient, μ_s') are calculated from the measured frequency- and distance-dependent behavior by fitting the experimental results to an appropriate theoretical framework. Thus, FDPM can rapidly and quantitatively assess tissue optical properties in a single non-invasive measurement. It is important to point out that time and frequency domain methods are equivalent and related to each other through the Fourier transform. We employ the frequency-domain approach due to instrumentation advantages that include reduced cost, complexity, and simplicity of mathematical techniques used in frequency-domain signal analysis [35].

Instrumentation

In frequency-domain photon migration (FDPM), the intensity of light incident on an optically turbid sample is modulated at high frequencies (e.g., hundreds of megahertz), and the diffusely reflected, transmitted, or re-emitted (e.g., fluorescent) signal is measured with a phase-sensitive detector. Intensity-modulated light propagates through multiple-scattering media with a coherent front, forming photon density waves (PDWs). PDW dispersion is highly dependent on the optical properties of the medium. Exact absorption (μ_a) and reduced scattering (μ_s') parameters are calculated by comparing the measured frequency- or distance-dependent PDW phase and amplitude behavior to analytically derived non-linear model functions. Model functions are, in turn, derived from solutions to the photon diffusion equation which yield expressions for phase (*phi*) and amplitude (A) as a function of modulation frequency (ω) and tissue optical properties under various boundary conditions [36]. The values *phi*, A, and ω are defined in the usual manner where *phi*=the measured phase lag between the source (reference) and sample response; $A=AC_{sample}/AC_{source}$; and $\omega=2\pi f$ is the angular modulation frequency.

A schematic of our 1-GHz, portable FDPM device is shown in Figure 4 [37]. FDPM instrumentation and theoretical background have been described in detail elsewhere (Fishkin et al. [41]; Chance et al. [35]). Briefly, modulation is swept from 300 kHz to 1 GHz in less than 1 second, providing rapid, multi-wavelength (~670 to 960 nm) characterization of most tissues in a single measurement. The instrument is compact and can easily be transported to operating rooms and bedridden patients. By incorporating several NIR laser diodes, a number of wavelength-dependent physiological parameters are determined. Source modulation frequencies typically range from 300 kHz to 1 GHz, with FDPM data recorded in 5 MHz increments.

The core component of the FDPM apparatus is a network analyzer (Hewlett Packard, model 8753C), which is used to produce modulation swept from 300 kHz to 1 GHz (20 dB m RF output). RF from the network analyzer is serially superimposed (via the AC switch) on the direct current of up to eight different diode lasers (e.g., SDL, Inc. models 7421, 5420, 5421, and 6321 at 674, 811, 849, and 956 nm, respectively) using individual bias-tees (model 5575A, Picosecond Pulse Labs) and an RF switch (model 8768K, Hewlett Packard). One-hundred-micrometer-diameter gradient-index fibers are used to couple each light source to an 8×8 optical multiplexer (model GP700, DiCon Instruments). The 8×8 optical multiplexer allows for up to eight different diode laser light sources and eight different optical fiber positions.

Light is launched onto the tissue (or test object) using the above-mentioned unique wavelengths and one source fiber.

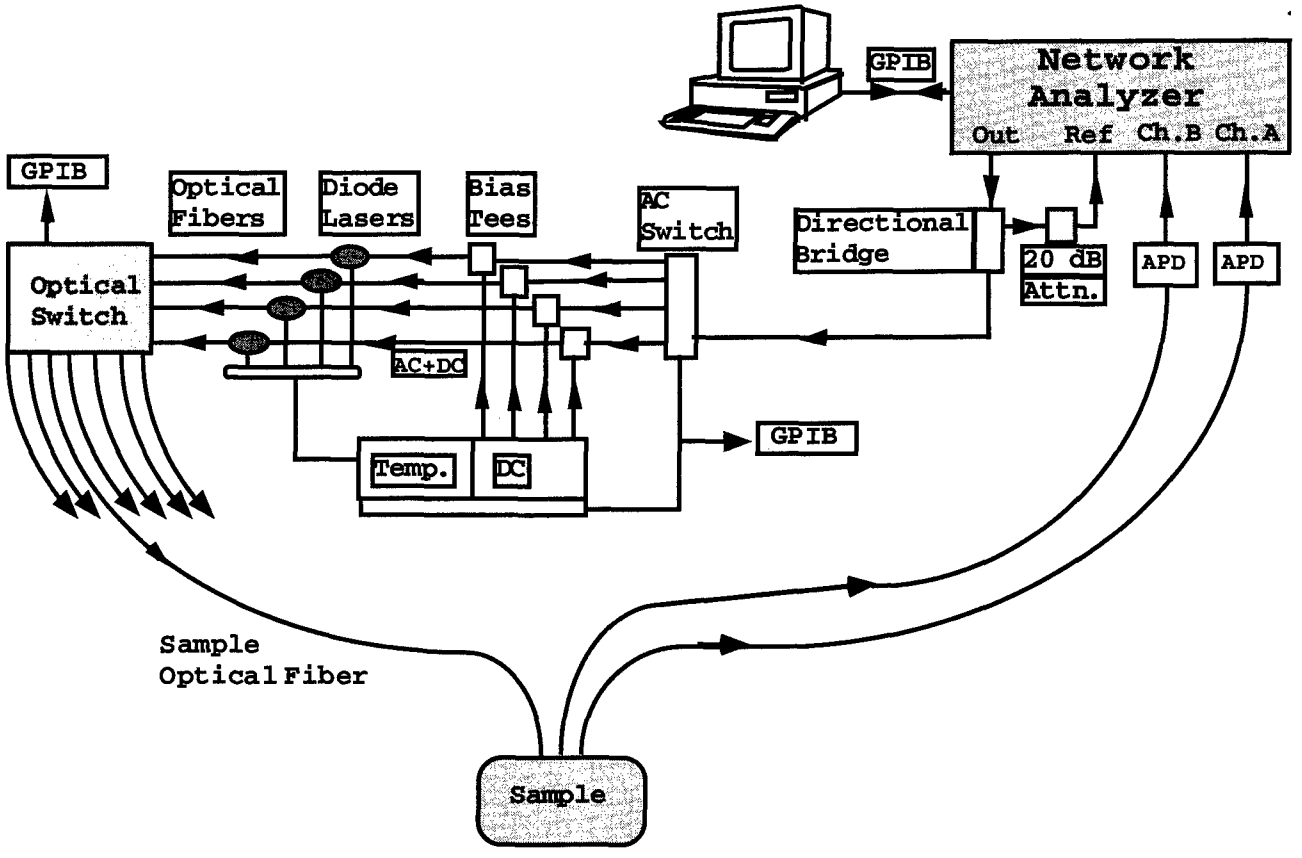

Figure 4. *One-gigahertz, multi-frequency, multi-wavelength FDPM instrument. See text for complete description.*

An avalanche photodiode (APD, Hamamatsu, model C5658) is used to detect the diffuse optical signal that propagates through the biological tissue. Both the APD and probe end of the source optical fiber are in direct contact with the patient (i.e., a "semi-infinite medium" measurement geometry). The optical power coupled into the tissue averages approximately 10 to 30 mW. Measurement time depends on the precision required, the number of sweeps performed, and RF/optical switch times. For human subject studies, approximately 0.1 second is used to sweep over the entire 1 GHz band of modulation frequencies. However, total elapsed time for four diodes (typically 12 to 16 sweeps/diode), data transfer, display, and source switching is approximately 40 seconds. Most components, including the network analyzer, RF/optical switches, diode power supplies and temperature of diode mounts are controlled by computer using virtual instrument software (LabView, National Instruments).

As shown schematically in Figure 5, phase and amplitude data (represented by *phi* and *A*, respectively) obtained from frequency-dependent FDPM tissue measurements are fit to theoretical model functions. This results in calculation of the optical absorption coefficient, μ_a, and the reduced scattering coefficient, μ_s', at a given λ and source–detector separation ρ. Minimization of the χ^2 surface is achieved for simultaneous, error-weighted fitting of the *phi* and *A* versus frequency data using a Marquardt-Levenberg algorithm. Typical μ_a, and μ_s' uncertainties, determined from the χ^2 distribution of phase and amplitude fits, range from 0.5% to 5% of the mean value. When optical properties (μ_s' and μ_a) are recovered for various source wavelengths, the spectral dependence of absorption can be combined with known values of molecular extinction coefficients to calculate physiologically relevant parameters, such as oxygenated, deoxygenated, and total hemoglobin concentration; oxygen saturation; drug concentration; blood volume fraction; and water concentration. The spectral dependence of scattering is used to provide insight into the mean density and size of scattering structures.

Application to Solid Tumor Characterization

The sensitivity of optical properties to tissue structure and function suggests that differences between normal and diseased tissues may provide a means for assessing the probability that processes such as malignant transformation, inflammation, or infection are occurring. Indeed, previous studies have shown unique scattering and/or absorption signatures associated with dysplastic [25,38,39], malignant [41] and benign [45] tissue transformations.

Characterization of solid tumors in thick tissues poses unique challenges. These structures are typically found embedded beneath epithelial layers and require methods capable of probing deep tissue structure and function.

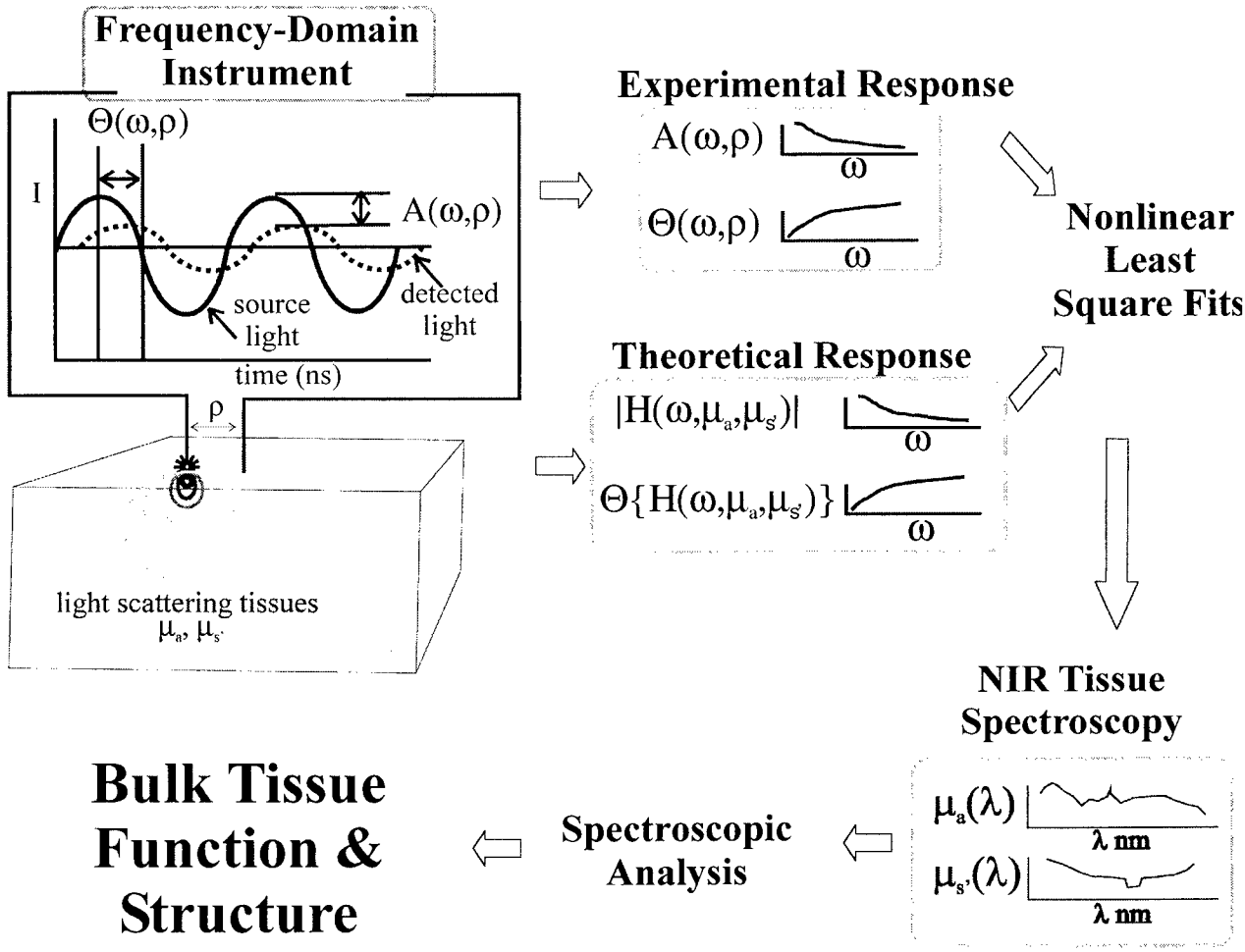

Figure 5. *FDPM measurement overview: intensity-modulated light is launched into tissue, resulting in the propagation of diffuse photon density waves. The frequency-dependent experimental response (phase, phi, and amplitude, A vs. frequency, ω) is compared to a theoretical model. Model-data fits provide calculated values for absorption, μ_a, and reduced scattering, μ_s', coefficients at each optical wavelength. Absorption and scattering spectra are generated. Absorption spectra are used to calculate concentration of principal tissue chromophores.*

Because of multiple light scattering, spatial resolution using "diffuse methods" is intrinsically rather poor, on the order of 1 to 5 mm [40]. Nevertheless, imposing temporal resolution can confine the photon interrogation volume to specific regions (see Figure 3) and improve sensitivity to buried tumors. This is achieved by examining the temporal point spread function of a short light pulse, as illustrated in Figure 3, or by measuring the phase and amplitude of photon density waves, as illustrated in Figure 5. By measuring *phi* and *A* at multiple modulation frequencies (ω), information that is comparable to recording the temporal profile of the diffusely propagating pulse is obtained. When these data are recorded at multiple wavelengths (λ), FDPM becomes a quantitative spectroscopic technique.

Structural components that contribute to FDPM signals in thick tissues are shown in Figure 6*A*. The appearance and progression of tumors alter the fractional contribution of cells, extracellular matrix, and vasculature to the absorption and scattering spectra. In addition, spatial variations in optical properties may be evident for poorly differentiated tumor versus well-differentiated normal tissues. This is due to the fact that, with disease progression, there is typically an increase in tumor cell density, nuclear volume fraction, and stromal/inflammatory cells. Extracellular matrix degrades with increasing tumor invasion, and neovasculature is recruited, forming a tortuous, leaky network complete with flow anomolies. These alterations in tissue architecture affect both the absolute value and wavelength dependence of the reduced scattering parameter. From a molecular perspective, we assume that the chromophores contributing to μ_a at a given NIR wavelength are principally oxy- and deoxy-hemoglobin, water, and fat. The total absorption measured at a given wavelength is a linear sum of each. Thus, in order to achieve optimal sensitivity, it is desirable to illuminate the tissue with light source wavelengths that correspond to high-contrast absorption features. For example, in Figure 6*B*, fractional spectral contributions are shown for physiological concentrations of principal components in a typical breast tissue: deoxy- and oxy-hemoglobin, fat, and water. Sources at about 670, 810, 920, and 960 nm are most

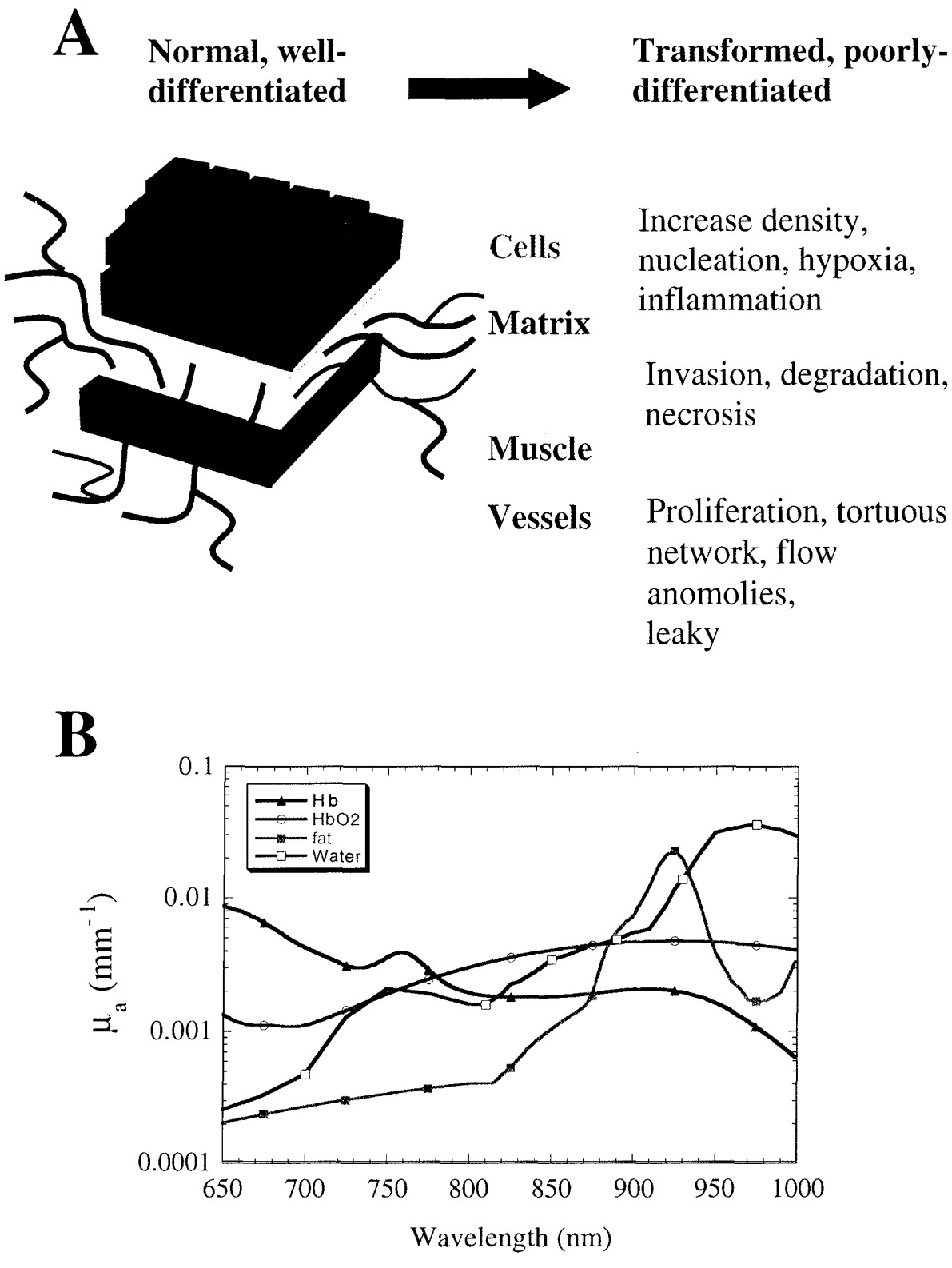

Figure 6. *(A) Structural and functional components of the optical signal in normal and transformed tissue. (B) Absorption spectra of tissue with composition similar to human post-menopausal breast: 10 μM deoxyhemoglobin [Hb], 15 μM oxyhemoglobin [HbO_2], fat (80% volume fraction), and water (15% volume fraction).*

sensitive to each. In order to calculate tissue concentrations, μ_a measurements at a minimum of four different wavelengths are combined with known values of molecular extinction coefficients [41]. Due to the metabolic demands of rapidly proliferating tumor cells and increased tumor vasculature, these biochemical constituents can vary substantially in relative abundance for normal versus diseased tissue.

Breast Measurements: Results and Discussion

The relative impact of these physiological features on photon migration can be determined by examining normal breast tissue optical properties (see Ref. [42] for a description of breast tissue optics). Figure 7 shows results of FDPM measurements obtained from two pre-menopausal and two post-menopausal subjects (27, 29 and 63, 67 years old, respectively). Data were collected from the right upper outer quadrants of each subject while in a reclining position. The probe was applied with gentle pressure (i.e., no external compression) using a source–detector separation of 2.5 cm.

Pre- and post-menopausal normal breasts exhibit clear wavelength-dependent differences in both absorption and scattering parameters. Figure 7*B* shows that scattering is approximately 20% greater in pre-menopausal (μ_s'~0.8 to 1.1 mm^{-1}) versus post-menopausal women (μ_s'~0.6 to 0.7 mm^{-1}). In addition, the wavelength dependence of scattering is steeper for pre- versus post-menopausal subjects. These findings are consistent with known changes in breast physiology. Breast tissue, while under hormonal control, has higher glandular/cellular content and collagen is required in the extracellular matrix in order to support the structural demands of cellular proliferation. After menopause, the absence of hormonal stimulation results in glandular shrinkage, collagen remodeling to fat, and diminished vasculature. Since small tissue structures such as collagen fibers and subcellular organelles are likely to be the primary contributors to tissue scattering, it is not surprising that the wavelength dependence of scattering is relatively steep for pre-menopausal subjects. In contrast, following conversion to a principally large-particle fatty matrix, a much more gradual wavelength dependence of scattering is observed. Thus, the diminished contribution of the glands and collagenous stroma leads to a clear wavelength-dependent scattering reduction.

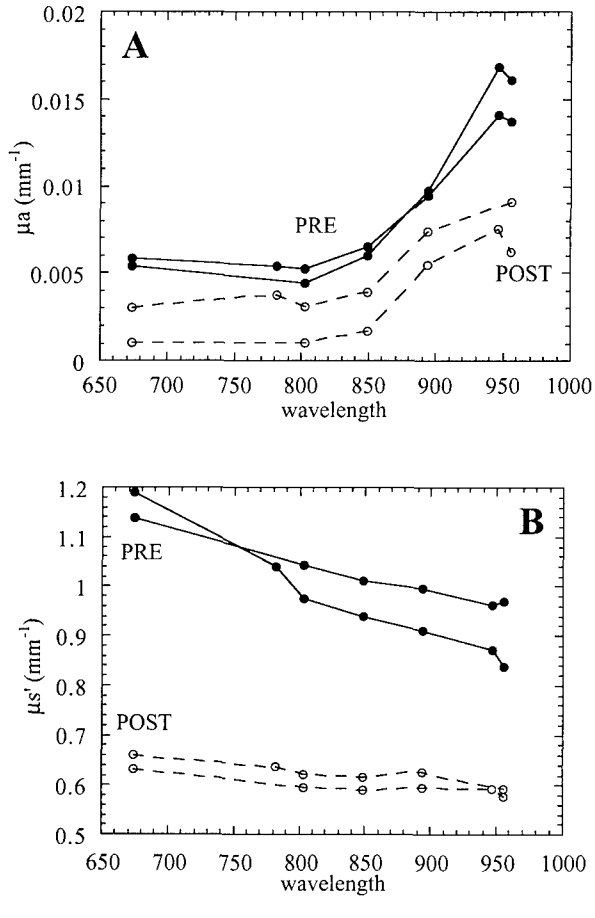

Figure 7. *FDPM measurements in PRE (●) and POST (○) menopausal normal breast (four subjects). (A) Calculated values of absorption coefficients, μ_a, vs. wavelength. (B) Calculated values of reduced scattering coefficients, μ_s', vs. wavelength.*

Variations in absorption can be explained in a similar manner. Absorption contrast due to enhanced perfusion is clearly detectable while breast tissue is under hormonal control. This is reflected in Figure 7*A* values of absorption coefficients that are consistently higher for pre-menopausal subjects. Following menopause, the absence of substantial metabolic demand leads to reduced perfusion and lower absorption values. This is well-correlated with the low blood, high fat content of post-menopausal tissue. Similar changes in optical properties have been observed by others [43,44].

These results demonstrate the intrinsic sensitivity of FDPM to breast tissue physiological states. In order to address the origin of photon migration signals in solid tumors, we have initiated breast tumor studies in human subjects [45]. Our goal is to carefully define the level of accuracy and precision required from our measurement techniques so that malignant lesions can be identified and resolved from normal structures with a reasonable level of confidence. The practical impact of increasing diagnostic specificity would be two-fold: 1) enhanced early detection of relatively small (0.5 to 1 cm diameter) tumors is likely to lead to mortality improvements (mammographic performance is highly variable in pre-menopausal subjects); and 2) more specific characterization of benign versus malignant lesions would lead to reductions in the large number of unnecessary surgical biopsies. As a result, there is considerable room for the development of new, non-invasive optical methods for characterizing breast tissue.

In the following discussion, we present results from three individuals. Experiments were performed under the guidelines of UC Irvine IRB-approved protocol #95-563. Patient 1 was a 67-year-old post-menopausal subject with a single palpable mass 7.4 mm beneath the skin surface in the upper outer quadrant of the left breast. Histological examination following surgical biopsy and ultrasound revealed a 1.8×0.9 cm ductal carcinoma in situ (DCIS) (malignant tumor). Patient 2 was a 63-year-old post-menopausal subject with a non-palpable spiculated left breast mass. Histological examination following surgical biopsy revealed a 0.6×0.4×0.7 cm invasive ductal carcinoma (malignant tumor). Patient 3 was a 22-year-old, pre-menopausal subject patient with a 2×2 cm palpable mass 3–7 mm below the surface in the upper medial portion of the right breast. Surgical biopsy revealed the presence of a benign fibroadenoma.

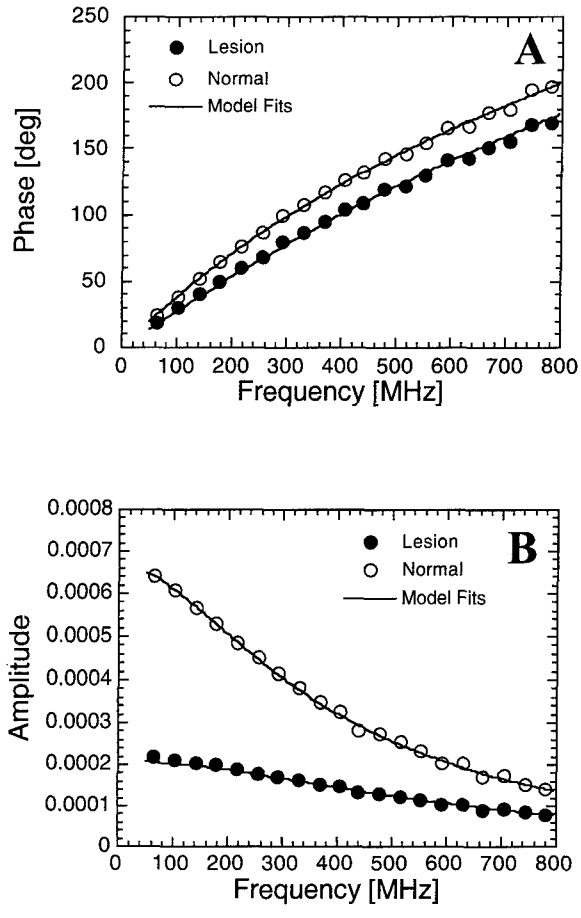

Figure 8. *FDPM measurements of phase (A) and amplitude (B) vs. source modulation frequency obtained from normal and tumor sites on patient 1 (ductal carcinoma in situ, DCIS). Source–detector distance = 2.5 cm; λ = 674 nm. Solid lines are best simultaneous fits to phase and amplitude data from tumor (●) and normal (○) data points, respectively. Ten percent of 200 frequency-domain data points is shown for clarity.*

Measurements are performed on each patient by gently placing the FDPM probe on both normal and tumor-containing breast. Data are acquired using a hand-held scanning probe placed in nine discrete locations covering a 2×2 cm^2 grid mapping the breast surface. The probe incorporates source–detector (s–d) pairs ranging from 1 to 2.5 cm in separation. The 2.5 cm s–d configuration is placed on the tissue with the source and detector bracketing the tumor. Tumor location, dimension, and depth are monitored immediately prior to FDPM measurements by ultrasound. Photon migration data are acquired by moving the probe in 0.5 mm increments along inferior–superior and medial–lateral paths. Repeat measurements immediately above tumor center are obtained at least three times. Both normal and tumor-containing breasts are studied. Each tissue location is characterized in terms of wavelength-dependent absorption and scattering parameters which, in turn, are used to calculate physiological properties.

Sequential scans of the same location following probe removal and replacement revealed no significant variations in optical properties. Normal tissue measurements are acquired in the same manner from a symmetric site on the opposite, uninvolved breast. Phase and amplitude data (represented by *phi* and *A*, respectively) obtained from FDPM tissue measurements are compared to semi-infinite model functions to extract the optical absorption coefficient, μ_a, and the reduced scattering coefficient, μ_s', at a given λ and source–detector separation. Typical μ_a and μ_s' uncertainties, determined from the phase and amplitude fits, range from 0.5% to 5% of the mean value.

Results of 674-nm FDPM measurements are shown for patient 1 in Figure 8. Raw data reveal clear differences in both phase (Figure 8*A*) and amplitude (Figure 8*B*) for normal and tumor sites. Solid lines are results of model-fits data demonstrating good agreement between measurements and the photon migration theoretical model. Only 10% of the actual data points is shown in each figure for clarity.

Optical properties calculated from each scan position are compared to mean values obtained from 11 discrete locations on the normal side. Figure 9*A* presents the ratio of absorption coefficients (tumor/normal) acquired in medial–lateral and superior–inferior scans at 674 nm.

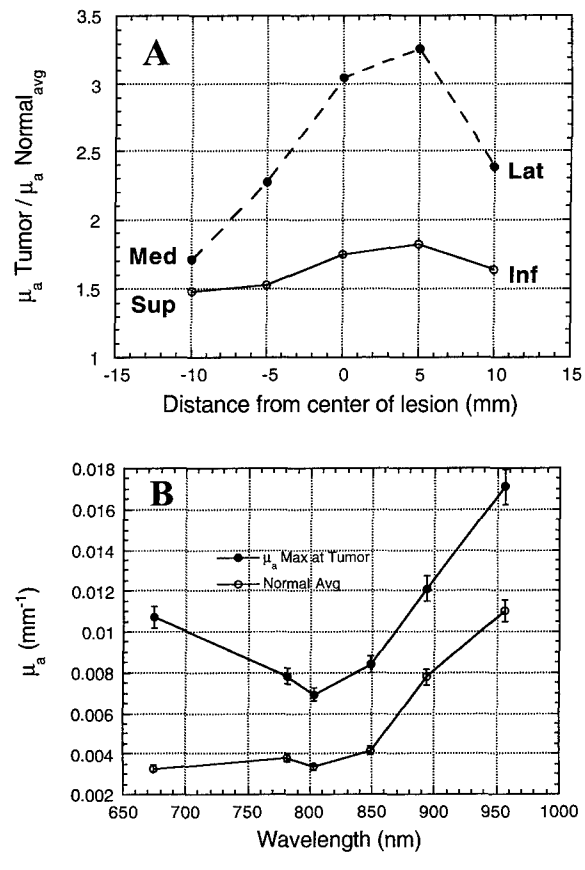

Figure 9. *(A) Ratio of absorption coefficients (tumor/normal) acquired in medial–lateral and superior–inferior scans at 674 nm for patient 1 (ductal carcinoma in situ, DCIS). Normal side represents average of 11 multiple site measurements. Contrast of approximately three-fold is observed for tumor vs. normal sites when the probe is placed 5 mm lateral of the estimated tumor center. (B) Wavelength dependence of optical properties acquired from the peak contrast location (5 mm lateral, medial–lateral axis) and symmetric location on normal side.*

Contrast of approximately three-fold is observed for tumor versus normal sites when the probe is placed just 5 mm lateral of the tumor center. A clearly discernable tumor shape is apparent in this horizontal scan direction. Reduced tumor/normal absorption contrast is observed in the superior–inferior scan, most probably due to differences in tumor orientation along this axis.

Wavelength-dependent optical properties acquired from the peak contrast location (5 mm lateral, medial–lateral axis) are displayed in Figure 9*B*. Absolute tumor μ_a

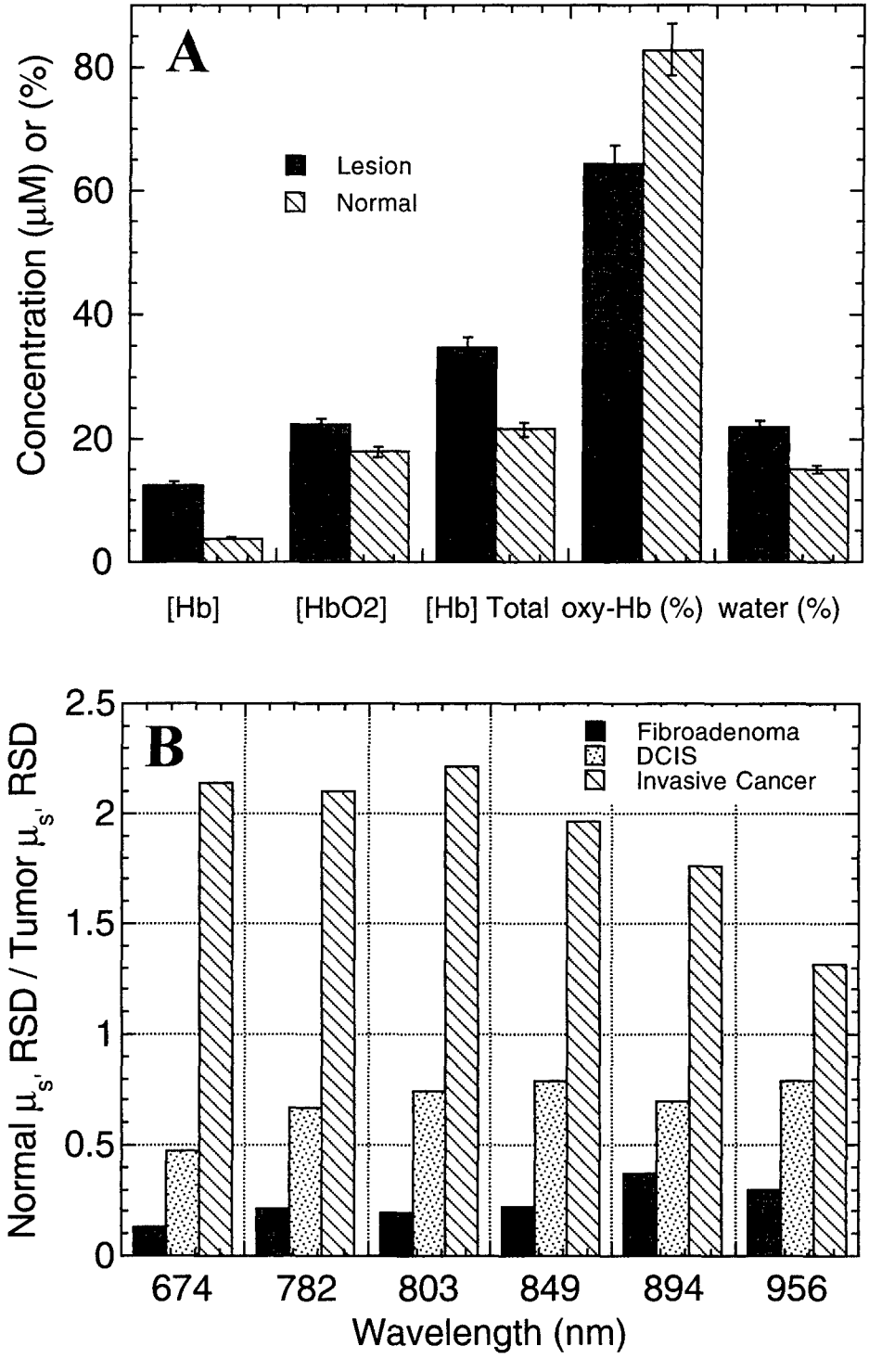

Figure 10. *(A) Hemoglobin concentration (μM) in deoxy- [Hb], oxy- [HbO_2], and total forms; %oxygen saturation (100× [HbO_2]/[Hb(tot)]), and water content (%) for normal and tumor breast, patient 1. Values calculated from wavelength dependence of absorption (Figure 9B). (B) The ratio of μ_s' RSD values for normal/tumor tissues at each measurement wavelength for patients 1 (DCIS), 2 (invasive ductal carcinoma), and 3 (benign fibroadenoma). RSD is determined from the mean and standard deviation of 11 measurements and nine discrete locations on normal and tumor sides. A RSD ratio of 1 implies that tumor and normal tissue have equivalent structural variation.*

values range from a minimum of about 0.007 mm^{-1} at 803 nm to a maximum of 0.017 mm^{-1} at 956 nm. Regardless of wavelength, tumor absorption is consistently on the order of 2- to 3.5-fold greater than normal tissue. This is due to the enhanced tumor versus normal blood supply (perfusion) and higher hemoglobin content. Tumor and normal tissue absorption spectra also have different shapes. The slope between 674 and 803 nm features is negative for tumor, positive for normal tissue. The significance of this is related to the increased contribution of de-oxyhemoglobin to light absorption in spectral regions that are shorter in wavelength than the ~800 nm isosbestic point (i.e., the point of equivalent absorption efficiency for both oxy- and deoxy-hemoglobin forms).

Physiologic differences between tumor and normal tissue are further amplified by calculations of water and blood content. The concentrations of water, deoxy-, oxy-, and total hemoglobin in DCIS and normal breast are determined from known extinction coefficients and Figure 9*B* absorption data. Results, shown in Figure 10*A*, clearly reveal elevated tumor levels for each physiological parameter. Total tumor hemoglobin ($[Hb(tot)]=[Hb]+[HbO_2]$) is 35 μM, nearly twice the 20 μM level typical of normal postmenopausal breast. Deoxy-hemoglobin ($[Hb]$) values of about 15 μM are roughly three-fold greater than normal. Together, these values can be used to determine percent oxygen saturation, Y, where $Y\%=100\times[HbO_2]/[Hb(tot)]$. In this case, $Y(tumor)\sim65\%$ and $Y(normal)\sim80\%$. Differences are due to the oxygen extraction demands of rapidly proliferating, metabolically active tumor cells. The reduced Y value is consistent with the measured elevation in hemoglobin at the tumor since both blood and oxygen are required to sustain tumor growth. Others have reported similar changes in tumor hemoglobin concentration and oxygen saturation using non-invasive photon migration techniques in the breast [46,47].

Tissue water concentration is also displayed in Figure 10*A*. It is difficult to confirm the accuracy of these values since they are based on pure water extinction coefficients (as opposed to protein-bound forms) at 25°C and our calculations do not take into account the contribution of fat to the 956 nm signal. Nevertheless, results fall within the 11.4% to 30.5% range given in the literature for percentage water in human fatty adipose tissue [48]. In addition, tumors develop high interstitial fluid pressure due to lack of lymphatic drainage. Thus, increased fluid retention, blood content, and cellularity are likely to be the cause of the slightly elevated tumor water percentage observed in this patient (20% vs. 15%).

Despite these clear biochemical differences, it is not yet known whether malignant tumors can be distinguished from benign lesions using this technology. In fact, it is our experience that both malignant and benign tumors generally display elevated hemoglobin and reduced $Y\%$ values. Although these observations are for a limited number of patients, it is likely that additional diagnostic specificity is required. This can be provided by examining spatial variations in the tissue-scattering parameter, μ_s'. As illustrated schematically in Figure 8, normal well-differentiated tissue is composed of distinct structural/functional domains. The appearance of disease perturbs this intrinsic organization, resulting in a gradual loss of structural heterogeneity. Ultimately, the growth of an invasive tumor will lead to a chaotic, poorly differentiated environment.

The precise relationship between disease progression stage and photon migration-scattering signature is poorly understood. In order to explore this more carefully, we have mapped tumor optical properties from three patients with benign, malignant invasive, and malignant in situ breast disease. As described above, data are acquired from at least 11 measurements (nine discrete locations in 5 mm increments) using a 2×2 cm^2 scanning pattern on the breast surface. Absorption and scattering coefficients are computed and mean±standard deviation (SD) values calculated for all measurements of normal and tumor-containing sites. The relative standard deviation (RSD) of optical properties obtained from tumor and normal sites is expressed in the usual manner, $RSD=100\times(SD/mean)$. Figure 10*B* shows the ratio of μ_s' RSD values for normal/tumor tissues at each measurement wavelength. A RSD ratio of 1 implies that tumor and normal tissue have equivalent structural variation. Interestingly, in the case of invasive cancer, the normal/tumor RSD is consistently greater than 1 for all wavelengths. This suggests greater scattering spatial heterogeneity in the well-differentiated normal tissue than in the lesion. These observations are consistent with the idea that disease progression leads to loss of differentiation, and that differentiation provides the fundamental origin for spatially varying scattering signals.

RSD ratios of about 0.5 and less are consistently observed with malignant DCIS and benign fibroadenomas. In the case of the fibroadenoma, this is likely due to enhanced structural variation (versus normal tissue) introduced by well-defined zones of dense collagen fiber synthesis and glandular shrinkage. DCIS appears to be midway between these two extremes, possibly due to the absence of invasion and general preservation/stimulation of extracellular matrix. These data further confirm the sensitivity of FDPM to the cell and matrix alterations seen in Figure 7. However, by measuring spatially varying properties, the perturbative effect tumors have on normal tissue architecture is detected with enhanced sensitivity.

Conclusions

FDPM is a non-invasive optical technique that utilizes NIR light to monitor physiology in bulk tissues. Optical properties derived from FDPM measurements can be used to construct low-resolution functional maps and, consequently, provide a relatively low-cost adjunct to many conventional diagnostic tools. Substantial work remains to accurately describe heterogeneous tissues that vary in geometry, structure, and composition. Despite these limitations, several unique applications of photon migration

measurements are currently underway, particularly in solid tumor characterization. Preliminary studies show that unique breast tumor optical signatures are, in fact, detectable in human subjects. Changes in blood flow, oxygen consumption, and tissue structure (cellular and matrix) can be measured quantitatively. Most importantly, these signals appear to reflect fundamental physiological processes associated with malignancy, disease progression, age and menopausal status. Because many attributes related to the origin, progression, and therapeutic response of breast cancer are common to other types of tumors, we expect continued optical technology development will have a broad impact on optical diagnosis and therapy.

Acknowledgements

The authors wish to thank Andy Dunn and Joon You for assistance with Monte Carlo simulations.

References

[1] Cutler M (1929). Transilluminating as an aid in the diagnosis of breast lesions. *Surg Gynecol Obstet* **48**, 721–728.

[2] Vastag B (1999). Shining light on breast tumors. *J Nat Cancer Inst* **91** (24), 2072–2073.

[3] Bonner RF, Nossal R, Havlin S, and Weiss GH (1987). Model for photon migration in turbid biological media. *J Opt Soc Am A* **4**, 423–432.

[4] Boulnois JL (1986). Photophysical processes in recent medical laser developments: a review. *Lasers Med Sci* **1**, 47–66.

[5] Svaasand L (1990). On the Physical Rationale of Photodynamic Therapy. In *Future Directions and Application in Photodynamic Therapy.* CJ Gomer (Ed.). SPIE Institute Series for Advanced Optical Technologies, IS6. pp. 233–248.

[6] Cheong WF, Prahl SA, and Welch AJ (1990). A review of the optical properties of biological tissues. *IEEE JQE* **26**, 2166–2185.

[7] Chance B, Leigh J, Miyake H, Smith D, Nioka S, Greenfield R, Finlander M, Kaufmann K, Levy W, Yound M, Cohen P, Yodshioka H, and Boretsky R (1988). Comparison of time-resolved and -unresolved measurements of deoxyhemoglobin in brain. *Proc Natl Acad Sci* **85**, 4971–4975.

[8] Delpy DT, Cope M, van de Zee P, Arridge S, Wray S, and Wyatt J (1988). Estimation of optical pathlength through tissue from direct time of flight measurement. *Phys Med Biol* **33**, 1433–1442.

[9] Wilson BC, Sevick EM, Patterson MS, and Chance B (1992). Time-dependent optical spectroscopy and imaging for biomedical applications. *Proc IEEE* **80**, 918–930.

[10] Cubeddu R, Pifferi A, Taroni P, Torricelli A, and Valentini G (1996). Experimental test of theoretical models for time-resolved reflectance. *Med Phys* **23** (9), 1625–1633.

[11] Zaccanti G, Bruscaglioni P, Ismaelli A, Carraresi L, Gurioli M, and Wei Q (1992). Transmission of a pulsed thin light beam through thick turbid media; experimental results. *Appl Opt* **31** (12), 2141–2147.

[12] Patterson MS, Chance B, and Wilson BC (1989). Time-resolved reflectance and transmittance for the non-invasive measurement of tissue optical properties. *Appl Opt* **28**, 2331–2336.

[13] Yoo KM, and Alfano RR (1990). Determination of the scattering and absorption lengths from the temporal profile of a backscattered pulse. *Opt Lett* **15**, 276–278.

[14] Singer JR, Grunbaum FA, Kohn P, and Zubelli JP (1990). Image reconstruction of the interior of bodies that diffuse radiation. *Science* **248**, 990–993.

[15] Barbour RL, Graber HL, Aronson R, and Lubowsky J (1991). Imaging of subsurface regions of random media by remote sensing. *Proc SPIE (Los Angeles)* **1431**, 192–203.

[16] Benaron D, and Stevenson D (1993). Optical time of flight and absorbance imaging of biologic media. *Science* **259**, 1463–1466.

[17] Ts'o DY, Frostig RD, Lieke EE, and Grinvald A (1990). Functional organization of primate visual cortex revealed by high resolution optical imaging. *Science* **249**, 417–420.

[18] Gratton E, Fantini S, Franceschini MA, Gratton G, and Fabini M (1997). Measurements of scattering and absorption changes in muscle and brain. *Philos Trans Biol Sci* **352**, 727–735.

[19] Sevick EM, Chance B, Leigh J, Nioka S, and Maris M (1991). Quantitation of time and frequency-resolved optical spectra for the determination of tissue oxygenation. *Anal Biochem* **195**, 330–351.

[20] Chance B, Nioka S, Kent J, McCully K, Fountain M, Greenfeld R, and Holtom G (1988). Time-resolved spectroscopy of hemoglobin and myoglobin in resting and ischemic muscle. *Anal Biochem* **174**, 698.

[21] Schmitt JM, and Zhou G-X (1992). Measurement of blood hematocrit by dual-wavelength near-IR photoplethysmography. In *Proc. SPIE 1641, Physiological Monitoring and Early Detection Diagnostic Methods.* TS Mang (Ed.). pp. 150–161.

[22] De Blasi RA, Fantini S, Franceschini MA, Ferrari M, and Gratton E (1995). Cerebral and muscle oxygen saturation measurement by a novel frequency-domain near-infrared spectrometer. *Med Biol Eng Commun* **33**, 228–230.

[23] Franceschini MA, Gratton E, and Fantini S (1999). Noninvasive optical method of measuring tissue and arterial saturation: an application to absolute pulse oximetry of the brain. *Opt Lett* **24** (12), 829–831.

[24] Patterson MS, Wilson BC, Feather JW, Burns DM, and Pushka W (1987). The measurement of dihematoporphyrin ether by reflectance spectrophotometry. *Photochem Photobiol* **46**, 337–343.

[25] Hornung R, Pham T, Keefe KA, Berns MW, Tadir Y, and Tromberg BJ (1999). Quantitative near-infrared spectroscopy of cervical dysplasia *in vivo. Hum Reprod* **14** (11), 2908–2916.

[26] Jacques SL, and Prahl SA (1987). Modeling optical and thermal distributions in tissue during laser irradiation. *Lasers Surg Med* **6**, 494–503.

[27] Furutsu K (1980). Diffusion equation derived from space–time transport equation. *J Opt Soc Am* **70**, 360.

[28] Patterson MS, Wilson BC, and Wyman DR (1991). The propagation of optical radiation in tissue: I. Models of radiation transport and their application. *Lasers Med Sci* **6**, 155–168.

[29] Jacques SL (1989). Time-resolved propagation of ultrashort laser pulses within turbid tissues. *Appl Opt* **28**, 2223–2229.

[30] Flock ST, Patterson MS, Wilson BC, and Wyman DR (1989). Monte Carlo modeling of light propagation in scattering tissues: I. Model prediction and comparison with diffusion theory. *IEEE Trans Biomed Eng* **36**, 1162–1168.

[31] Hasegawa Y, Yamada Y, Tamura M, and Nomura Y (1991). Monte Carlo simulation of light transmission through living tissues. *Appl Opt* **31**, 4515–4520.

[32] Ishimaru A (1989). Diffusion of light in urbid materials. *Appl Opt* **28**, 2210–2215.

[33] Dunn AK, Wallace VP, Coleno M, Berns MW, and Tromberg BJ Influence of optical properties on two-photon fluorescence imaging in turbid samples. *Appl Opt*, submitted.

[34] Fishkin J, and Gratton E (1993). Propagation of photon density waves in strongly scattering media containing an absorbing "semi-infinite" plane bounded by a straight edge. *J Opt Soc Am A* **10** (1), 127–140.

[35] Chance B, Cope M, Gratton E, Ramanujam N, and Tromberg B (1998). Phase measurement of light absorption and scatter in human tissues. *Rev Sci Instrum* **689**, 3457–3481.

[36] Haskell RC, Svaasand LO, Tsay T-T, Feng T-C, McAdams MS, and Tromberg BJ (1994). Boundary conditions for the diffusion equation in radiative transfer. *J Opt Soc Am A* **11**, 2727–2741.

[37] Madsen SJ, Anderson ER, Haskell RC, and Tromberg BJ (1994). A portable, high-bandwidth frequency-domain photon migration instrument for tissue spectroscopy. *Opt Lett* **19**, 1934–1936.

[38] Bigio IJ, and Mourant JR (1997). Ultraviolet and visible spectroscopies for tissue diagnostics: fluorescence spectroscopy and elastic-scattering spectroscopy. *Phys Med Biol* **42**, 803–814.

[39] Perelmand LT, Backman V, Wallace M, Zonios G, Manoharan R, Nusrat A, Shields S, Seiler M, Lima C, Hamano T, Itzkan I, Van Dam J, Crawford JM, and Feld MS (1998). Observation of periodic fine structure in reflectance from biological tissue: a new technique for measuring nuclear size distribution. *Phys Rev Lett* **80** (3), 627–630.

[40] Boas DA, O'Leary MA, Chance B, and Yodh AG (1997). Detection and characterization of optical inhomegeneities with diffuse photon density waves: a signal-to-noise analysis. *Appl Opt* **36**, 75–92.

[41] Fishkin JB, Coquoz O, Anderson EA, Brenner M, and Tromberg BJ (1997). Frequency-domain photon migration measurements of normal and malignant tissue optical properties in a human subject. *Appl Opt* **36**, 10–20.

[42] Thompsen S, and Tatman D (1998). Physiological and pathological

factors of human breast disease that can influence optical diagnostics. *Ann NY Acad Sci* **838**, 171–193.

[43] Suzuki K, Yamashita Y, Ohta K, Kaneko M, Yoshida M, and Chance B (1996). Quantitative measurement of optical parameters in normal breasts using time-resolved spectroscopy: *in vivo* results of 30 Japanese women. *J Biomed Opt* **1** (3), 330–334.

[44] Quaresima V, Matcher SJ, and Ferrari M (1998). Identification of intrinsic optical contrast for near-infrared mammography. *Photochem Photobiol* **67** (1), 4–14.

[45] Tromberg BJ, Coquoz O, Fishkin JB, Pham T, Anderson ER, Butler J, Cahn M, Gross JD, Venugopalan V, and Pham D (1997). Non-invasive measurements of breast tissue optical properties using frequency-domain photon migration. *Philos Trans R Soc London B* **352**, 661–668.

[46] Fantini S, Walker SA, Franceschini MA, Moesta KT, Schlag PM, Kaschke M, and Gratton E (1998). Assessment of the size, position, and optical properties of breast tumors *in vivo* by non-invasive optical methods. *Appl Opt* **37**, 1982–1989.

[47] McBride TO, Pogue B, Gerety ED, Poplack SB, Osterberg UL, and Paulsen KD (1999). Spectroscopic diffuse optical tomography for the quantitative assessment of hemoglobin concentration and oxygen saturation in breast tissue. *Appl Opt* **38** (25), 5480–5491.

[48] Duck FA (1990). *Physical Properties of Tissue*. London, Academic Press. pp. 320–328.

Broadband absorption spectroscopy in turbid media by combining frequency-domain and steady-state methods

Frédéric Bevilacqua,[§] Andrew J. Berger,[§¶*]Albert E. Cerussi,[§]

Dorota Jakubowski,[§] and Bruce J. Tromberg[§†]

[§]Beckman Laser Institute, University of California, Irvine

Irvine, CA 92612

[¶]*current address:* The Institute of Optics, University of Rochester

Rochester, NY 14627

August 17, 2000

*Co-first author (with Bevilacqua).

†Corresponding author. Email: *tromberg@bli.uci.edu*

Abstract

A technique for measuring broadband near-infrared absoprtion spectra of turbid media is presented using a combination of frequency-domain (FD) and steady-state (SS) reflectance methods. Most of the wavelength coverage is provided by a white-light SS measurement, while the FD data are acquired at a few selected wavelengths. Coefficients of absorption (μ_a) and reduced scattering (μ_s') derived from the FD data are used to intensity-calibrate the SS measurements and to estimate μ_s' at all wavelengths in the spectral window of interest. After these steps are performed, μ_a can be determined by comparing the SS reflectance values to the predictions of diffusion theory, wavelength by wavelength. Absorption spectra of a turbid phantom and of human breast tissue *in vivo*, derived using the combined SSFD technique, agree well with expected reference values. All measurements can be performed at a single source-detector separation distance, reducing variations in sampling volume that exist in multi-distance methods. The technique uses relatively inexpensive light sources and detectors and is easily implemented on an existing multi-wavelength FD system.

OCIS codes: 170.1470, Blood/tissue constituent monitoring; 170.4090, modulation techniques; 170.5280, photon migration; 170.7050, turbid media.

1 Introduction

Reflectance spectroscopy has become a widely used technique for characterizing turbid media, including many medical applications to human tissue. In many cases, the quantification of chromophore concentrations is desired, and this requires the ability to separate the effects of absorption from those of scattering. Fundamentally, the coefficients of absorption, μ_a, and reduced scattering, μ_s', can be determined by a series of reflectance measurements performed in one of three domains, namely time[1–3] (using a fast pulse of light), frequency[4–7] (using a sinusoidally modulated source of light), or steady state[8–15] (using a source of constant intensity but multiple detectors at different distances). Unsurprisingly, these three techniques have different merits and limitations. Spatially-resolved steady-state techniques are relatively inexpensive, and more readily suited for the determination of μ_a and μ_s' over large, continuous ranges of wavelengths than the other methods. However, the steady-state approach works best when measurements are performed using a combination of both short ($\sim$ 1 transport mean free path) and long (many transport mean free paths) source-detector separations.[11] Ideally, the optical properties of the sample should not vary over the range of different volumes probed by the different measurements. The larger the spread of distances probed, the more likely that heterogeneities, such as those found in biological tissue, will distort the data from the predictions of the model. One approach to limiting this effect, given that the shortest separations provide great stability to the calculation of μ_s', is to use relatively short source-detector separations (<10 mm).[12,13] Since the mean probing depth scales with the source-detecor separation, this makes such measurements sensitive

to superficial components (to depths of less than 5 mm for typical biological tissues).

Time– and frequency-domain techniques are well suited for deeper investigations (>1 cm for biological tissue). Moreover, they can be performed using only one or a few source-detector separations, which makes them more robust in studying heterogeneous samples. Because such techniques require sources that can be pulsed or modulated rapidly, covering a large wavelength range requires a tunable laser or an extensive collection of laser diodes, both of which can be expensive, difficult to maintain, and slow to cover the entire spectrum. This is an important drawback, since, as discussed by Hull *et al.*,[14] the quantification of chromophore concentrations can be significantly affected by using a limited number of wavelengths.

In this article, we suggest a way to use steady-state (SS) and frequency-domain (FD) reflectance measurements in tandem to obtain broad wavelength coverage with increased penetration depth. This method is especially promising for tissue near-infrared spectroscopy, such as breast physiology characterization. For such applications, the method proposed here enables rapid data acquisition, deep tissue probing, and robust resolution of the contributions from the four major NIR tissue absorbers: oxy– and deoxy-hemoglobin, water, and fat. The central innovations are a) using FD-derived μ_a and μ_s' values to convert the SS measurements into units of absolute reflectance, and b) using the power-law wavelength dependence of μ_s' to obtain interpolated and extrapolated values at non-laser wavelengths. FD measurements are performed at a handful of diode laser wavelengths spanning the range of interest (650–1000 nm), while the SS measurements are performed continuously

across the entire range. Unlike spatially-resolved SS, however, only a single, large source-detector separation is used, preferably the same one as for the FD measurements. The instrumentation is straightforward and particularly easy to add to an existing FD system.

After describing our method of combining the SS and FD methods ("SSFD"), we test the SSFD technique by using it to measure the absorption spectra of turbid samples. First, we analyze a liquid tissue phantom whose absorption spectrum is known (via direct spectrophotometry of its absorbing component prior to mixing) and to which the SSFD result can be compared. We also measure locations on the breast of two human female volunteers, demonstrating that data can be gathered *in vivo* and analyzed to provide pertinent physiological parameters. Differences among the measured breast spectra can be interpreted in terms of different relative levels of water, fat, and hemoglobin present in the explored tissue volumes. In addition, estimates of absolute concentrations are comparable to those reported in other recent broadband *in vivo* studies. Lastly, we discuss possible reasons for imperfect spectral fits, and we compare concentration predictions derived from SSFD analysis to those derived from FD data alone.

2 Experimental methods

2.1 Optical measurements

Figure 1 shows the experimental arrangement for SSFD measurements. In all cases, light is delivered via optical fiber to the surface of the sample and collected at some distance ρ

away. For the liquid phantom measurements, ρ was 15.5 mm; for the breast, 21.5 (FD) and 24 (SS) mm (the slight difference was due to instrumental limitations; a future instrument will utilize identical distances). In FD mode (upper box), the light arrives sequentially from one of seven amplitude-modulated diode lasers (672, 800, 806, 852, 896, 913, and 978 nm, all with output powers of < 20 mW at the sample) and is detected by an avalanche photodiode unit (Hamamatsu C556P-56045-03) that amplifies the AC component of the signal. A network analyzer (Hewlett Packard 8753C) delivers 251 modulation frequencies between 100 and 700 MHz and measures phase and modulation amplitude of the photon intensity signal, as described elsewhere.[7,16] In SS mode (lower box), light comes from a 150W halogen lamp (Fiber-Lite) and is analyzed via a fiber-coupled spectrograph (Ocean Optics S2000) with a linear CCD detector between 525 and 1155 nm, with the useful range for our experiments being 650–1000 nm. The spectrograph records a total of 2048 points (0.35 nm/pixel), and the spectral resolution is 5 nm (full width at half maximum). Light is delivered to the sample using a bundle of four fibers (bundle diameter 600 μm) and collected using a single fiber of diameter 1 mm. The spectrum of the light source is measured separately by inserting the source and detector fibers into different ports of an integrating sphere (Labsphere, IS-040-SF). Relative reflectance is calculated to be the sample spectrum divided by the source spectrum (note that both measurements use the same delivery fiber, collection fiber, and detector apparaturs). Total acquisition time per sample for SSFD measurements is on the order of 40 s (30 for FD and 10 for SS). Calculation of $\mu_a(\lambda)$ was performed according to the methods of the next section using in-house Matlab

(The MathWorks, Inc.) code, making use of the optimization toolbox.

2.2 Samples

The phantom contained 17 mg of green dye (naphthol) and 50 ml of an aqueous scattering suspension (Intralipid-20%, Pharmacia, Inc.) dissolved in 950 ml of water. Prior to the addition of Intralipid, the absorbance spectrum of the dye-water solution was measured in a 1 cm plastic cuvette via spectrophotometer (Beckman Instruments, DU630) with water as a reference. Optical measurements were performed as indicated in Figure 1, with source and detector fibers placed at the surface of the samples.

In vivo measurements were performed on the left breasts of two supine female volunteers, ages 37 and 21. Data were gathered from two regions on one volunteer (a region on the areolar border and a region of "inner breast", *i.e.* close to the middle of the chest) and one region on the other volunteer (inner breast only), resulting in three total samples. In this modality, the source light was again delivered by optical fiber but the FD detector was placed directly against the tissue, without a collection fiber. Fiber and detector were bundled into a single handheld device that was placed gently against the breast. SS reflectance was measured subsequently, at the exact same location, in the two-fiber mode described above. All procedures were approved by the Institutional Review Board of the University of California, Irvine (study 95-563).

3 Background Theory

3.1 Diffusion model

The measured reflectance signal R (see Figure 1) can be predicted theoretically using the diffusion approximation to the radiative transfer equation, as many groups have discussed.[7,17–21] In this theoretical framework, the reflectance is a function of the optical properties of the medium, defined by the absorption coefficient μ_a, reduced scattering coefficient μ_s', and index of refraction n. The diffusion approximation is valid for large source-detector separation r $[r > 10(\mu_a + \mu_s')^{-1}]$ and high (reduced) albedo $[\mu_s'/(\mu_a + \mu_s') > 0.95]$. The SS and FD cases can be described using a single formalism in which the solution for the reflectance is built from the Green's function for the diffusion equation, *i.e.* the fluence [W/cm^2] due to an isotropic point source in an infinite, homogeneous medium. This function takes the form $\exp(-kr)/(Dr)$, where $D \equiv [3(\mu_a + \mu_s')]^{-1}$, the complex wavenumber $k = k_{real} + ik_{imag}$, and

$$k_{real} = \left[\frac{3}{2}\mu_a(\mu_a + \mu_s')\right]^{1/2}\left\{\left[1 + \left(\frac{\omega}{\mu_a c}\right)^2\right]^{1/2} + 1\right\}^{1/2}$$

$$k_{imag} = \left[\frac{3}{2}\mu_a(\mu_a + \mu_s')\right]^{1/2}\left\{\left[1 + \left(\frac{\omega}{\mu_a c}\right)^2\right]^{1/2} - 1\right\}^{1/2},$$

with ω being the modulation frequency in radians/sec. The steady-state solution is simply the limit when ω=0. In this case, the solution for R is a real number ($k_{real} = \sqrt{3\mu_a(\mu_a + \mu_s')}$ and $k_{imag} = 0$). When $\omega > 0$, R becomes a complex number $A\exp(-i\phi)$, where A is the

modulation amplitude and ϕ is the phase shift relative to the source. As explained in next section, these quantities can be obtained from the FD measurement.

In treating reflectance problems, the sample/air interface is modeled using an extrapolated boundary condition,[21] in which the fluence is set to zero at a distance $z_b = 2D(1 + R_{\text{eff}})/(1 - R_{\text{eff}})$ above the sample (R_{eff} depends upon the refractive mismatch and equals 0.493 for tissue of $n = 1.4$ and air of $n = 1.0$). The method of images is employed, with an isotropic point source at a depth $z_o = (\mu_a + \mu_s')^{-1}$ contributing a signal S_r, and a negative image point at a height $z_o + z_b$ above the extrapolated boundary contributing S_i. This gives the fluence Φ at any point in the sample. The detected signal along the boundary is then written as a combination of terms proportional to the fluence and to its flux normal to the surface:

$$R = c_1\Phi - c_2 D\nabla\Phi \cdot (-\hat{z}), \tag{1}$$

where values for the constants c_1 and c_2 are determined by the refractive index mismatch between the two media[21] (for tissue of $n = 1.40$ and air of $n = 1$, these constants assume the values of 0.118 and 0.306, respectively), $-\hat{z}$ is a unit vector pointing normally upwards out of the sample, and

$$\begin{aligned} \Phi &= \frac{P}{4\pi D}\left[\frac{\exp(-kr_s)}{r_s} - \frac{\exp(-kr_i)}{r_i}\right] \\ D\nabla\Phi\cdot\hat{z} &= \frac{P}{4\pi}\left[z_o\left(k+\frac{1}{r_s}\right)\frac{\exp(-kr_s)}{r_s^2} + (z_o+2z_b)\left(k+\frac{1}{r_i}\right)\frac{\exp(-kr_i)}{r_i^2}\right], \end{aligned} \tag{2}$$

where P is the incident power and r_s (r_i) is the distance from the source (image) to the

detector.

3.2 Frequency domain fitting

Like the theory of the previous section, our frequency-domain fitting process, which provides μ_a and μ_s' values at a few wavelengths, has been described at length elsewhere,[7,16] and is provided here as background.

Each FD measurement contains instrumental artifacts; *i.e.*, the measured reflectance is actually

$$R = C_o A \exp\left[-i(\phi + \phi_o)\right], \tag{3}$$

where C_o and ϕ_o are sample-independent instrumental constants. A and ϕ are respectively the modulation amplitude and phase of the frequency-domain reflectance, as defined in the previous section.

For calibration, we gather FD data from a prepared sample whose μ_a and μ_s' values are known *a priori* from a set of two-distance frequency-domain measurements.[7] Frequency-dependent values of ϕ_o and C_o are calculated from the discrepancies between measured (Eq. 3) and predicted (Eq. 1) phase and modulation amplitude, thus calibrating our future measurements.

With the instrumental constants thus determined, the 502 data points per sample (251 each for both phase and amplitude vs. ω) depend upon two unknowns: μ_a and μ_s'. We select the best μ_a and μ_s' values to fit the predictions of Eq. 1 to the data using the iterative, nonlinear, least-squares method of Levenberg and Marquardt,[22] alternating between fitting

the phase and the amplitude until overall convergence is achieved.[7] As noted by various authors,[2,21] the reflectance in Eq. 1 is very nearly proportional to either the flux or the fluence term alone (*i.e.*, the ratio of the two is independent of μ_a and μ_s') for the large source-detector separations that we employ ($> 10\,(\mu_a + \mu_s')^{-1}$). We therefore use only the fluence term Φ from Eq. 1, absorbing the additional proportionality factor into the instrumental contstant C_o.

4 Determination of broadband μ_a spectrum

The previous section provided background information regarding diffusion theory models and a method for extracting μ_a and μ_s' values from FD measurements at specific wavelengths. We now describe how FD and SS measurements can be combined to obtain quantitative, broadband μ_a spectra.

Our goal is to compute μ_a at each wavelength, given the measured SS reflectance. However, single-distance SS reflectance cannot itself provide μ_a: R depends upon μ_s' as well as μ_a, so one measurement cannot provide a unique determination of either parameter. In addition, the instrumental constant C_o is not known. The single SS measurement at each wavelength therefore needs to be supplemented with:

1. A means of establishing the absolute reflectance intensity.

2. An additional piece of information about μ_a or μ_s' (or a combination of the two).

4.1 Use of FD data to provide additional information

The FD system can provide both pieces of necessary information at each SS wavelength. At first glance this is surprising, as the FD system operates at only seven wavelengths, while the SS system covers 450 nm with continuous 5 nm resolution. It would seem then that the needed values of μ_s' and C_o could be determined only at these seven wavelengths, and strictly speaking this is indeed the case. Significantly, however, the wavelength dependence of both μ_s' and C_o are smooth and predictable in shape, as will be discussed below. It is this fact that enables us to use the discrete FD information to supplement our broadband SS measurements at *all* desired wavelengths.

Amplitude calibration of reflectance spectrum The FD measurements enable calculation of the instrumental factor C_o at all wavelengths because we expect no wavelength dependence at all: the sample and source spectra are measured using the same delivery and collection system and only a few seconds apart, so there should be negligible wavelength-dependent artifacts in the ratio of the two. As such, the task reduces to that of calculating C_o at a single wavelength. This is readily done at any of the FD wavelengths, as μ_a and μ_s' are both known, and absolute reflectance is a function of only these variables (cf. Eqs. 1 and 2 in the $\omega = 0$ limit). Using all of the FD data to increase robustness, we can calculate the value of C_o that scales the measured SS reflectances to match the predicted reflectances as closely as possible (in the least-squares sense). Once this is done, the scale factor C_o is known for the entire spectrum. Examples of this scaling will be shown below.

Determination of $\mu_s'(\lambda)$ The FD values of μ_s' also allow us to obtain information about μ_s' across the entire wavelength range. As numerous groups have observed,[23–25] the particle size distribution of scatterers (0.1–10μm) in many biological media and phantoms tends to have smooth wavelength dependence over the range 650-1000 nm, well-described by a power function of the form

$$\mu_s'(\lambda) = A\lambda^{-B} \tag{4}$$

(the parameter A here having no relation to the modulation amplitude). As a result, measuring several μ_s' values allows us to fit them to a simple function of wavelength and obtain good estimates of μ_s' at all other wavelengths needed.

Iterative solving for $\mu_a(\lambda)$ spectrum With $\mu_s'(\lambda)$ calculated and the reflectance correctly scaled, the equation for steady-state reflectance (Eq. 1) contains only one unknown, μ_a. Because it is difficult to obtain an analytical solution for μ_a from this equation, numerical solving methods were employed. Proceeding one wavelength at a time, we used the MATLAB nonlinear zero-finding function `fzero` to choose μ_a such that $R_{meas} - R_{thy}(\mu_a) = 0$, where R_{meas} is the calibrated SS reflectance measurement and $R_{thy}(\mu_a)$ is the theoretical reflectance predicted by Eqs. 1 and 2 for a given trial value of μ_a. Solving for for the entire μ_a spectrum required about 10 seconds on a personal computer.

5 Results

Figure 2 displays the SS reflectance measured from the phantom and the predicted absolute reflectance calculated from diffusion theory based upon the FD measurements of μ_a and μ_s'. Because of strong absorption at wavelengths above 950 nm, the FD measurement at 978 nm was very noisy at short integration times, which in turn made calculation of SS data at wavelengths above 950 unstable. Data are therefore presented between 650–950 nm, for the phantom only. As anticipated, all of the measurements differ from the predictions by essentially the same scale factor. The entire SS spectrum is thus converted to absolute reflectance units. Similar results were observed for the three breast samples, as shown in Figure 3. In the order presented, sample 1 is the inner breast region of the 37-year-old volunteer, and samples 2 and 3 are respectively from the areolar border and inner breast of the 21-year-old volunteer.

Figure 4 shows the least-squares power-law fit to the μ_s' values measured by FD on the phantom. As expected, the wavelength dependence is fairly smooth and easily described by the fit. Corresponding fits for the three breast samples appear in Figure 5. Note that the values only change by a factor of 2 over the entire range, so the wavelength dependence is weak in addition to being predictable.

Figure 6 summarizes the absorption values calculated for the dye-Intralipid phantom. The thick line shows the μ_a values that were found to make Eq. 1 reproduce the measured reflectance data as closely as possible, using the `fzero` algorithm as previously described. The thin line represents a linear least-squares fit to the thick line based upon reference

spectra of pure water (from Kou *et al.*[26]) and pure dye (measured by spectrophotometer as described above). As the figure shows, the two-component fit accurately models the measured spectrum across the entire spectral range. The least-squares fitting coefficient for the dye spectrum is 1.00. Also shown are the values of μ_a derived by FD analysis alone, demonstrating an agreement between the FD and SSFD methods at these wavelengths, as would be expected because the FD data have been used to calibrate the SS data.

Corresponding plots showing absorption spectra of the three breast samples appear in Figures 7 through 9. As before, the thick line is the experimental data, the thin line is a full-spectrum fit, and the circles are FD values. In these cases, however, the fit is built from published spectra (see Figure 10) of oxy– and deoxy-hemoglobin,[27] water,[26] and fat,[28] which are commonly regarded as the four major absorbers in breast tissue in the 650–1000 nm regime. Coefficients from the fit thus provide estimates of these components' concentrations. The estimates are useful for comparing one sample to another; no attempt at independent concentration validation has been performed (however, they are approximately correct in magnitude and, as noted in the next section, the values are consistent with others from the recent literature[3,15]). For comparison purposes, the additional dotted line shows the spectral fit obtained when only the FD wavelengths are weighted, as in a customary FD-only experiment. The two spectral reconstructions are clearly different, which leads to different concentration estimates. All of the concentration predictions, both SSFD and FD, are listed in Table 1, along with a final column indicating the percent deviation of the FD value from the SSFD value. The hemoglobin results are reported in terms of total

hemoglobin (oxy plus deoxy) and oxygen saturation (oxy divided by total).

6 Discussion

In order to extract μ_a from a single SS reflectance spectrum, one has to convert the data into absolute units (*i.e.*, the instrumental factor C_o must be removed) and determine μ_s' values at all wavelengths. We have demonstrated that FD measurements at a few wavelengths can accomplish these goals across the entire 650–1000 nm spectrum. This somewhat surprising result arises because $\mu_s'(\lambda)$ follows a power law, while C_o has no wavelength dependence at all. Two innovations that combine FD and SS methods are thus available. First, by scaling SS reflectance to match FD predictions of absolute reflectance, the entire reflectance spectrum is automatically calibrated. Secondly, by fitting the FD μ_s' values to a wavelength-dependent function, the extra information needed to extract μ_a from diffusion theory (Eqs. 1 and 2) is obtained. We note that the FD-derived μ_a and μ_s' values could just as readily be supplied by time-domain measurements at a single source-detector separation.

The interpolation of the reduced scattering spectra by using a fit is an important point of this technique. The lower two plots in Figure 5 show excellent agreement with the power law. The top plot shows reasonably good agreement, but small discrepancies can nevertheless be observed (on the order of 5-8%). This behavior is likely not to be an actual divergence from the power law, but is probably due to a coupling effect between the scattering and absorption quantification in the FD fit. Such a coupling appears when the diffusion model's assumptions are not sufficiently fulfilled. The tissue heterogeneity, *i.e.* the

layered superficial structure and the mix of deeper fat lobules and fibrous tissue, could be a possible source of deviation from the model. Interestingly, the highest fat concentration was measured for this breast location (cf. Table 1). As described recently by Doornbos *et al.*,[15] using a power law fit to calculate the μ_s' spectrum can in fact provide an advantage in computing μ_a. Indeed, by smoothing the spectrum, it reduces the spurious coupling between scattering and absorption caused by inaccurate modeling.

When compared to discrete-wavelength FD measurements, the access to a continuous absorption spectrum offers two important advantages: better chromophore identification and improved concentration quantification. The ability of the method to recover the continuous shape of the true absorption spectrum is evidenced by the phantom measurement. Figure 6 shows that the experimental spectrum is accurately fitted using known spectra of dye and water. The fitting coefficient of 1.00 for the dye additionally demonstrates the accurate recovery of chromophore concentrations.

The breast spectra (Figures 7 through 9) further illustrate the usefulness of the SSFD technique for clinical investigations. As expected, the fit using oxy–and deoxy-hemoglobin, fat, and water accounts for most of the absorption in the 650-1000 nm in breast tissues. The quality of the fit is especially striking for wavelengths longer than 800 nm. In particular, the fat spectrum used in the fit seems accurate, matching the main peak at 928 nm and the shoulder at 895 nm. These results are surprisingly good considering that the pure fat spectrum was measured on soybean oil.[28] These measurements stress the important contribution of fat to tissue absorption, as this chromophore has been sometimes neglected

in previous work.[6,15] The water peak at 976 nm is also well reproduced in the measurements. We observe that the highest water content was measured for the areolar border sample (sample #2). Interestingly, we note that for both dye and breast tissue, data fits to the water spectrum of Kou *et al.* are superior to Hale and Querry,[29] particularly in the 920–960 nm regime where their water absorption spectrum increases sharply.

In the 650-800 nm region, the major features of tissue absorption are clearly due to oxy– and deoxy-hemoglobin. The deoxy-hemoglobin peak at 760 nm is distinctly visible in the experimental data. Nevertheless, we observe small but consistent spectral differences on the order of 0.001 mm^{-1} between the fit and measurement in this regime (see Figures 7 through 9). These discrepancies, revealed in the full SSFD spectrum, are not evident when fitting the FD data alone. Two reasons for the imperfect fits can be suggested. First, the oxy-and deoxy-hemoglobin absorption spectra we used could be slightly incorrect. Indeed, small variations are found between various published spectra, and changes could be also expected between *in vitro* and *in vivo* values. Second, other "background" chromophores should probably be taken into account. For example, the tails of several protein absorption bands, not included in the modeling, might contribute in this wavelength region. A more extensive spectral library is therefore desirable for future studies. Alternatively, one could model the background empirically, either with predetermined mathematical functions of wavelength (*e.g.* Hull *et al.*[14]) or via a principal-component analysis of several background residuals once many samples have been studied.[30]

For the sake of comparison, we used the same least-square fitting algorithm to calculate

the spectral fits and concentrations twice, once using the full spectrum and once using only the FD wavelengths, even though this second procedure does not fully exploit the potential of the SSFD method. Interesting differences are found between the FD and SSFD calculations. Figure 7 and Table 1 show that FD significantly underestimates the fat concentration in the first breast sample: 0.75 g/cm^3 using SSFD versus 0.44 g/cm^3 using FD. The reason for this discrepancy lies in the fact that no laser wavelength is close enough to the fat peak (at present, commercial laser diodes at this particular wavelength are uncommon). Thus, with no weighting in this region, the FD fit tolerates large fitting errors near the absorption maximum of fat (as seen in Figure 7), leading to large errors in the fat concentration. Such a discrepancy is naturally enhanced for this sample, where the fat concentration is highest. This example illustrates the shortcomings of using a limited number of sources (*i.e.* wavelengths), especially when a significant chromophore lies in an undersampled specral region. A similar error is seen in the fitting of the areolar breast location (Figure 8), where this time it is the water peak that is poorly addressed by the FD analysis.

The total hemoglobin determination is more consistent between the FD and SSFD calculations, due to the smoother spectral features of these chromophores and better diode coverage of the 650–850 nm regime. However, the oxygenation determination by FD is systematically higher. As discussed before, consistent small differences occur between the fit and the experiments in the 650-800 nm region due to some incompleteness in our library of fitting lineshapes. Fitting the curve with a limited number of wavelengths naturally

exacerbates the incompleteness and produces a bias in the results.

As mentioned above, Cubeddu *et al.*[3] obtained similar optical properties and physiological parameters for premenopausal breast, working in the time domain. Conceptually, the two experiments exploit the same optical phenomena and are essentially complementary techniques in different domains. A technical advantage of the SSFD measurement is the use of a white light source rather than a tunable laser. As such, the SS measurement covers all wavelengths simultaneously, whereas the laser(s) must be tuned separately to each wavelength.[3] Additionally, the heart of the SSFD system (a few laser diodes, a frequency generator, an avalanche photodiode, a network analyzer or lock-in amplifier, and a SS reflectance system) is inexpensive and easy to maintain compared to a tunable laser system and a single-photon-counting detection apparatus.

As already stated, the method presented here has the advantage of being compatible with a single, large source-detector separation ($\gg$10 transport mean free paths). In contrast to spatially-resolved methods, it is well suited for interrogating deep strucures in relatively heterogeneous samples. As numerous groups have shown[15,31,32] the layered structure of tissue affects reflectance differently at different source-detector separations, raising doubts about the applicability of spatially-resolved techniques that assume sample homogeneity over a large range. While variations in the FD modulation frequency ω do change the optically-explored tissue volume, these effects are modest in comparison to changes in ρ, particularly at high absorption.[21] Consequently, the assumption of homogeneity is less extreme for the single-distance measurements proposed here. The essence is that all mea-

surements at one wavelength explore a more consistent volume; this does not mean that different wavelengths will explore the same volume. Indeed, less-absorbed wavelengths will explore larger regions than wavelengths that attentuate more rapidly.

7 Conclusion

A combination of SS and FD reflectance measurements has been described for absorption spectroscopy of turbid media, featuring beneficial aspects of both techniques. As with SS, the wavelength coverage is continuous, detecting absorption features that may elude the discrete wavelengths chosen for FD. The prediction of constituent concentrations, for instance in breast tissue, is substantially improved using full-spectrum absorption data rather than a handful of wavelengths. As with FD, however, only a single source-detector separation is required, making the technique more amenable to reporting volume-averaged values for heterogeneous samples. In addition, the source-detector separation can be large, allowing for centimeter-scale mean probing depths that cannot be achieved with spatially-resolved SS techniques. This advantage for deeply-probing studies is significant for many clinical purposes. An application to breast analysis has been demonstrated, with quantitative *in vivo* spectra of human breast obtained rapidly (<1 min.). The total hemoglobin content, oxygen saturation, water, and fat content of the breast samples have been calculated from the spectra, and failures of FD-only fitting have been highlighted. The technique is relatively inexpensive and could prove valuable for improving accuracy in the development of quantitative photon migration for clinical instruments.

8 Acknowledgments

This work was supported by the National Institutes of Health (NIH) under grant Nos. GM50958 and RR01192 (Laser Microbeam and Medical Program: LAMMP), the Department of Energy (DOE No. DE-FG03-91ER61227), and the Office of Naval Research (ONR No. N00014-91-C-0134). The authors gratefully acknowledge postdoctoral fellowships from the George E. Hewitt Foundation for Medical Research (AJB), the Swiss National Science Foundation (FB), and US Army grant DAMD17-98-1-8186 (AEC). Facilities and support of the Avon breast center in the Chao Family Comprehensive Cancer Center at UC Irvine were utilized to complete clinical portions of this study.

References

[1] M. S. Patterson, B. Chance, and B. C. Wilson, "Time resolved reflectance and transmittance for the noninvasive measurement of tissue optical properties," Appl. Opt. **28,** 2331–2336 (1989).

[2] A. Kienle and M. S. Patterson, "Improved solutions of the steady-state and the time-resolved diffusion equations for reflectance from a seni-infinite medium," J. Opt. Soc. Am. **14,** 246–254 (1997).

[3] R. Cubeddu, A. Pifferi, P. Taroni, A. Torricelli, and G. Valentini, "Noninvasive absorption and scattering spectroscopy of bulk diffusive media: An application to the optical characterization of human breast," Apl. Phys. Lett. **74,** 874–876 (1999).

[4] B. W. Pogue and M. S. Patterson, "Frequency-domain optical absorption spectroscopy of finite tissue volumes using diffusion theory," Phys. Med. Biol. **39,** 1157–1180 (1994).

[5] S. Fantini, M. A. Franceschini-Fantini, J. S. Maier, S. A. Walker, B. Barbieri, and E. Gratton, "Frequency-domain multichannel optical detector for noninvasive tissue spectroscopy and oximetry," Opt. Eng. **34,** 32–42 (1995).

[6] J. B. Fishkin, O. Coquoz, E. R. Anderson, M. Brenner, and B. J. Tromberg, "Frequncy-domain photon migration measurements of normal and malignant tissue optical properties in a human subject," Appl. Opt. **36,** 10–20 (1997).

[7] T. H. Pham, O. Coquoz, J. B. Fishkin, E. Anderson, and B. J. Tromberg, "Broad bandwidth frequency domain instrument for quantitative tissue optical spectroscopy," Rev. Sci. Inst. **71,** 2500–2513 (2000).

[8] L. Reynolds, C. Johnson, and A. Ishimaru, "Diffuse reflectance from a finite blood medium: applications to the modeling of fiber optic catheters," Appl. Opt. **15,** 2059–2067 (1976).

[9] T. J. Farrell, M. S. Patterson, and B. C. Wilson, "A diffusion theory model of spatially-resolved, steady-state diffuse reflectance for the noninvasive determination of tissue optical properties *in vivo*," Med. Phys. **19,** 879–888 (1992).

[10] A. Kienle, L. Lilge, M. S. Patterson, R. Hibst, R. Steiner, and B. C. Wilson, "Spatially resolved absolute diffuse reflectance measurements for noninvasive determination of the optical scattering and absorption coefficients of biological tissue," Appl. Opt. **35,** 2304–2314 (1996).

[11] R. Bays, G. Wagnières, D. Robert, D. Braichotte, J.-F. Savary, P. Monnier, and H. van den Bergh, "Clinical determination of tissue optical properties by endoscopic spatially resolved reflectometry," Appl. Opt. **35,** 1756–1766 (1996).

[12] R.A.Weersink, J. Hayward, K. Diamond, and M. Patterson, "Accuracy of noninvasive in vivo measurements of photosensitizer uptake based on a diffusion model of reflectance spectroscopy," Photochem. Photobiol. **66,** 326–335 (1997).

[13] F. Bevilacqua, D. Piguet, P. Marquet, J. Gross, B. Tromberg, and C. Depeursinge, "In vivo local determination of tissue optical properties: applications to human brain," Appl. Opt. **38,** 4939–4950 (1999).

[14] E. L. Hull, M. G. Nichols, and T. H. Foster, "Quantitative broadband near-infrared spectroscopy of tissue-simulating phantoms containing erythrocytes," Phys. Med. Biol. **43,** 3381–3404 (1998).

[15] R. M. P. Doornbos, R. Lang, M. C. Aalders, F. W. Cross, and H. J. C. M. Sterenborg, "The determination of *in vivo* human tissue optical properties and absolute chromophore concentrations using spatially resolved steady-state diffuse reflectance spectroscopy," Phys. Med. Biol. **44,** 967–981 (1999).

[16] B. J. Tromberg, O. Coquoz, J. B. Fishkin, T. Pham, E. R. Anderson, J. Butler, M. Cahn, J. D. Gross, V. Venugopalan, and D. Pham, "Non-invasive measurements of breast tissue optical properties using frequency-domain photon migration," Phil. Trans. R. Soc. Lond. **352,** 661–668 (1997).

[17] A. Ishimaru, *Wave Propagation and Scattering in Random Media* (Academic Press, 1978).

[18] J. B. Fishkin and E. Gratton, "Propagation of photon-density waves in strongly scattering media containing an absorbing semi-infinite plane bounded by a straight edge," J. Opt. Soc. Am. **10,** 127–140 (1993).

[19] B. J. Tromberg, L. O. Svaasand, T.-T. Tsay, and R. C. Haskell, "Properties of Photon Density Waves in Multiple-Scattering Media," Appl. Opt. **32,** 607–616 (1993).

[20] S. Fantini, M. A. Franceschini, J. B. Fishkin, B. Barbieri, and E. Gratton, "Quantitative determination of the absorption spectra of chromophores in strongly scattering media: a light-emitting-diode based technique," Appl. Opt. **33,** 5204–5213 (1994).

[21] R. C. Haskell, L. O. Svaasand, T.-T. Tsay, T.-C. Feng, M. S. McAdams, and B. J. Tromberg, "Boundary conditions for the diffusion equation in radiative transfer," J. Opt. Soc. Am. **11,** 2727–2741 (1994).

[22] W. H. Press, S. A. Teukolsky, W. T. Vetterling, and B. P. Flannery, in *Numerical Recipes in C: The Art of Scientific Computing*, 2nd ed. (Cambridge University Press, 1993), Chap. 15, pp. 683–688.

[23] R. Graaff, J. G. Aarnoose, J. R. Zijp, P. M. A. Sloot, F. F. M. de Mul, J. Greve, and M. H. Koelink, "Reduced light-scattering properties for mixtures of spherical particles: a simple approximation derived from Mie calculations," Appl. Opt. **31,** 1370–1376 (1992).

[24] J. R. Mourant, T. Fuselier, J. Boyer, T. Johnson, and I. J. Bigio, "Predictions and measurements of scattering and absorption over broad wavelength ranges in tissue phantoms," Appl. Opt. **36,** 949–957 (1997).

[25] J. M. Schmitt and G. Kumar, "Optical scattering properties of soft tissue: a discrete particle model," Appl. Opt. **37,** 2788–2797 (1998).

[26] L. H. Kou, D. Labric, and P. Chylek, "Refractive indexes of water and ice in the 0.65 μm to 2.5 μm spectral range," Appl. Opt. **32,** 3531–3540 (1993).

[27] S. Wray, M. Cope, D. T. Delpy, J. S. Wyatt, and E. O. R. Reynolds, "Characterization of the near-infrared absorption spectra of cytochrome-AA3 and hemoglobin for the non-invasive monitoring of cerebral oxygenation," Biochim. et Biophys. Acta **933,** 184–192 (1988).

[28] C. Eker, Ph.D. thesis, Lund University, 1999, *Optical characterization of tissue for medical diagnostics.*

[29] G. M. Hale and M. R. Querry, "Optical Constants of Water in the 200-nm to 200-μm wavelength region," Appl. Opt. **12,** 555–63 (1973).

[30] A. J. Berger, T.-W. Koo, I. Itzkan, and M. S. Feld, "An Enhanced Algorithm for Linear Multivariate Calibration," Anal. Chem. **70,** 623–628 (1998).

[31] G. Alexandrakis, T. J. Farrell, and M. S. Patterson, "Accuracy of the diffusion approximation in determining the optical properties of a two-layer turbid medium," Appl. Opt. **37,** 7401–7409 (1998).

[32] M. A. Franceschini, S. Fantini, L. A. Paunescu, J. S. Maier, and E. Gratton, "Influence of a superficial layer in the quantitative spectroscopic study of strongly scattering media," Appl. Opt. **37,** 7447–7458 (1998).

List of Figures

1 Configuration of light sources, optical fibers, and detectors. Key: APD, avalanche photodiode. The two dotted rectangles denote components belonging to the FD and SS systems, respectively. 31

2 SS reflectance spectrum acquired from dye-Intralipid phantom, scaled to fit the discrete reflectance values (circles) predicted by Eqs. 1 and 2 using FD-derived values of μ_s' and μ_a. This scaling causes the entire spectrum to be converted into absolute reflectance units; see text for discussion. Error in FD reflectance is estimated at $\pm 3 \times 10^{-7}$/mm; in SS reflectance, $\pm 1 \times 10^{-7}$/mm. 32

3 SS reflectance spectra acquired from three locations on breast tissue of female volunteers. The spectra have been scaled to fit reflectance values (circles) calculated from FD data in the same manner as Figure 2. Errors are same as previous figure. 33

4 Determination of broadband μ_s' spectrum for the dye-Intralipid phantom. Circles are the discrete μ_s' values measured by the FD technique, while the solid line is the best power-law fit to Eq. 4. Fitting parameters: A = 2200, B = -0.82. Error bars on μ_s' are 3%.[7] 34

5 Determination of broadband μ_s' spectra for the three breast samples. Circles are the discrete μ_s' values measured by the FD technique, while the solid lines are the best power-law fit to Eq. 4. Fitting parameters (A,B) are (240,-0.86), (2700,-12), and (250,-0.85), respectively. Error bars on μ_s' are 3%.[7] 35

6 Comparison of μ_a values generated by FD (dots) and by SSFD (thick line) for the dye-Intralipid phantom. Also shown is the best fit (thin line) to the SSFD data using spectra of naphthol (measured on a spectrophotometer) and water (from Kou *et al.*[26]). Circles are the discrete μ_a values from FD alone. Error bars are ± 0.0005 mm^{-1} or 5%, whichever is larger. 36

7 μ_a predictions for the first breast measurement (inner breast, 37-year-old volunteer). The thick line is the SSFD data; the thin line is the least-squares fit using a superposition of Hb, HbO_2, water, and fat spectra; the circles are the FD values (error bars are ± 0.0005 mm^{-1} or 5%, whichever is larger); the dotted line is the least-squares fit when only the FD values are weighted. Physiological parameters from SSFD spectral fit: total hemoglobin concentration, 22 μM; oxygen saturation, 73%; water, 15 g/cm^3; and fat, 0.75 g/cm^3. See Table 1 for more details. Note that the fat peak between 900 and 950 nm is significantly underfit by the FD calculation. 37

8 μ_a predictions for the second breast measurement (areolar border, 21-year-old volunteer). Lines and circles have the same assignments as described in Figure 7. Physiological parameters: total hemoglobin concentration, 30 μM; oxygen saturation, 70%; water, 0.51 g/cm^3; and fat, 0.42 g/cm^3. See Table 1 for more details. 38

9 μ_a predictions for the third breast measurement (inner breast, 21-year-old volunteer). Lines and circles have the same assignments as described in Figure 7. Physiological parameters: total hemoglobin concentration, 19 μM; oxygen saturation, 72%; water, 28 g/cm^3; and fat, 0.56 g/cm^3. See Table 1 for more details. 39

10 Absorption spectra of major absorbers in breast tissue. Upper left: oxyhemoglobin, 1 μM; upper right, deoxyhemoglobin, 1 μM; lower left, water, 1 g/cm^3; lower right, fat (soybean oil), 0.9 g/cm^3. The hemoglobin spectra are from Wray *et al.*,[27] the water is from Kou *et al.*,[26] and the fat is from the doctoral thesis of Eker.[28] 40

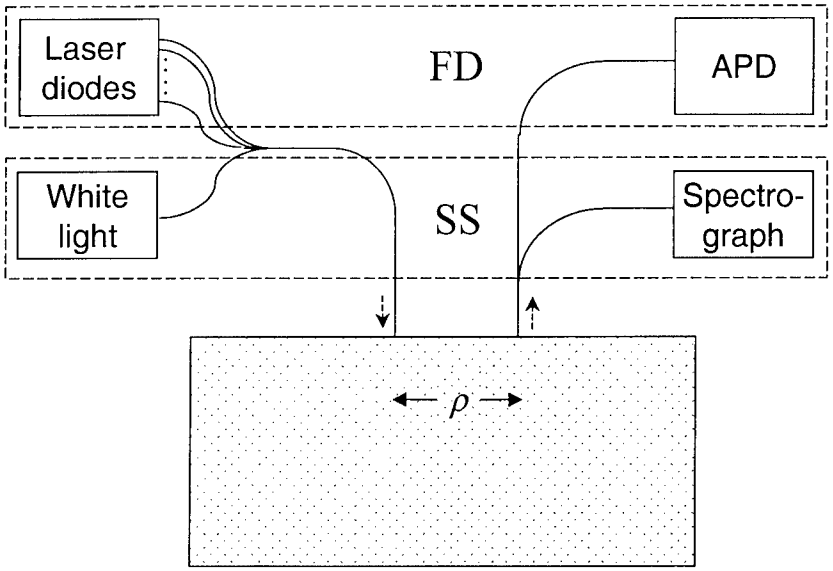

Figure 1: Configuration of light sources, optical fibers, and detectors. Key: APD, avalanche photodiode. The two dotted rectangles denote components belonging to the FD and SS systems, respectively.

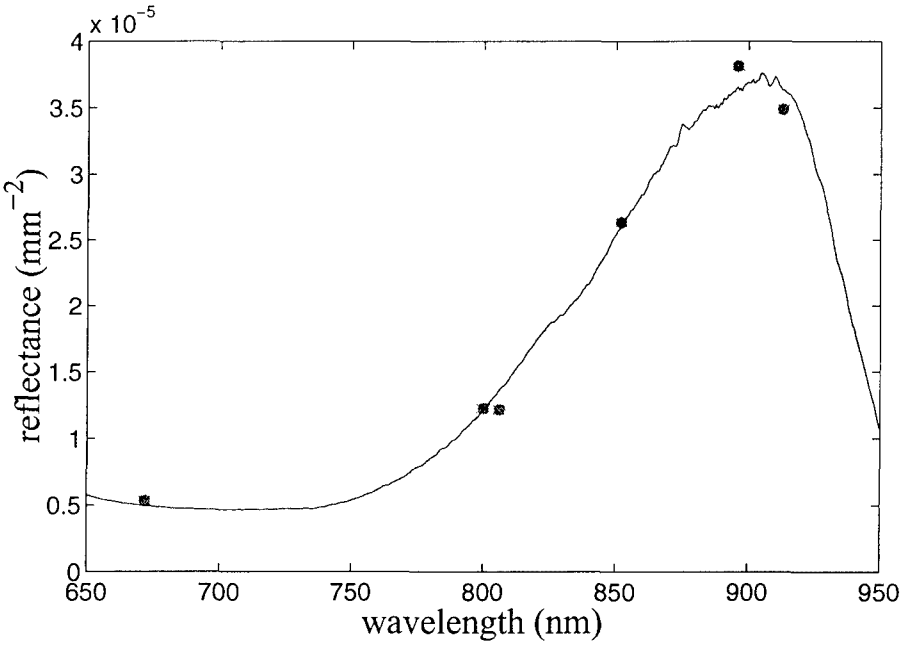

Figure 2: SS reflectance spectrum acquired from dye-Intralipid phantom, scaled to fit the discrete reflectance values (circles) predicted by Eqs. 1 and 2 using FD-derived values of μ_s' and μ_a. This scaling causes the entire spectrum to be converted into absolute reflectance units; see text for discussion. Error in FD reflectance is estimated at $\pm 3 \times 10^{-7}$/mm; in SS reflectance, $\pm 1 \times 10^{-7}$/mm.

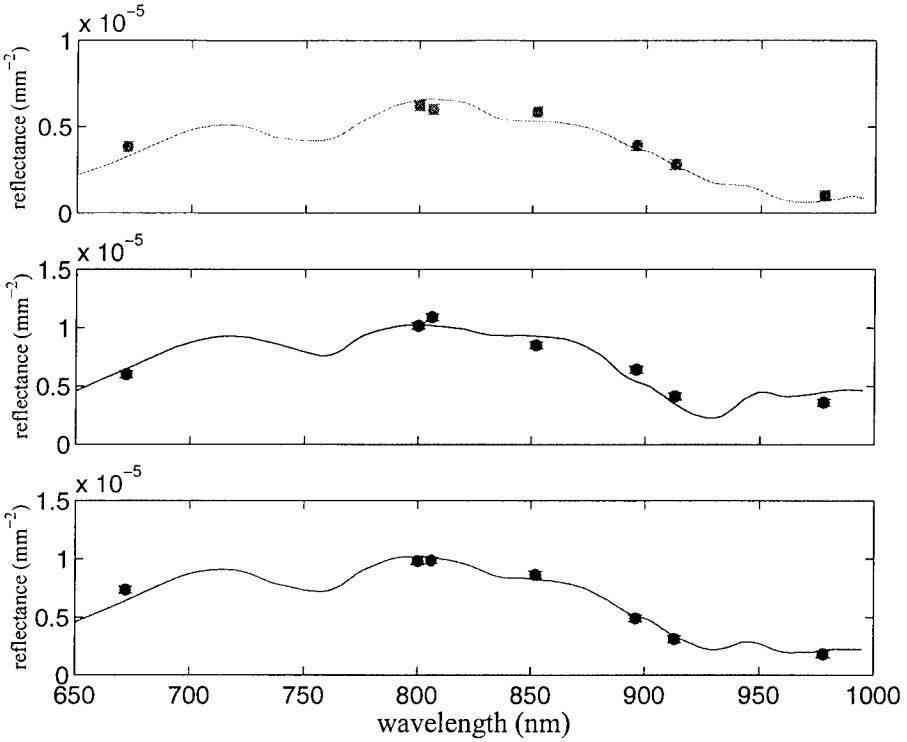

Figure 3: SS reflectance spectra acquired from three locations on breast tissue of female volunteers. The spectra have been scaled to fit reflectance values (circles) calculated from FD data in the same manner as Figure 2. Errors are same as previous figure.

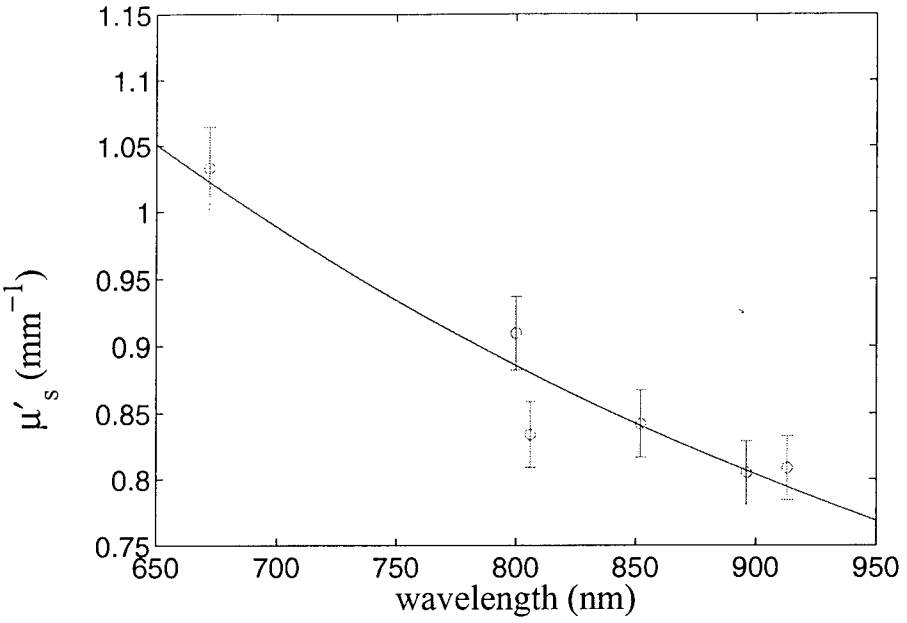

Figure 4: Determination of broadband μ_s' spectrum for the dye-Intralipid phantom. Circles are the discrete μ_s' values measured by the FD technique, while the solid line is the best power-law fit to Eq. 4. Fitting parameters: A = 2200, B = -0.82. Error bars on μ_s' are 3%.[7]

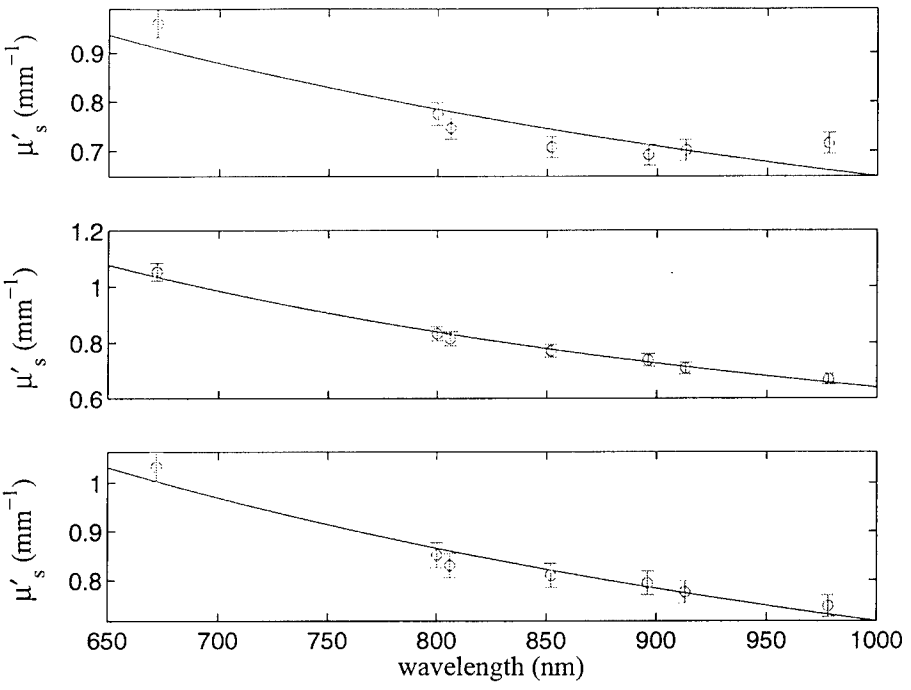

Figure 5: Determination of broadband μ_s' spectra for the three breast samples. Circles are the discrete μ_s' values measured by the FD technique, while the solid lines are the best power-law fit to Eq. 4. Fitting parameters (A,B) are (240,-0.86), (2700,-12), and (250,-0.85), respectively. Error bars on μ_s' are 3%.[7]

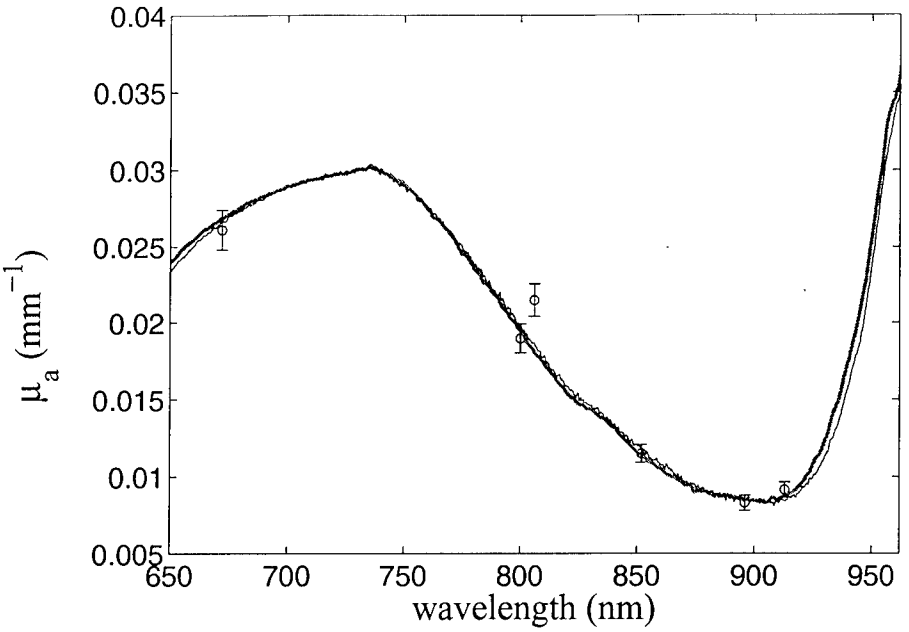

Figure 6: Comparison of μ_a values generated by FD (dots) and by SSFD (thick line) for the dye-Intralipid phantom. Also shown is the best fit (thin line) to the SSFD data using spectra of naphthol (measured on a spectrophotometer) and water (from Kou *et al.*[26]). Circles are the discrete μ_a values from FD alone. Error bars are ± 0.0005 mm^{-1} or 5%, whichever is larger.

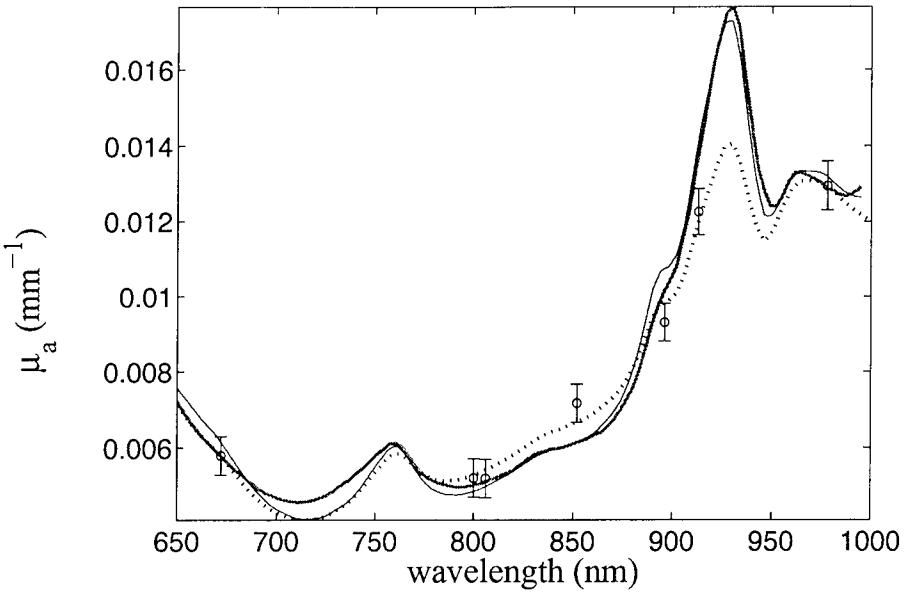

Figure 7: μ_a predictions for the first breast measurement (inner breast, 37-year-old volunteer). The thick line is the SSFD data; the thin line is the least-squares fit using a superposition of Hb, HbO_2, water, and fat spectra; the circles are the FD values (error bars are ± 0.0005 mm^{-1} or 5%, whichever is larger); the dotted line is the least-squares fit when only the FD values are weighted. Physiological parameters from SSFD spectral fit: total hemoglobin concentration, 22 μM; oxygen saturation, 73%; water, 15 g/cm^3; and fat, 0.75 g/cm^3. See Table 1 for more details. Note that the fat peak between 900 and 950 nm is significantly underfit by the FD calculation.

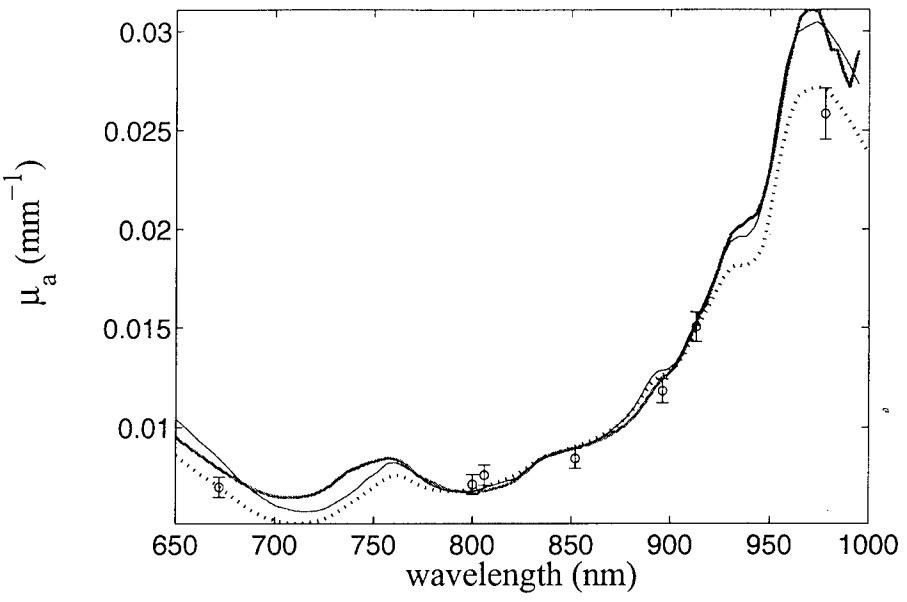

Figure 8: μ_a predictions for the second breast measurement (areolar border, 21-year-old volunteer). Lines and circles have the same assignments as described in Figure 7. Physiological parameters: total hemoglobin concentration, 30 μM; oxygen saturation, 70%; water, 0.51 g/cm^3; and fat, 0.42 g/cm^3. See Table 1 for more details.

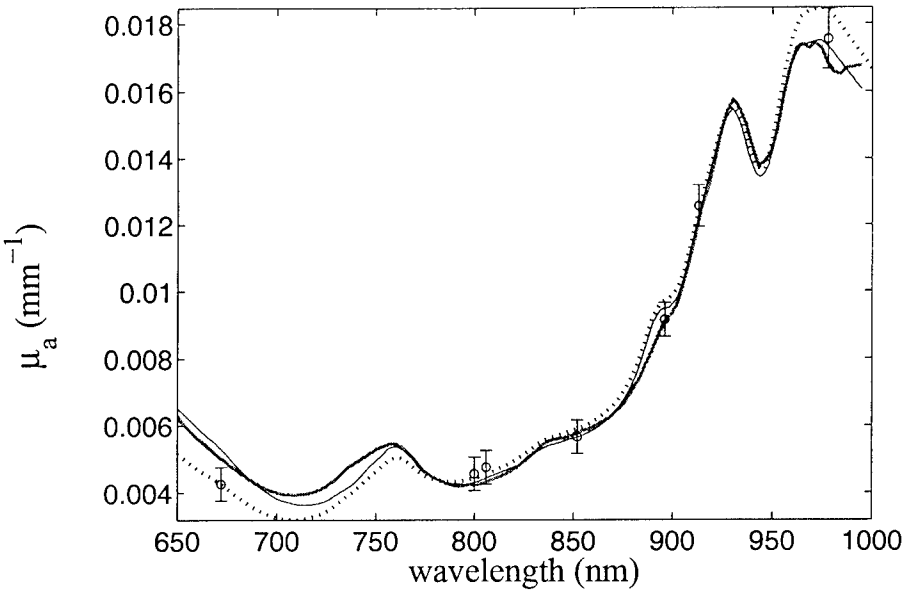

Figure 9: μ_a predictions for the third breast measurement (inner breast, 21-year-old volunteer). Lines and circles have the same assignments as described in Figure 7. Physiological parameters: total hemoglobin concentration, 19 μM; oxygen saturation, 72%; water, 28 g/cm^3; and fat, 0.56 g/cm^3. See Table 1 for more details.

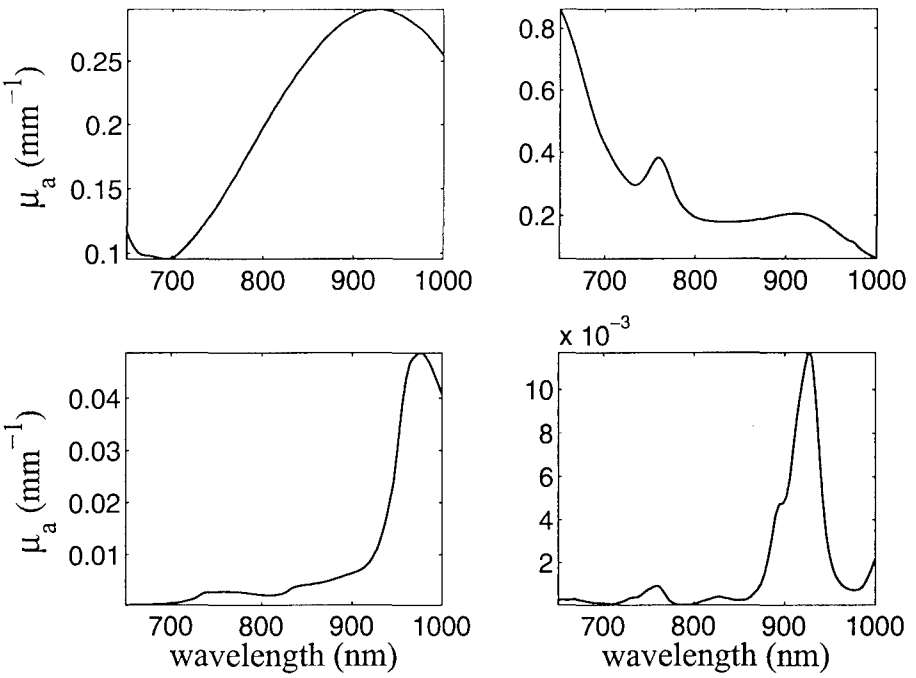

Figure 10: Absorption spectra of major absorbers in breast tissue. Upper left: oxyhemoglobin, 1 μM; upper right, deoxyhemoglobin, 1 μM; lower left, water, 1 g/cm^3; lower right, fat (soybean oil), 0.9 g/cm^3. The hemoglobin spectra are from Wray *et al.*,[27] the water is from Kou *et al.*,[26] and the fat is from the doctoral thesis of Eker.[28]

List of Tables

1 Results of physiological predictions for breast samples 1–3. The final column gives the % difference between the FD and SSFD values, defined as 100×(FD- SSFD)/SSFD. 42

	component	SSFD	FD only	% difference
breast 1	total Hb (μM)	22	25	13
	O_2 saturation (%)	73	78	7
	water (g/cm^3)	0.15	0.14	-7
	fat (g/cm^3)	0.75	0.44	-41
breast 2	total Hb (μM)	30	30	0
	O_2 saturation (%)	70	79	13
	water (g/cm^3)	0.51	0.40	-22
	fat (g/cm^3)	0.42	0.39	-7
breast 3	total Hb (μM)	19	19	0
	O_2 saturation (%)	72	81	13
	water (g/cm^3)	0.28	0.27	-4
	fat (g/cm^3)	0.56	0.54	-4

Table 1: Results of physiological predictions for breast samples 1–3. The final column gives the % difference between the FD and SSFD values, defined as 100×(FD- SSFD)/SSFD.

Sources of absorption and scattering contrast for non-invasive optical mammography

A. E. Cerussi, Ph D[1], A. J. Berger, Ph D[1], F. Bevilacqua, Ph D[1], N. Shah, B S[1], D. Jakubowski, M S[1], J. Butler, MD[2], R. F. Holcombe, MD[3], and B. J. Tromberg, Ph D[1*]

Beckman Laser Institute and Medical Clinic[1]

University of California, Irvine

phone:(949)824-4713

fax:(949)824-8413

Department of General Surgery[2]

University of California, Irvine Medical Center

(714)456-8030

Division of Hematology/Oncology[3]

University of California, Irvine

(714)456-5153

*corresponding author

email of corresponding author: tromberg@bli.uci.edu

Original Research Submission

Sources of absorption and scattering contrast for non-invasive optical mammography

Original Research Submission

ABSTRACT

Purpose: Near infrared (NIR) diffuse optical spectroscopy and imaging may enhance existing technologies for breast cancer screening, diagnosis, and treatment. NIR techniques are based on sensitive, quantitative measurements of functional contrast between healthy and diseased tissue. In this study we quantified the origins of this contrast in healthy breast.

Materials and Methods: Non-invasive NIR measurements were performed on the breasts of 28 healthy women. Subjects included pre- and post-menopausal women between the ages of 18 and 64. A diffusive model of light transport quantified oxygenated and deoxygenated hemoglobin, water, and lipid by their absorption signatures. Cellular density, fat, and collagen content were inferred from measured light-scattering spectra.

Results: Substantial quantitative differences were observed in the optical properties of breast as a function of age. Changes were consistent with long-term hormone-dependent transformations that occur in breast. Instrument response was not adversely affected by subject age or menopausal status.

Conclusions: These measurements provide new insight into endogenous optical absorption and scattering contrast mechanisms and have implications for the development of optical mammography. NIR spectroscopy yields quantitative functional information that cannot be obtained with other non-invasive radiological techniques. The prototype bedside-capable instrument is comparable in cost to commercialized ultrasound.

Key Words: breast, breast radiography, blood, fat

INTRODUCTION

A. Scope of This Work

This paper describes the application of a new class of near-infrared (NIR) spectroscopy tools for non-invasive, quantitative characterization of breast tissue physiology. Diagnostic methods currently in use, such as mammography, magnetic resonance imaging, and ultrasound offer excellent anatomical lesion-detection capabilities, but are generally unable to provide quantitative information regarding tissue function and composition [1]. Positron emission tomography shows great promise in evaluating the metabolic demands of tissue, but requires exogenous radionuclides and is insensitive to tissue hemodynamics. NIR optical spectroscopy is intrinsically sensitive to the principal components of breast: blood, water, and adipose, as well as epithelial and connective tissues. Preliminary studies suggest that the fractional contribution of each to NIR signals depends strongly on factors such as age, menopausal status, and the progression of disease. Thus, NIR optical spectroscopy provides an opportunity for revealing physiological information that is unobtainable by other non-invasive techniques.

As optical diagnostic methods move rapidly towards the clinic, there is a growing need to identify and quantify sources of endogenous contrast in breast [2-11]. This paper presents the results of quantitative NIR spectroscopic studies in a population of 28 subjects ranging in age from 18 to 64. We provide evidence that NIR tissue spectroscopy is inherently sensitive to long-term age and hormone-dependent dynamics. Similar studies have been initiated [12-14] but on

only a few subjects or with limited sensitivity to physiological parameters. These data are expected to play an important role in characterizing the sensitivity of optical spectroscopy and imaging for applications such as tumor detection, therapeutic monitoring, and risk assessment.

B. Near-Infrared Tissue Spectroscopy

NIR photons (600-1000 nm) are non-ionizing and weakly absorbed by tissue. Many have exploited their enhanced penetrance relative to that of visible or ultra-violet radiation to explore non-invasively into brain, breast, and muscle [1]. In breast tissue, the principal NIR absorbers are assumed to be reduced hemoglobin (Hb-R), oxygenated hemoglobin ($Hb\text{-}O_2$), water (H_2O), and lipids [15]. NIR tissue spectroscopy offers a safe way to quantify these components and to view unique functional information with low-cost "point-of-care" devices. Multiple light scattering complicates quantitative measurements of light absorption in the NIR. The process of using frequency-domain photon migration (FDPM) techniques to separate the effects of absorption from scattering has been described in detail [16, 17]. FDPM enables the use of quantitative spectroscopic analysis tools to determine the composition and structure of tissue non-invasively [18].

The application of FDPM techniques to NIR tissue spectroscopy differs substantially from conventional bulk NIR methods, such as diaphanography [19]. FDPM employs computational models that allow the quantitative separation of the effects of absorption and scattering. Thus, within the limits of applicability of the light-transport models to the breast, all parameters measured in this study are absolute values.

MATERIALS AND METHODS

A. Patient Selection

All volunteers enrolled in this study competently provided informed consent for participating in one of two trials (#95-563 and #99-2183) under the guidelines of an Institutional Review Board. The 28 volunteer ages ranged between 18 and 64. Fifteen of the volunteers were pre-menopausal (average age 28 +/- 9). Seven were post-menopausal (average age 56 +/- 2). The remaining six (average age 56 +/- 5) were women taking some form of hormone replacement therapy (HRT); three of these six women classified themselves as peri-menopausal. None of the women had any known cancerous lesions or other known forms of breast disease.

B. Measurement Technique

Each volunteer rested in a supine position during the measurement. The instrument probe, which is slightly larger than an ultrasound probe (Figure 1), was the only item placed in contact with the volunteer. This probe consisted of a sealed avalanche photodiode (APD) module and an optical fiber placed 22 mm away from the APD. All measurements were performed in a reflection-style geometry. The probe was placed on the breast with minimal pressure using only the force of gravity; no compression was used. In this configuration, we estimate that the light sampled approximately 1 cm below the skin. We report data only on measurements performed in the center of the left upper outer quadrant (measurements on the right upper quadrant yielded

similar results). Error bars in Figures and Tables represent the standard deviation of repeated measurements.

C. Instrumentation

A schematic of our 1 GHz, portable FDPM device is shown in Figure 1. The specific details of this FDPM instrument have been described in detail elsewhere [20], but the relevant technical information is mentioned here. The instrument employs multiple diode lasers that provide visible and NIR light at seven wavelengths (672, 800, 806, 852, 896, 913, and 978 nm). A hand-held probe has been designed to house an APD that records the modulated diffuse light signals after propagation through the tissue. This probe has a plastic attachment on the casing to position a source optical fiber a fixed distance from the APD. A 100-μm-diameter graded index optical fiber positioned 22 mm from the APD detector was used to deliver the diode laser outputs to the tissue surface. A network analyzer measured the phase and amplitude of the detected electronic signal from the APD. A steady-state current source was mixed with RF power provided by the network analyzer in a bias network. This bias network serially distributed power to each laser diode and produced intensity-modulated light. An optical switch delivered light serially from each diode to the tissue via the single optical fiber described in the handheld probe. The optical power launched into the tissue ranged from 5-25 mW for each wavelength.

A sweep over all seven wavelengths ranged from approximately 35 to 60 s. The system acquired data in less than 3 s per wavelength, with a 2 s delay between each laser diode in the system because of switching considerations. The system was wheeled into a medical clinic for the each

measurement. Instrumental artifacts were removed by calibrating on a tissue-simulating phantom with known absorption and scattering properties.

D. Measured Parameters and Data Analysis

The amplitude and phase of a NIR diffusive light wave demodulates and retards, respectively, as the wave propagates through multiple-scattering media such as tissue. The real and imaginary parts of this diffuse wave were fit simultaneously to a light-diffusion model (the P_1 Approximation to the Boltzmann Transport Equation) [21,22] by minimizing the chi-squared (χ^2) surface with a Marquardt-Levenberg algorithm. This fit determined the absolute optical absorption coefficient, μ_a and the absolute optical reduced scattering coefficient, μ_s' at each wavelength. Typical μ_a, and μ_s' uncertainties, determined from the χ^2 distribution of the fits, are 1% to 3% of their mean values. In actual tissue measurements, precision error is less than 10% for μ_a and 5% for μ_s'.

When the optical properties μ_s' and μ_a are recovered for the seven wavelengths, the spectral-dependence of the absorption may be combined with known values of molecular extinction coefficients to calculate physiologically-relevant parameters. We assume that bulk breast tissue is composed principally of four NIR absorbers Hb-R, Hb-O_2, H_2O, and lipids. The concentrations of these absorbers (c) were quantified by solving the equation $\vec{\mu}_a = \mathrm{E}\,\vec{c}$, where E is a 7 x 4 matrix that contains the molar extinction coefficients of the four chromophores at the seven source wavelengths ([23]-[25]).

For each measurement we report four hemoglobin parameters: [Hb-R], [Hb-O_2], total hemoglobin concentration (THC = [Hb-R]+[Hb-O_2]), and the tissue hemoglobin saturation (S_tO_2=[Hb-O_2] / THC x 100%), where the characters [] denote concentration (M L^{-1}). Values for water and lipid content are reported as percentages. The water percentage is the concentration of measured tissue water divided by the concentration of pure water (55.6 M). The lipid percentage is the kilograms per liter of lipid measured relative to an assumed 'pure' lipid density of 0.9 Kg L^{-1}. Thus, the water and lipid percentages we report are relative figures of merit compared to pure solutions of the substance, and are not strict volume or mass fractions.

The scattering properties of the tissue also yield important physiological information. NIR scattering in tissue has the following dependence: $\mu_s' = A\,\lambda^{-SP}$, where A is a constant, λ is the wavelength (nm), and SP is the scatter power. Scatter power is related to the scattering center size (d) compared to the optical wavelength. As an example, scatter power is 4 in the case of Rayleigh scattering ($d<<\lambda$) and is ~1 for large Mie-like scatterers ($d \sim \lambda$).

RESULTS

A. Sensitivity: Pre- versus Post-Menopausal

Both Figure 2 and Figure 3 present a typical series of measurements of seven absorption and scattering coefficients, respectively. The points represent an average of several measurements in the center of the left upper outer quadrants of two volunteers; a 32-year old pre-menopausal woman (squares) and a 54-year-old post-menopausal woman (triangles). Error bars show the standard deviation of repeated measurements. There are vast absorption and scattering differences between pre- and post-menopausal breast tissue. The solid lines of Figure 2 represent a weighted-least-squares fit of the seven absorption coefficients using published extinction coefficients for Hb-R, Hb-O_2, H_2O, and lipids [23-25]. Lines between the measured points have been interpolated. The solid lines of Figure 3 represent a fit of the scattering coefficients to the equation: $\mu_s' = A\,\lambda^{-SP}$.

These optical spectra provide unique insight into breast tissue composition. There are higher concentrations of hemoglobin (i.e., both Hb-R and Hb-O_2) in the pre-menopausal subject, as evidenced by the overall higher absorption in the 670 to 850 nm range. There is also more water relative to lipids in the pre-menopausal subject, as revealed by the large water absorption peak at 980 nm. Recovery of the absorption spectra allows calculations of the tissue concentrations of Hb-R, Hb-O_2, H_2O, and lipids. In addition, the light scattering intensity is significantly lower in the post-menopausal breast. Table 1 provides a summary of the fitted physiological properties for these two subjects represented in both Figure 2 and Figure 3.

B. Quantities vs. Age

The next three figures present FDPM-measured quantities as a function of volunteer age. Figure 4 shows the THC, Figure 5 shows the tissue water percent (referenced to the concentration of pure water), and Figure 6 shows the scatter power. Premenopausal subjects (i.e., age <50) display a variety of values in all three plots. This spread is the result of inter-subject variations, including, but not limited to, menstrual cycle differences and gynecological age.

There is a general decrease with age in THC, water, and scatter power for peri- and post-menopausal volunteers (i.e., $\geq$ 50 years old). The decrease in THC correlates well with previous histological studies showing both the atrophy of well-vascularized lobular tissue and the increase of the fat-to-collagen ratio after menopause [15]. This is consistent with compositional analysis data showing lower blood and water content for fat versus glandular tissue [26]. Scatter power also decreases with age after 50. Compared with fat, collagen and glandular tissue scatter light with a higher intensity and a steeper spectral dependence [27]. Thus, smaller scatter powers are expected in fatty tissue. Exact knowledge of the weighted biological contributions to optical tissue scattering is a matter of debate.

C. Correlation Between Absorption and Scattering Information

Figure 7 displays a correlation plot of the measured water (open squares) and lipid (triangles) percents vs. scatter power. The lipid percent is the mass density of lipids in the tissue referenced to the mass density of soybean oil. Note that neither the water nor lipid percents represent a strict mass or volume fraction for the tissue (i.e., all components are not normalized to 100%). Lines represent fits of water (solid) and lipids (broken) as functions of scatter power.

Tissue scattering correlates well with the parenchyma composition measured via absorption. As scatter power increases, the lipid percent decreases ($R^2 = -0.841$, $p < 10^{-3}$) and water percent increases ($R^2 = +0.850$, $p < 10^{-3}$). The absorption spectra of water and lipids overlap which can lead to errors in measuring these chromophores. However, Figure 7 clearly shows that both scattering and absorption provide complementary information regarding breast composition, indicating that such errors do not significantly distort our findings.

D. Tissue Metabolism and Menopause

S_tO_2 is the percent fraction of arterial and venous Hb-O_2 that contributes to the tissue THC, and should not be confused with the S_aO_2, measured via pulse oximetry (which is the arterial saturation). Table 2 presents the measured S_tO_2 in all subjects with a body-mass-index below 40. The S_tO_2 of the pre-menopausal volunteers and the HRT volunteers both averaged approximately 76%. Their means were not statistically significantly different. However, the S_tO_2 values for the post-menopausal women not taking HRT were significantly higher, averaging $81.9 \pm 8.8\%$ ($p = 0.062$).

Decreases in S_tO_2 are associated with increased metabolism. Tumors for example have been shown to have lower S_tO_2 values than non-tumor tissue [18]. The post-menopausal increase in S_tO_2 relative to the pre-menopausal/HRT women is plausible since general tissue metabolism in the breast should decrease after menopause as the tissue begins to atrophy. The similarity between the S_tO_2 values of pre-menopausal and HRT women suggests that their metabolisms are similar, reflecting the effects of both endogenous and exogenous hormones.

DISCUSSION

Although it is difficult to directly validate non-invasive *in vivo* measurements, these initial results indicate that the sensitivity of NIR spectroscopy is a reasonable reflection of long-term hormone-controlled breast remodeling. Additional work in the field has demonstrated that short-term menstrual-cycle changes are detectible using a similar NIR technique [28]. Our results provide indirect validation of the general accuracy of NIR breast spectroscopy. It must be stressed that this quantitative physiological information is not obtainable by any other non-invasive radiologic method.

An important feature of NIR methods is the ability to characterize quantitatively the breast tissue of women regardless of age, hormonal status, or mammographic density. Increased mammographic density contributes to a 22% false negative rate as well as a high false positive rate (56.2% cumulative risk after ten exams) in women less than 50 years of age [29, 30]. A recent study found that routine initial mammography was not clinically advantageous for women less than 35 years of age [31]. Furthermore, the use of HRT in post-menopausal women is known to increase mammographic density [32] and has been recently shown to impede the efficacy of mammographic screening [33, 34]. The sensitivity of NIR spectroscopy to known biological processes suggests optical methods may provide important information complementary to conventional diagnostic techniques, particularly in the case of radiographically dense breast tissue.

In general, pre-menopausal breast is more optically attenuating than post-menopausal breast, both in absorption and scattering. It is important to note that this trend, particularly in scattering, is also true for mammographic density. Radiographically dense breast tissue is due to differing amounts of fat, collagen, epithelium, and water [35]. Although x-rays are inherently sensitive to dense electron structures in tissue, such as micro-calcifications, NIR photons are naturally sensitive to tissue constituents. Thus NIR spectroscopy has unique potential for quantifying the elements of breast tissue that contribute to mammographic density. This observation may be of importance in screening, since it may identify breast tissue at physiological risk for malignant transformation and can be performed easily in all women.

In addition to scattering contrast, we report age-dependent variations in the THC, H_2O, and lipids, as well as changes in S_tO_2 for pre- and post-menopausal subjects. Knowledge of the "normal" values of these chromophores will play a role in evaluating the usefulness of optical methods in detecting and characterizing lesions in the breast. Several investigators have reported a 2-4 fold THC contrast between normal and tumor structures. In vivo tumor S_tO_2 values are also typically lower than normal tissue. [18, 6, 36]. Thus, detailed studies of normal tissue are essential for determining the sensitivity required of optical instrumentation for detecting lesions in women of varying age and hormonal status. Furthermore, as baseline levels are characterized, data on an individual's absorption and scattering variations could provide important insight into disease appearance and progression. When applied to patients receiving chemotherapy and/or HRT, this information could also be used to generate feedback that would permit customized treatment planning based upon individual physiologic response.

ACKNOWLEDGEMENTS

This work was supported by the following grants and gifts: National Institutes of Health (NIH) Laser Microbeam and Medical Program (#RR-01192), NIH (#R29-GM50958), Department of Energy (DOE #DE-FG03-91ER61227), Office of Naval Research (ONR #N00014-91-C-0134), California Breast Cancer Research Program, and Avon. A.E.C. cheerfully acknowledges support from the U. S. Army Medical Research and Material Command (DAMD17-98-1-8186). The authors also acknowledge additional support from the George E. Hewitt Foundation (AJB) and the Swiss National Science Foundation (FB).

REFERENCES

1. An assortment of applications may be found in: The Philosophical Transactions of the Royal Society. 1997; 352.

2. An assortment of applications to the breast may be found in: Advances in Optical Biopsy and Optical Mammography. Conference proceedings. The Annals of the New York Academy of Sciences. 1998; 838.

3. Heusmann, H, Kölzer, J, Mitic, G. Characterization of female breasts in vivo by time-resolved and spectroscopic measurements in near infrared spectroscopy. J Biomed Opt 1996; 1:425-434.

4. Franceschini, MA, Moesta, KT, Fantini, S et al. Frequency-domain techniques enhance optical mammography: Initial clinical results. Proc Natl Acad Sci USA 1997; 94:6468-6473.

5. Moesta, KT, Fantini, S, Jess, H et al. Contrast features of breast cancer in frequency-domain laser scanning mammography. J Biomed Opt 1998; 3:129-136.

6. McBride, TO, Pogue, BW, Gerety, ED, Poplack, SB, Osterberg, UL, Paulsen, KD. Spectroscopic diffuse optical tomography for the quantitative assessment of hemoglobin concentration and oxygen saturation in breast tissue. Appl Opt 1999; 38:5480-5490.

7. Grosenick, D, Wabnitz, H, Rinneberg, HH, Moesta, KT, Schlag, PM. Development of a time-domain optical mammograph and first in vivo applications. Appl Opt 1999; 38:2927-2943.

8. Colak, SB, van der Mark, MB, W.'t Hooft, G, Hoogenraad, JH, van der Linden, ES, Kuijpers, FA. Clinical optical tomography and NIR spectroscopy for breast cancer detection. IEEE J Sel Top Quant 1999; 5:1143-1158.

9. Tromberg, BJ, Shah, N, Lanning, R et al. Non-invasive in vivo characterization of breast tumors using photon migrati on spectroscopy. Neoplasia 2000; 2:1-15.

10. Holboke, MJ, Tromberg, BJ, Li, X et al. Three-dimensional diffuse optical mammography with ultrasound localization in a human subject. J Biomed Opt 2000; 5:237-247.

11. Ntziachristos, V, Yodh, AG, Schnall, M, Chance, B. Concurrent MRI and diffuse optical tomography of breast after indocyanine green enhancement. Proc Natl Acad Sci USA 2000; 97:2767-2772.

12. Suzuki, K, Yamashita, Y, Ohta, K, Kaneko, M, Yoshida, M, Chance, B. Quantitative measurement of optical parameters in normal breasts using time-resolved spectroscopy: In vivo results of 30 Japanese women. J Biomed Opt 1996; 1:330-334.

13. Quaresima, V, Matcher, SJ, Ferrari, M. Identification and quantification of intrinsic optical contrast for near-infrared mammography. Photochem Photobiol 1998; 67:4-14.

14. Cubeddu, R, Pifferi, A, Taroni, P, Torricelli, A, Valentini, G. Noninvasive absorption and scattering spectroscopy of bulk diffusive media: An application to the optical characterization of human breast. Appl Phys Lett 1999; 74:874-876.

15. Thomsen, S, Tatman, D. Physiological and pathological factors of human breast disease that can influence optical diagnosis. Ann N Y Acad Sci 1998; 838:171-193.

16. Fishkin, JB, Gratton, E. Propagation of photon-density waves in strongly scattering media containing an absorbing semi-infinite plane bounded by a straight edge. J Opt Soc Amer A 1993; 10:127-140.

17. Yodh, A, Chance, B. Spectroscopy and imaging with diffusing light. Phys Today 1996; 48:34-40.

18. Fishkin, JB, Coquoz, O, Anderson, ER, Brenner, M, Tromberg, BJ. Frequency-domain photon migration measurements of normal and malignant tissue optical properties in a human subject. Appl Opt 1997; 36:10-20.

19. Cutler, M. Transillumination as an aid in the diagnosis of breast lesions. Surg Gynecol Obstet 1929; 48:721-728.

20. Pham, T, Coquoz, O, Fishkin, J, Anderson, EA, Tromberg, BJ. A Broad bandwidth frequency domain instrument for quantitative tissue optical spectroscopy. Rev Sci Instrum 2000; 71:1-14.

21. Kaltenbach, JM, Kaschke, M. Frequency- and time-domain modeling of light transport in random media In: Müller, G et al. eds. Book Frequency- and time-domain modeling of light transport in random media. Bellingham: Society of Photo-Optical Instrumentation Engineers, 1993; 65-86.

22. Fishkin, JB, Fantini, S, vandeVen, MJ, Gratton, E. Gigahertz photon density waves in a turbid medium: Theory and experiments. Phys Rev E 1996; 53:2307-2319.

23. Wray, S, Cope, M, Delpy, DT, Wyatt, JS, Reynolds, EO. Characterization of the near infrared absorption spectra of cytochrome aa3 and haemoglobin for the non-invasive monitoring of cerebral oxygenation. Biochim Biophys Acta 1988; 933:184-192.

24. Hale, GM, Querry, MR. Optical constants of water in the 200-nm to 200- mu m wavelength region. Appl Opt 1973; 12:555-563.

25. Eker, C. Optical characterization of tissue for medical diagnostics. Lund Institute of Technology, 1999.

26. Duck, FA. Physical Properties of Tissue. London: Academic Press, 1990; 320-328.

27. Peters, VG, Wyman, DR, Patterson, MS, Frank, GL. Optical properties of normal and diseased human breast tissues in the visible and near infrared. Phys Med Biol 1990; 35:1317-1334.

28. Cubeddu, R, D'Andrea, C, Pifferi, A, Taroni, P, Torricelli, A, Valentini, G. Effects of the menstrual cycle on the red and near-infrared optical properties of the human breast. Photochem Photobiol 2000; 72:383-391.

29. Kerlikowske, K, Barclay, J, Grady, D, Sickles, EA, Ernster, V. Comparison of risk factors for ductal carcinoma in situ and invasive breast cancer. J Natl Cancer Inst 1997; 89:76-82.

30. Elmore, JG, Barton, MB, Moceri, VM, Polk, S, Arena, PJ, Fletcher, SW. Ten-year risk of false positive screening mammograms and clinical breast examinations [see comments]. N Engl J Med 1998; 338:1089-1096.

31. Hindle, WH, Davis, L, Wright, D. Clinical value of mammography for symptomatic women 35 years of age and younger. Amer J Obstet Gynecol 1999; 180:1484-1490.

32. Baines, CJ, Dayan, R. A tangled web: factors likely to affect the efficacy of screening mammography. J Natl Cancer Inst 1999; 91:833-838.

33. Laya, MB, Larson, EB, Taplin, SH, White, E. Effect of estrogen replacement therapy on the specificity and sensitivity of screening mammography [see comments]. J Natl Cancer Inst 1996; 88:643-649.

34. Litherland, JC, Stallard, S, Hole, D, Cordiner, C. The effect of hormone replacement therapy on the sensitivity of screening mammograms. Clin Radiol 1999; 54:285-288.

35. Oza, AM, Boyd, NF. Mammographic parenchymal patterns: a marker of breast cancer risk. Epidemiol Rev 1993; 15:196-208.

36. Fantini, S, Walker, SA, Franceschini, MA, Kaschke, M, Schlag, PM, Moesta, KT. Assessment of the size, position, and optical properties of breast tumors in vivo by noninvasive optical methods. Appl Opt 1998; 37:1982-1989.

Table 1 – Measured physiological properties of a pre-menopausal and a post-menopausal breast

	[Hb-R] (μM)	[Hb-O_2] (μM)	S_tO_2 (%)	THC (μM)	[H_2O][a] (%)	LIPID[b] (%)	SP
PRE	12.6±0.7	27.9±2.7	68.9 ± 1.3	40.4 ± 2.7	45.1 ± 3.6	29.8 ± 5.6	0.864 ± 0.068
POST	2.36±0.49	12.2±1.6	83.7±2.5	14.4±1.9	10.3±0.8	67.5±3.7	0.555±0.036

[a] Measured concentration relative to pure water

[b] Measured mass density relative to pure lipid

Hb-R: reduced hemoglobin

Hb-O_2: oxygenated hemoglobin

S_tO_2: total hemoglobin saturation

THC: total hemoglobin concentration

SP: scatter power

PRE: pre-menopausal volunteer

POST: post-menopausal

Table 2 - Comparison of tissue hemoglobin saturations

	S_tO_2 (%)	Observations (#)
PRE	76.3 ± 6.4	15
HRT	76.9 ± 9.2	6
POST	81.9 ± 8.8	6

PRE: pre-menopausal

POST: post-menopausal

HRT: hormone replacement therapy

S_tO_2: total hemoglobin saturation

Figure 1 - Schematic drawing of FDPM instrument, hand-held probe, and measurement map. The components of the instrument are: (1) diode lasers (2) avalanche photodiode (3) network analyzer (4) steady-state current source (5) bias network (6) optical switch. Measurements were performed with a hand-held probe (close-up on bottom of Figure) that contained the APD and a source optical fiber. The measurement location was in the center of the left upper outer quadrant as indicated.

Figure 2 - Measured absorption spectra for 32 year-old pre-menopausal (squares) and 54 year old post-menopausal (triangles) volunteers. Points represent the average of several measurements. The lines represent a least-squares fit (extrapolated to all wavelengths) assuming the breast absorption is due to only Hb-R, Hb-O_2, H_2O and lipids. Concentrations of chromophores from this measurement are listed in Table 1.

Figure 3 – Measured scattering spectra for same volunteers in Figure 2. The lines represent a fit to: $\mu_s' = A\,\lambda^{-SP}$, where S is the scattering (mm^{-1}), A is a constant, λ is the wavelength (nm) and $|SP|$ is the scatter power. Results of the fit from this measurement are listed in Table 1.

Figure 4 – Plot of the total hemoglobin concentration (micro-molar) versus volunteer age (years). Pre-menopausal volunteers (<50 years, $N = 15$) show considerable variation with age because of inter-subject variations such as menstrual cycle variations and overall hormone production differences. Post-menopausal ($N = 10$) and peri-menopausal ($N = 3$) volunteers (> 50 years) show a marked decrease in total hemoglobin concentration. ($N = 28$ total subjects.)

Figure 5 - Plot of the measured tissue water percentage (%) versus volunteer age (years). Pre-menopausal volunteers show considerable variation over age because of intra-subject variations such as menstrual cycle variations and overall hormone production differences. Post-menopausal and peri-menopausal volunteers show a marked decrease in water content. Percentages are water concentrations normalized to the concentration of pure water ($N = 28$ total subjects.)

Figure 6 - Plot of the measured optical scatter power (arbitrary) versus volunteer age (years). Optical scatter power refers to the magnitude of the slope of the scattering vs. wavelength curve. Pre-menopausal volunteers show considerably higher scatter power than the post-menopausal volunteers. This general pattern is the same for mammographic density. ($N = 28$ total subjects.)

Figure 7 – Correlation plot between water percent (open squares) and lipid percent (triangles) vs. scatter power. Percentages are referenced to the concentration of pure water and the mass density of pure fat. Scatter power correlates with water ($R^2 = +0.850$, $p < 10^{-3}$) and anti-correlates with lipids ($R^2 = -0.841$, $p < 10^{-3}$). ($N = 28$ total subjects.)

FIGURE 1

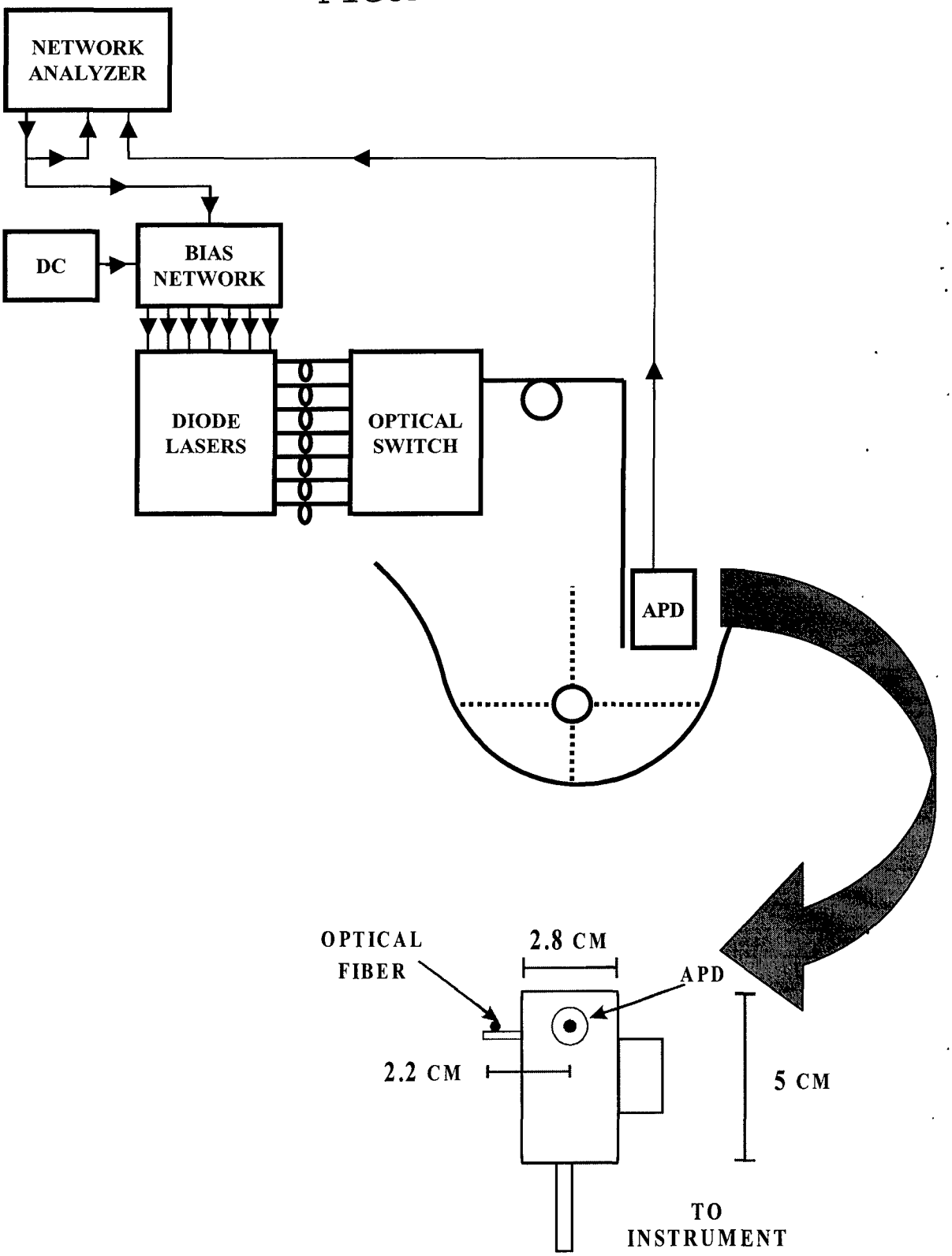
NETWORK ANALYZER
DC
BIAS NETWORK
DIODE LASERS
OPTICAL SWITCH
APD
OPTICAL FIBER
2.8 CM
APD
2.2 CM
5 CM
TO INSTRUMENT

FIGURE 2

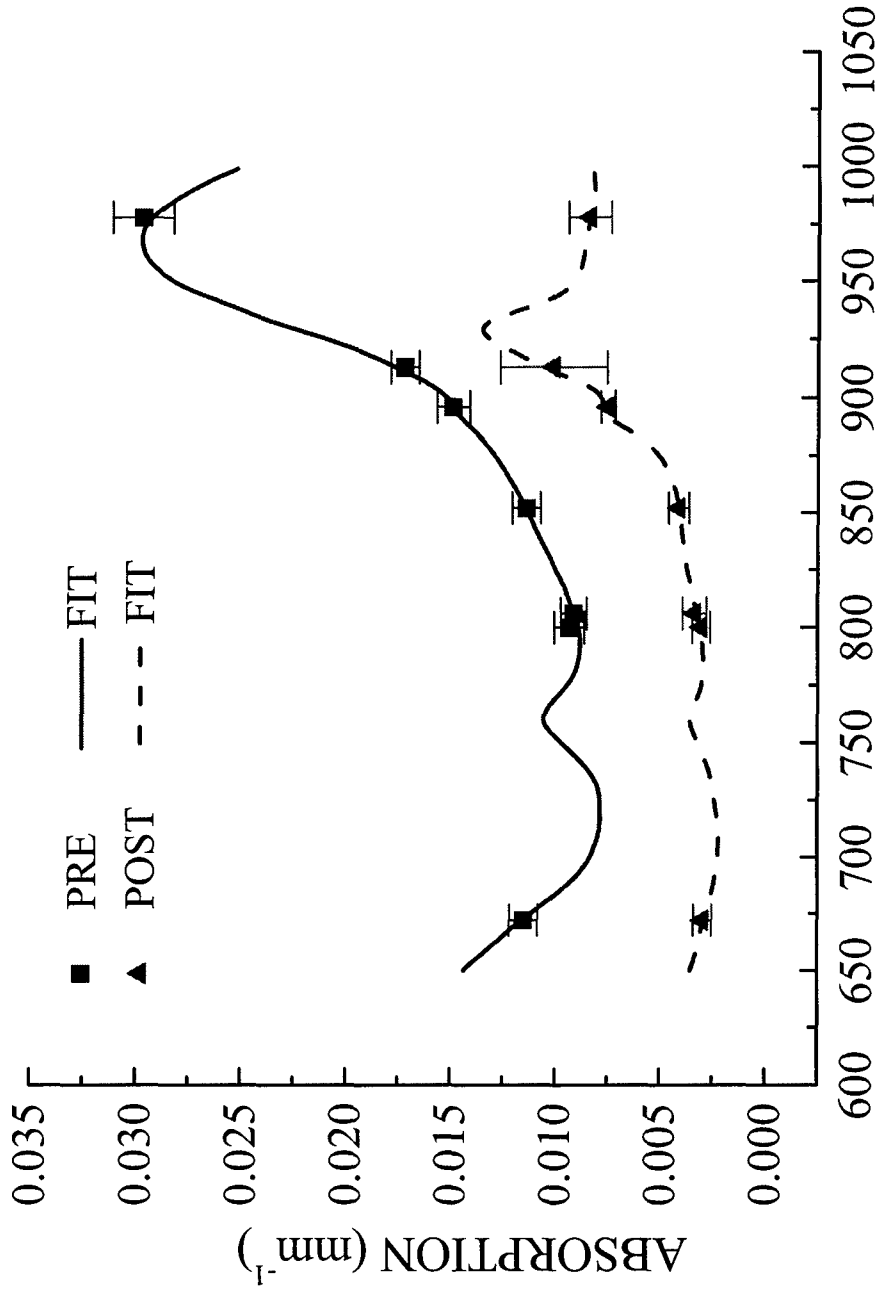
PRE
FIT
POST
FIT
ABSORPTION (mm-1)
0.035
0.030
0.025
0.020
0.015
0.010
0.005
0.000
600
650
700
750
800
850
900
950
1000
1050
WAVELENGTH (nm)

FIGURE 3

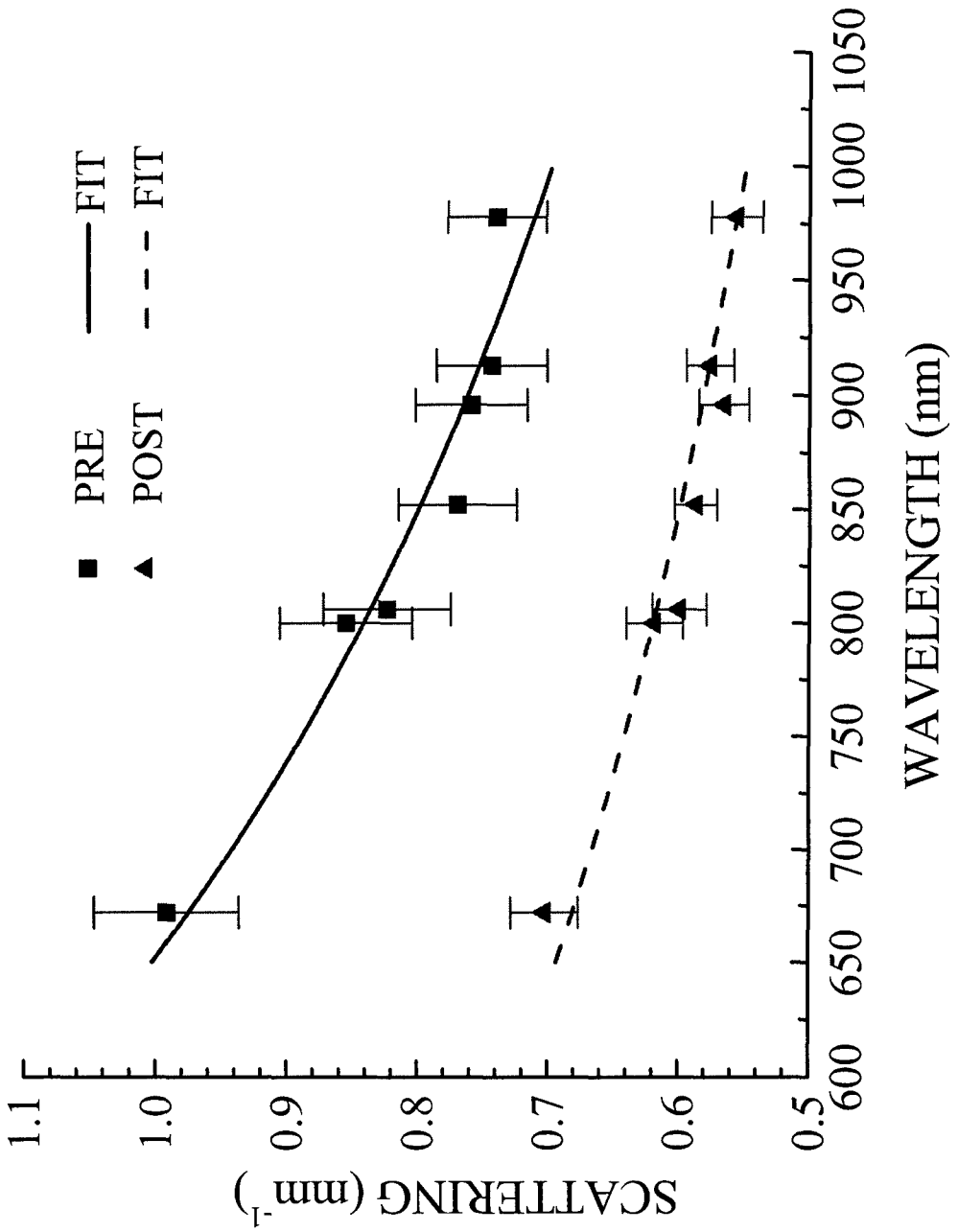
PRE
POST
FIT
FIT
SCATTERING (mm-1)
WAVELENGTH (nm)
1.1
1.0
0.9
0.8
0.7
0.6
0.5
600
650
700
750
800
850
900
950
1000
1050

FIGURE 4

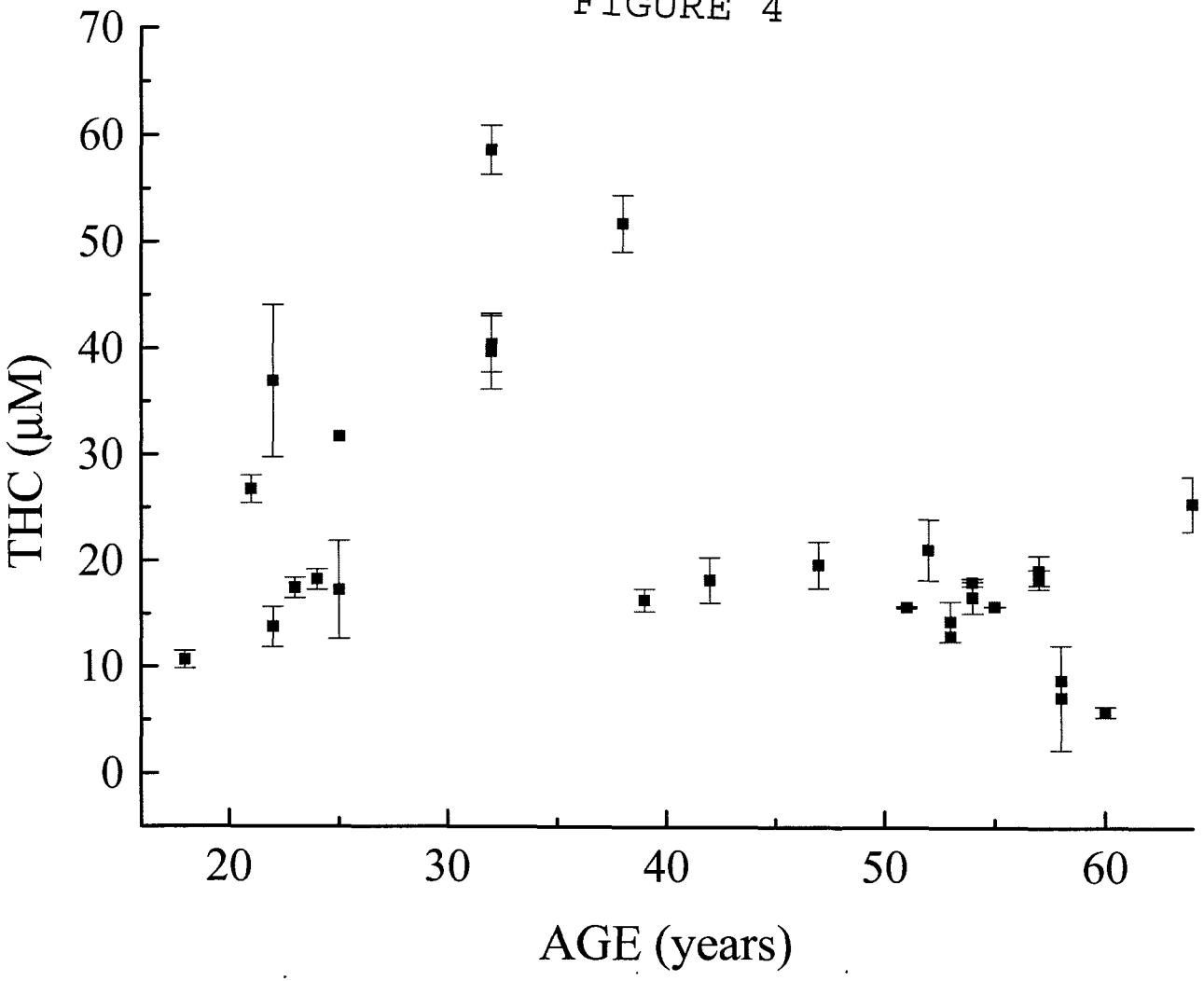

FIGURE 5

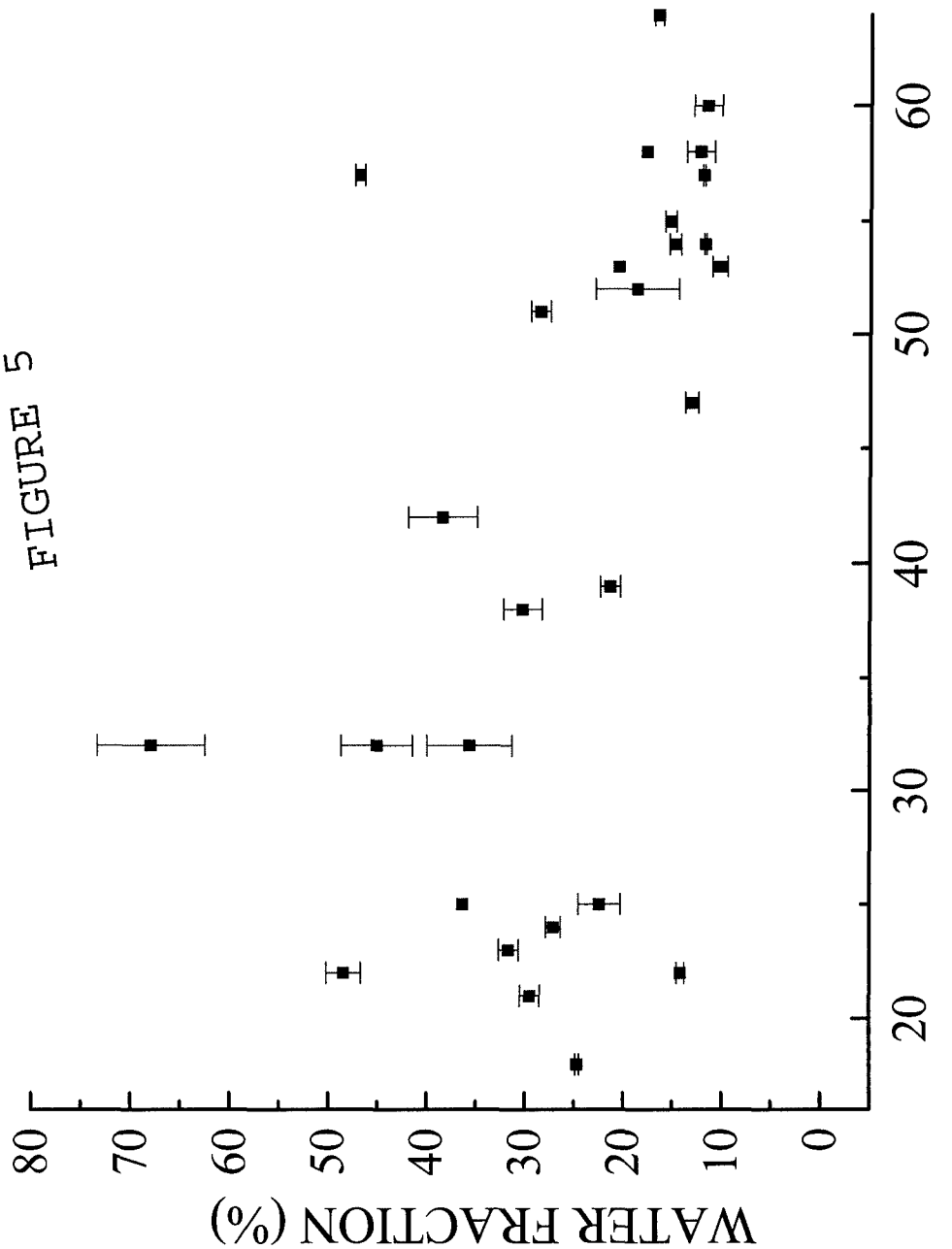

FIGURE 6

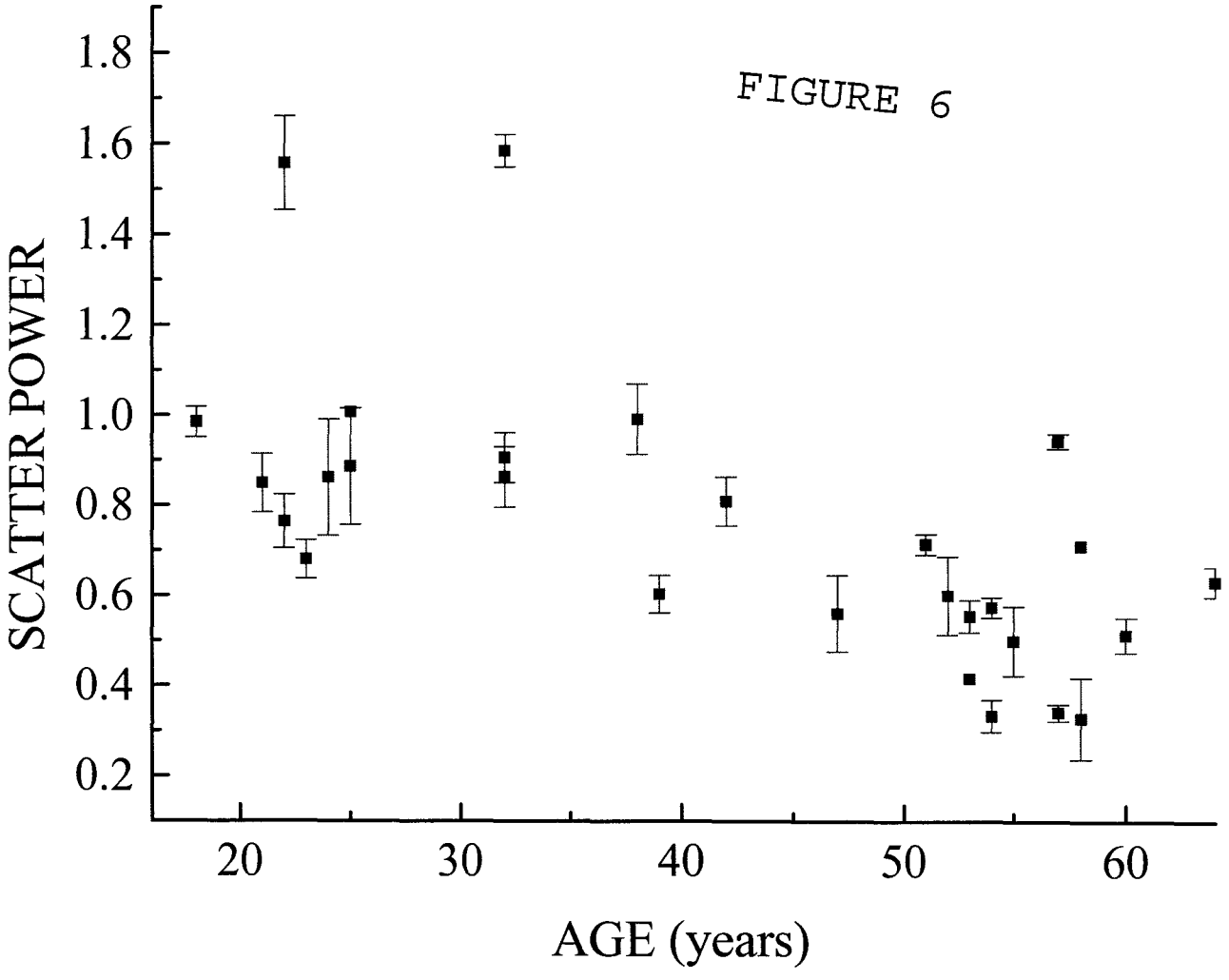

FIGURE 7

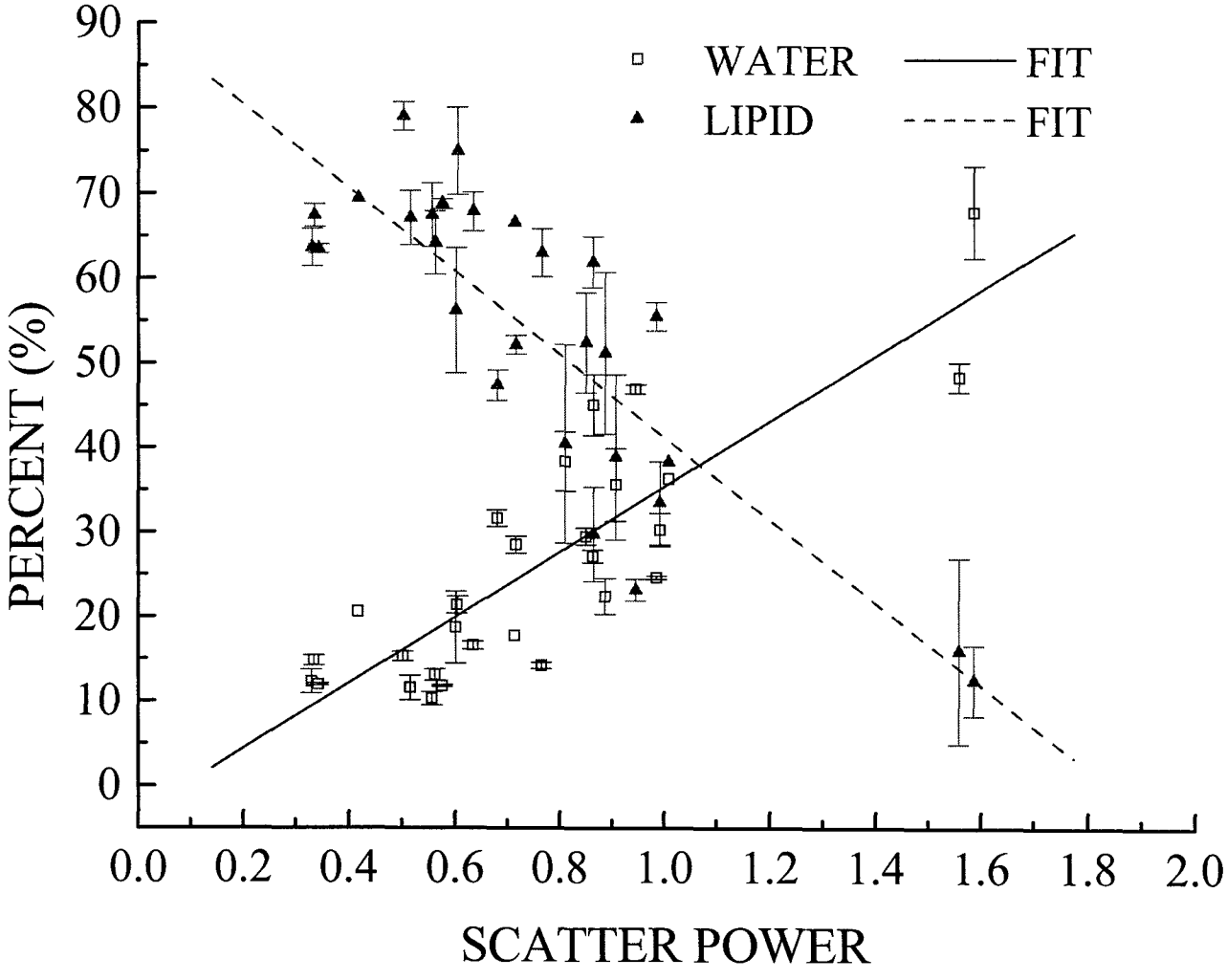
WATER
FIT
LIPID
FIT
PERCENT (%)
SCATTER POWER
0
10
20
30
40
50
60
70
80
90
0.0
0.2
0.4
0.6
0.8
1.0
1.2
1.4
1.6
1.8
2.0

Non-Invasive Functional Optical Spectroscopy of Human Breast Tissue

Natasha Shah[1,2], Albert Cerussi[1], Charlotta Eker[3] Jenny Espinoza[1], John Butler[4], Joshua Fishkin[1], Rene Hornung[1,5], Bruce Tromberg[1*]

1. Laser Microbeam and Medical Program, Beckman Laser Institute and Medical Clinic, University of California, Irvine, 1002 Health Sciences Road East, Irvine, Ca. 92612
Phone: 949/824-4713, Fax: 949/824-8413, email: tromberg@bli.uci.edu

2. Department of Chemistry, University of California, Irvine
516 Rowland Hall, Irvine, Ca. 92697-2025.

3. Department of Physics, Lund Institute of Technology, Sweden
P.O. Box 118, S-221 00 Lund, Sweden.

4. Department of Surgery, Div. of Surgical Oncology, Chao Cancer Center, University of California, Orange, California 92665.

5. Department of Obstetrics and Gynecology, University Hospital, Zurich, Switzerland.

*Corresponding Author

Classification: Biological Sciences, Biophysics

Manuscript:
21 pages
7 figures
1 table

Abstract: 269 words
Character Count: 46,653

Abbreviations:

FDPM – Frequency Domain Photon Migration
HRT – Hormone Replacement Therapy
μ_a – Absorption coefficient
μ_s' – Reduced scattering coefficient
Hb – Hemoglobin
HbO_2 – Oxy-hemoglobin
NIR – Near Infrared

Abstract

Near infrared (NIR) diffuse optical spectroscopy (DOS) and diffuse optical imaging (DOI) are promising methods that may eventually enhance or replace existing technologies for breast cancer screening and diagnosis. These techniques are based on highly sensitive, quantitative measurements of optical and functional contrast between healthy and diseased tissue. In this study we examine whether changes in breast physiology caused by exogenous hormones, aging, and fluctuations during the menstrual cycle result in significant alterations in breast tissue optical contrast. A non-invasive, quantitative DOS technique, Frequency-Domain Photon Migration (FDPM), was employed. Measurements were performed on fourteen volunteer subjects (UC Irvine IRB #95-563) using a hand-held, deep-tissue probe. Optical properties, i.e. intrinsic tissue absorption (μ_a) and reduced scattering (μ_s') parameters, were calculated from FDPM data. Wavelength-dependent absorption (μ_a at 674, 803, 849, 956nm) was used to determine tissue concentration of oxyhemoglobin (HbO_2), deoxy hemoglobin (Hb), and total hemoglobin ($Hb_{tot} = HbO_2 + Hb$); tissue hemoglobin oxygen saturation ($S_tO_2 = 100$ x (HbO_2/ Hb_{tot})) and bulk water content. Results show significant and dramatic differences in optical properties between menopausal states. Average pre-menopausal μ_a and μ'$_s$ values at each wavelength are 2.5 to 3-fold higher and 16-28% greater, respectively, than absorption and scattering for post-menopausal subjects. Absorption and scattering properties for women using HRT are intermediate between pre- and post- populations. Physiological properties show differences in mean total hemoglobin (7.0 μM, 11.8 μM and 19.2μM) and water concentration (10.9%, 15.3% and 27.3%) for post-, HRT, and pre- subjects, respectively. Because of their unique, quantitative information content,

diffuse optical methods may play an important role in breast diagnostics and improving our understanding of breast disease.

Introduction:

X-ray mammography is widely used for breast cancer screening, the most common form of cancer in women. Because of uncertainties associated with radiographic density, mammography has up to a 22% false negative rate as well as a high false positive rate (56.2% cumulative risk after ten exams) in women under 50 years of age[1, 2]. A growing body of evidence supports the notion that mammography cannot accurately distinguish between benign and malignant tumors in younger women[3]. A recent study found that routine initial mammography was not clinically advantageous for women under 35 years of age[4]. Furthermore the use of hormone replacement therapy (HRT) in post-menopausal women is known to increase mammographic density[5] and has been recently shown to impede the efficacy of mammographic screening[6, 7]. Techniques such as magnetic resonance imaging (MRI) and ultrasound (US) are used only as secondary procedures due to factors as high cost and poor specificity (MRI) or low sensitivity (US).

Currently, invasive procedures such as fine needle aspiration or surgical biopsy are implemented in order to provide a definitive diagnosis. Given the sub-optimal performance of x-ray mammography in pre- and peri-menopausal women, the majority of invasive follow-up procedures are performed on normal or benign tissue that present no malignant disease[8]. As a result, the use of non-invasive, near-infrared optical methods as a supplement to present techniques for diagnosing and detecting breast cancer has generated considerable interest.

Optical methods are advantageous because they are non-invasive, quanitative, relatively inexpensive, do not require compression, and pose no risk of ionizing radiation. A promising NIR optical technique currently under development is frequency domain

photon migration (FDPM). FDPM methods have successfully detected the presence of small palpable breast lesions *in vivo* in women with previously diagnosed breast abnormalities[9-11].

FDPM employs intensity-modulated NIR light to quantitatively characterize tissue in terms of its optical parameters, i.e. the reduced scattering coefficient (μ_s') and the absorption coefficient (μ_a). The concentration of significant NIR absorbers (deoxy- and oxy-hemoglobin, water and adipose) can be calculated using measured μ_a values[12, 13]. Multiple light scattering in breast tissue occurs as a consequence of spatial variations in refractive index which, in turn, are influenced by cellular and extracellular matrix density[14,15]. Both μ_a and μ_s' together provide an understanding of changes in tissue cellularity, metabolic activity, physiology and host response to cancer. Detection of lesions is based upon functional contrast between normal and diseased tissue in the same patient. However the physiology of healthy breast tissue is complex, influenced by multiple internal and external factors such as menstrual cycle phase, menopausal status, exogenous hormones, lactation and pregnancy. Consequently, in order to establish a better basis for optical detection and diagnosis based on differential functional contrast, the optical properties of normal breast tissue must be carefully examined and characterized.

There has been increasing attention paid to the study of normal breast tissue optical properties and changes that occur with age, menopausal status, and hormone replacement therapy[16-18]. During the reproductive years, the breast is comprised mostly of glandular tissue. With menopause, there is a progressive atrophy of glandular tissue, mitotic activity slows down and vascular requirements decrease. Some of these changes

have been monitored qualitatively by mammography and magnetic resonance imaging[4, 19-21]. Involution of breast glandular tissue can be impeded by the use of exogenous hormones, such as estrogen and progesterone[22]. Presently up to 20% of U.S. women use hormone replacement therapy, (HRT) to alleviate symptoms of menopause. However, long term use has, under certain conditions, been linked with increased risk for breast cancer[23]. Magnetic resonance imaging studies further suggest that fluctuations in endogenous hormones may alter menstrual cycle patterns and impact breast cancer risk.[24, 25, 26, 27]. In addition, the phase of the menstrual cycle has been shown to influence mammographic accuracy and survival rates following tumor resection[28, 29].

In this paper we provide initial results examining differences in both optical and physiological properties of healthy breast tissue of fourteen women. Our results show that the population studied can be well-differentiated based on quantitative near-infrared spectroscopic measurements. Optical contrast is based upon physiological changes accompanying menstrual cycle variations, exogenous hormone levels and menopausal status. We believe this study is particularly important because standard-of-care screening using x-ray mammography has diminished efficacy in two of the populations we examine; i.e. pre-menopausal and HRT subjects. The sensitivity of our technique to known biological processes suggests our methods may provide important information complementary to conventional diagnostic techniques, particularly in the case of radiographically dense breast tissue. Ultimately, this may enhance our understanding of pathophysiological changes that accompany malignant transformation and provide insight into processes associated with increased disease risk.

Materials and Methods

a. FDPM instrument

A portable, multi-wavelength, high-bandwidth frequency-domain photon migration instrument has been designed and optimized for clinical optical property studies (figure 1a). The instrument employs multiple diode lasers (1) to provide visible and near-infrared light at six wavelengths (674nm, 803nm, 849nm, 894nm, 947nm and 956nm or 980nm). The FDPM instrument is described in detail in Tromberg *et. al.*, 1997[11] and Pham *et. al.*, 1999[30]. A hand-held probe has been designed to house an avalanche photodiode (APD) that records the diffuse light signals after propagation through the tissue (2). This probe has multiple grooves on the casing to position source optical fibers a fixed distance from the APD (Figure 1b). A 100-μm-diameter graded index optical fiber positioned 25mm from the APD detector delivers the diode laser output to the tissue surface. The network analyzer (3) measures the phase and amplitude of the electronic signal. A DC current source (4) is mixed with RF power provided by the network analyzer in a bias network (5). This distributes power to each laser diode and produces amplitude modulated light. An optical switch (6) delivers light serially from each diode to the tissue. The optical power launched into the subject ranged from 10-20mW for each wavelength.

b. Measurement technique

Subjects were measured in the supine position. Measurements were made in reflectance geometry by placing the hand-held probe on the skin surface with light pressure. The phase shift and amplitude of the photon density wave was measured at each wavelength for 201 modulation frequencies between 50 and 1000MHz at a source-detector separation of 25 mm. The range of modulation frequencies was swept repetitively so that each amplitude and phase value represents up to twelve measurements. Four to six wavelengths were utilized for the measurements.

c. Subjects

A total of fourteen subjects were studied: subjects Pre 1 through Pre 6 were pre-menopausal volunteers 18 to 33 years of age. Post 1 through Post 3 were post-menopausal women age 57-67. The remaining five volunteers were post-menopausal women 51-60 years of age using hormone replacement therapy. HRT 1 and HRT 5 were on combination HRT (progesterone and estrogen) and HRT 2 through HRT 4 were taking estrogen–only HRT. All HRT subjects have been taking exogenous hormone for at least 2 years. Experiments were conducted in adherence to UC Irvine IRB approved protocols 95-563 and 99-2183. The volunteers were healthy with no known breast diseases. After providing informed consent, volunteers filled out a brief questionnaire which surveyed pertinent medical history.

When using four wavelengths, the time required for a single measurement was approximately ninety seconds. A total of twelve sites, six per breast, for each volunteer was measured during volunteer visits. The measurement map is shown in Figure 1a.

Measurements were made in each of the four quadrants placed approximately halfway from the center of the breast to the edge of the breast laterally. Additional measurements were made on the superior areolar border and the axillary tail. Calibration measurements were made approximately every ten minutes on a tissue phantom of known optical properties.

A separate subject (Pre 6) was studied at two different points in her menstrual cycle. One measurement was performed near ovulation (day 14) of the subject's regular 28 day cycle, and another measurement performed during the luteal phase (day 25) of the menstrual cycle.

d. Model

The P_1 approximation to the Boltzmann transport equation[31] was used to analyze the frequency-domain data and is valid when probing homogeneous turbid media at source-detector separations greater than 1cm and modulation frequencies less than a few GHz. The model employs an extrapolated boundary condition for a semi-infinite geometry[32]. The solution to the P_1 approximation relates the frequency-dependent phase and amplitude to the optical absorption (μ_a) and reduced scattering (μ_s') coefficients[33]. To determine the optical properties from a given set of frequency-dependent data a Marquardt-Levenburg χ^2 minimization algorithm was used to simultaneously fit the amplitude $A(\omega)$, and phase $\Phi(\omega)$ by minimizing the difference between the measured values and those predicted by the P_1 approximation.

Physiological properties were calculated from the determined μ_a values assuming that principal chromophores in breast tissue for the NIR wavelengths used are deoxy-

hemoglobin, oxy-hemoglobin and water. The concentrations in tissue of the three components were calculated using μ_a at four wavelengths: 674, 803, 849 and 956nm or 980nm. The contribution of each component to the total μ_a at a given wavelength is represented by the equation $2.303(\varepsilon_i c_i) = \mu_{ai}$, where ε_i is the extinction coefficient in units of cm^2/mole of a particular chromophore at a given wavelength λ, and c_i is the concentration of the chromophore. The total absorption at a given wavelength from the tissue chromophores is:

$$\varepsilon^{\lambda}_{(Hb)}[Hb] + \varepsilon^{\lambda}_{(Hbo2)}[HbO2] + \varepsilon^{\lambda}_{(H2O)}[H2O] = \mu_a{}^{\lambda}, \quad (1)$$

Where the brackets, [ ], indicate concentration. The matrix representation of the four equations is[12]:

$$\begin{bmatrix} 6.578x10^6 & 0.740x10^6 & 0.748 \\ 1{,}897x10^6 & 2.037x10^6 & 0.34 \\ 1.809x10^6 & 2.659x10^6 & 0.781 \\ 1.570x10^6 & 3.049x10^6 & 0.74 \end{bmatrix} \begin{bmatrix} [Hb] \\ [HbO_2] \\ [H_2O] \end{bmatrix} = \begin{bmatrix} \mu_a^{674} \\ \mu_a^{803} \\ \mu_a^{849} \\ \mu_a^{956} \end{bmatrix}, \quad (2)$$

Given that there are more wavelengths than principle chromophores we have 4 equations and 3 unknowns and there exists no general solution for c_i. The chromophore concentrations are determined using a least squares solution to $\mathbf{Ec} = \boldsymbol{\mu}_a$. In matrix representation the chromophore concentration is given by: $\mathbf{c} = (\mathbf{E}^T \mathbf{E})^{-1} \mathbf{E}^T \boldsymbol{\mu}_a$ where $\mathbf{E}^T$ and $\mathbf{E}^{-1}$ denote the transpose and inverse of the matrix $\mathbf{E}$ respectively.

e. Calibration

A measurement of the phase shift of intensity modulated light at source wavelength λ propagating through a turbid medium at a given source-detector separation can be expressed as follows:

$$\Phi_{meas} = \Phi_{medium} + \Phi_{instrument} \quad (3)$$

In order to extract Φ_{medium} from Φ_{meas} at a single source-detector separation, $\Phi_{instrument}$ must be explicitly evaluated (Eq. (3)). Similar arguments can be made for amplitude data (A); however A_{medium} is determined by evaluating measured and instrument response ratios. The instrument response was calculated by making a measurement on a homogenous phantom with known optical properties. A siloxane phantom cast from flexible silicone (RTV 615/700, GE Corporation) and titanium diode in a 400mL mold was used to calibrate the instrument response in phase and amplitude measurements. Optical properties of the phantom were determined by the two-distance technique described in Fantini *et. al.*, 1994[34]. Reference measurements are made on the phantom at the given source-detector separation during the time of the subject measurement. Calibrations were made at approximately ten-minute intervals to account for amplitude drift.

Results and Discussion:

The results of raw data and simultaneous fits to the P_1 approximation for Pre 1 and Post 1 are shown in Figure 2. Clear differences are detected between the two subjects

in both amplitude and phase data. In order to establish the range of optical property values characteristic of normal menopausal states, we examined eight volunteers (5 pre-menopausal) not receiving exogenous hormone therapy. Figure 3 shows a scatter plot of μ_a versus μ_s' at all four wavelengths for each subject. For comparative purposes data from the right upper outer quadrant measurements are shown. Glandular tissue is concentrated in the upper outer quadrant of the breast and consequently, more lesions appear in this region than any other[35].

In general, post-menopausal women have substantially lower μ_a and μ_s' values compared to pre-menopausal women. Average pre-menopausal μ_a values at each wavelength (0.0049 -0.016 mm^{-1}) are 2.5 to 3-fold higher than post-menopausal absorption (average μ_a = 0.0016-0.0064mm^{-1}). Pre-menopausal women have 16-28% higher scattering values at each wavelength (average μ_s' = 0.78-1.1mm^{-1}) than post-menopausal subjects (average μ_s' = 0.67-0.86 mm^{-1}). Since measurement uncertainties are less than 5% of the optical property value[30] these constitute significant and dramatic differences between menopausal states.

A deeper understanding of the underlying physiological reasons for optical property contrast can be obtained by examining μ_s' spectra (i.e. μ_s' vs. λ) for three individuals. Results shown in Figure 4 highlight the impact of estrogen on breast structure. The 29-year old pre-menopausal subject displays μ_s' values that are consistently greater than the 67-year old post-menopausal volunteer. Interestingly, μ_s' values for the 52-year old post-menopausal subject receiving estrogen-only HRT fall directly between pre-menopausal and post-menopausal data. This may be due to the fact that estrogen increases the rate of mitosis within ductal tissue. Thus, optical property

differences between HRT and post-menopausal subjects could be a consequence the impact of epithelial tissue proliferation. Scattering contrast between pre- and post-menopausal subjects is probably due to a combined effect of the loss of glandular epithelium as well as extracellular matrix remodeling. The more gradual μ_s' vs λ slope shown for the post-menopausal subjects reflects large particle scattering consistent with a high percentage of fatty parenchyma found in this age group. In younger women, the relatively steep μ_s' vs. λ slope is likely to be influenced by the presence of extracellular collagen in addition to cellular/epithelial factors.

These concepts are further substantiated by Figure 5, which illustrates an inverse correlation between μ_s' and age for subjects over 50. Whether the trend indicating increased scattering for HRT women is due to exogenous hormone use is not yet clear. Pre-menopausal μ_s' values appear to be independent of age, most likely due to the timing of the measurements. The five pre-menopausal subjects were measured at different points of their menstrual cycle, which can significantly affect optical properties.

Average tissue hemoglobin concentrations (oxy-, deoxy- and total) and tissue water concentration are shown in Figure 6. The concentration of blood vessels and blood flow, indicated by total hemoglobin concentration (THC = [Hb] + [HbO_2]), is greatest in pre-menopausal breast due to the high vascular demands of the tissue. Blood vessel density and blood flow decrease as a result of menopausal involution of glandular tissue. This effect can be detected from the significant total hemoglobin concentration difference between pre- and post-menopausal subject groups.

Women using HRT exhibit hemoglobin concentration values that are intermediate between pre- and post-menopausal subjects. Thus, FDPM measurements may be

sensitive to subtle HRT effects, including previously documented elevations in blood flow, fibroglandular volume, and epithelial cell proliferation [36-39]. The general decrease in total hemoglobin concentration with age after 50 (Figure 7) suggests it is difficult to determine from limited existing data whether the measured HRT hemoglobin effect is real or simply a consequence of age-related optical property changes.

Figure 6 data show that the average water percentage for pre-menopausal women (29 ± 6%) is more than a factor of two greater than the mean tissue water concentration for post-menopausal women (11 ± 2%). These differences reflect the high water content of epithelial connective tissue compartments in pre-menopausal tissue while post-menopausal breast is dominated by low-water content adipose. Water concentration in HRT subjects is slightly greater than the post-menopausal group (15 ± 7%). Differences may be due to hormone-induced accumulation of fluids, a commonly occurring side effect from HRT[39].

Investigating positional variations in optical properties between pre-menopausal (Pre 1) and post-menopausal (Post 1) subjects reveals a higher degree of variation in scattering for post-menopausal women (approximately 8% for all wavelengths) vs. pre-menopausal women (approximately 4%). These values were calculated by normalizing the standard deviation of the values from measurements in each of the four quadrants (n=4) to the mean (data not shown). This difference may represent the non-uniform glandular involution of breast tissue that accompanies menopause and results in palpable differences in density in the breast tissue of post-menopausal women[40]. The positional variation in the absorption coefficient is greater for wavelengths corresponding to hemoglobin absorption (674-849nm) for the post-menopausal subjects (23-33% vs. 17-

20% for pre-). However, wavelengths corresponding to fat and water concentrations (894, 947 and 956nm) show a higher variability in pre-menopausal subjects (13-16%) vs. only 7-8% in post.

Figures 3 - 7 strongly suggest that physiological changes due to hormonal fluctuations that occur over a period of many years can be detected and quantified. Previous studies[41] show these effects are also detectable within the menstrual cycle of pre-menopausal women. In order to test FDPM sensitivity to menstrual cycle variations, we examined a pre-menopausal subject during ovulation and before the onset of menses. Table 2 data summarizing these results show that μ_a and μ_s' are higher for the latter part of the cycle (Day25) than in mid-cycle (Day14). Absorption differences correspond to the calculated physiological properties. Our results show a 48.3% increase in hemoglobin and 28.1% increase in water concentration during the luteal phase, changes that are consistent with the physiological effects due to ovarian hormone fluctuations during the menstrual cycle. After ovulation, blood flow to the breast can increase by up to 50%, there is an increase in breast volume, and parenchymal water content changes by an average of 25% during the latter half cycle[25, 26]. Changes in scattering were 3-5% and not statistically significant.

Conclusions

A hand-held photon migration probe has been developed that can detect significant differences in absorption and scattering properties occurring with changes in age and menstrual cycle phase. The sensitivity of quantitative NIR spectroscopy to breast biology is unique among radiologic methods. Consequently, optical techniques may eventually provide a practical, non-invasive means for enhancing the accuracy of tumor diagnostics in pre- and peri-menopausal subjects and for increasing our understanding breast pathophysiology.

Acknowledgments:

This work was supported by the National Institutes of Health (NIH) Laser Microbeam and Medical Program (RR-01192), NIH (GM-50958), the Avon Breast Unit in the Chao Family Comprehensive Cancer Center (CA-62203), and Department of Energy (DOE DE-FG03-91ER61227). A.E.C., R.H., and C.E. acknowledge support from the U. S. Army Medical Research and Material Command (DAMD17-98-1-8186) the Swiss National Science Foundation, and the American Cancer Society, respectively.

References

1. Kerlikowske, K., Barclay, J.,Grady, D., Sickles, E.A. (1997) *JNCI* **89** (1), 76-82.

2. 2.Elmore, J. G., Barton, M. B., Moceri, V. M., Polk, S., Arena, P. J., Fletcher,S. W. (1998) *N. Engl. J. Med.* **338** (16), 1089-1096.

3. Homer, M. J. (1985) *Radiol. Clin. North Am.* **23**(3), 459-472

4. Hindle, W. H., Davis, L., Wright, D. (1999) *Am. J. Obstet. Gynecol.* **180** (6), 1484-1490.

5. 4 Baines, C. J., Dayan, R. (1999) *JNCI* **91** (10), 833-838.

6. Laya, M. B., Larson, E. B., Taplin, S. H., White, E. (1996) *JNCI* **88** (10), 643-649.

7. Litherland, J. C., Stallard, S., Hole, D., Cordiner, C. (1999) *Clin. Radiol.* **54** (5), 285-288.

8. Fletcher, S.W. (1997) *JNCI Monographs* **22**, 5-9.

9. Fantini, S., Walker, S. A., Franceschini, M. A., Kaschke, M, Sclag, P. M., Moesta, T. K. (1998) *Appl. Opt.* **37**(10), 1982-1989.

10. Franceschini, M. A., Moesta, K. T., Fantini ,S., Gaida, G., Gratton, E., Jess, H., Mantulin,W. W., Seeber, M., Schlag, P. M., Kaschke, M. (1997) *Proc. Nat. Acad. Sci. USA* **94** (12), 6468-6473.

11. Tromberg, B.J., Coquoz, O., Fishkin, J.B., Pham, T., Anderson, E. R., Butler, J., Cahn, M., Gross, J.D., Venugopalan, V., Pham, D., (1997*) Philos. Trans. R. Soc. London Ser. B-Biological Sciences* **352** (1354), 661-668.

12. Cope, M. (1991) Ph.D. thesis, University of London, Department of Medical Physics and Bioengineering, University College London.

13. Sevick, E,M., Chance, B., Leigh, J., Nioka, S. (1991) *Anal. Biochem.* **195** (2), 330-351.

14. Beauvoit, B., Kitai, T., Chance, B. (1994) *Biophys. J.* **67**(6), 2501-2510.

15. Thomsen, S., Tatman, D. (1998) *Ann. N. Y. Acad. Sci.* **838**, 171-193.

16. Suzuki, K., Yamashita ,Y., Ohta, K., Chance, B. (1994) *Invest. Radiol.* **29** (4), 410-414.

17. Suzuki, K., Yamashita, Y., Ohta, K., Kaneko, M., Yoshida, M., Chance, B. (1996) *J. Biomed. Opt.* **1**(3), 330-334.

18. Cubeddu, R., Pifferi, A., Taroni, P., Toricelli, A., Valentini, G., (1999) *Appl. Phys. Lett.* **74** (6), 874-876.

19. Brisson, J., Morrison, A. S., Khalid, N. (1998) *JNCI* **80** (19), 1534-1540.

20. Boyd, N. F., Greenberg, C., Lockwood, G., Little, L., Martin, L., Byng, J., Yaffe, M., Tritchler, D. *JNCI* **89** (7), 488-496.

21. Lee, N. A., Rusinek, H., Weinreb, J., Chandra, R., Toth, H., Singer, C., Newstead, G. (1997) *Am. J. Roentgenol.* **168**(2), 501-506.

22. Kaufman. Z., Garstin, W. I. H., Hayes, R., Michell, M. J. (1991) *Clin. Radiol.* **43** (6), 385-388.

23. Colditz, G. A. (1997) *Ann. N. Y. Acad. Sci.* **833**, 129-136.

24. Drife, J. O. (1989) *Int. J. Gynecol. Obstet. Suppl.* **1**, 19-24

25. Fowler, P. A., Casey, C. E., Cameron, G. G., Foster, M. A., Knight, C. H. (1990) *Br. J. Obstet. Gynaecol.* **97** (7), 595-602.

26. Graham, S. J., Stanchev, P. L., Lloydsmith, J. O. A., Bronskill, M. J., Plewes, D. B. (1995) *Journal of Magnetic Resonance Imaging* **5** (6), 695-701.

27. Whelan, E.A., Sandler, D.P., Root, J.L., Smith, K.R., Weinberg, C.R. (1994) *Am. J. Epidemiol.* **140** (12), 1081-1090.

28. White, E., Velentgas, P., Mandelson, M. T., Lehman, C. D. (1998) *JNCI* **90** (12), 906-910.

29. Hrushesky, W. J. M. (1993) *J. Surg. Oncol.* **53** (1), 1-3.

30. Pham, T. H., Coquoz, Fishkin, J. B., Anderson, E., Tromberg, B. J. (2000). *Rev. Sci Instrum.* **71**(6), 2500-2513.

31. Fishkin, J. B., Fantini, S., Vandeven, M. J., Gratton, E. (1996) *Phys. Rev. E.* **53**(3), 2307-2319.

32. Haskell, R. C., Svaasand L. O., Tsay T. T., Feng T. C., McAdams, M. S., Tromberg, B. J. (1994) *J. Opt. Soc. Am. [A]* **11** (10), 2727-2741.

33. Fishkin, J.B., Gratton, E. (1993) *J. Opt. Soc. Am. [A]* **10** (1), 127-140.

34. Fantini, S., Franceschini M. A., Gratton, E. (1994) *J. Opt. Soc. Am. [B]* **11** (10), 212-2138

35. Reichart, C. M., Moshiri, S., Austin, R. M., Norris,H. J. in *Diagnosis and Management of Breast Cancer,* eds. Lippman, M. E., Lichter, A. S., Danforth D. N., Jr., (Saunders, Philadelphia), pp.22-26.

36. Bourne, T., Hillard, T. C., Whitehead, M. I., Crook, D., Campbell S. (1990) *Lancet* **335**, 1470-1471.

37. Pines, A., Fisman, E. Z., Levo, Y., Averbuch, M., Lidor, A., Drory, Y., Finkelstein, A., Hetman-Peri, M., Moshkowitz, M., Ben-Ari, E., Ayalon, D. (1991) *Am. J. Obstet. Gynecol.* **164** (3), 806-812.

38. Berkowitz, J. E., Gatewood, O. M., Goldblum, L. E., Gayler B. W. (1990) *Radiology* **174** (1), 199-201. 41.Duck, F. A., (1990) *Physical Properties of Tissue*, (Academic Press, London), pp.320-321.

39. Key, T.J.A. (1995) *Mutat. Res.***333**(1-2), 59-67.

40. Wren, B. G. (1996) *Baillieres Clin. Obstet. Gynaecol.* **10** (3), 433-447.

41. Cubeddu, R., D'Andreal, C., Pifferi, A., Taroni, P., Torricelli, A., Valentino, G. (2000) *Photochem and Photobiol.* **72**(3), 383.

Figure Captions

Figure 1: (a) Schematic drawing of FDPM instrument, hand-held probe and measurement map of healthy volunteers. The components of the instrument are: (1) diode lasers (2) avalanche photodiode (3) network analyzer (4) DC current source (5) bias T (6) optical switch. See text for detailed description.. The breast is divided into four quadrants: upper outer (a), upper inner (b), lower outer (c) and lower inner (d). FDPM measurements are made in each quadrant, the areolar border (e), and on the glandular tail (f) that extends into the axilla.

Figure 2: FDPM measurements of (a) phase lag and (b) amplitude versus modulation frequency for a pre-menopausal woman (Pre 1) and a post-menopausal woman (Post 1). Source-detector separation = 2.5 cm, wavelength = 849nm. Solid lines represent best diffusion model function fits to phase and amplitude data for each subject. Error bars are on the order of the marker size.

Figure 3: Absorption coefficient μ_a versus μ_s' for five pre-menopausal and three post-menopausal subjects at all wavelengths. Values are calculated from best diffusion model fits to phase and amplitude data

Figure 4: Reduced scattering coefficient, μ_s' versus wavelength for three subjects of varied hormonal and menopausal status. Some values at 980nm represent values extrapolated from $A\lambda^{-B}$ linear regression analysis of the data.

Figure 5: μs' at 674nm versus age for all subjects.

Figure 6: Mean hemoglobin concentration (μM, oxy-, deoxy-, and total) and water concentration relative to pure water (%) for each subject group. Values are determined from wavelength-dependent absorption values at 674nm, 803nm, 849nm and 956nm or 980nm. Error bars represent the normalized standard deviation to the mean for 5 pre-menopausal, 5 HRT and 3 post-menopausal subjects. Confidence values are 80.9% for Hb, 86.7% for HbO_2, 86.3% for THC and 98.0% for H_2O.

Figure 7: Total hemoglobin concentration versus age for all subjects.

Table 1: Calculated physiological properties, hemoglobin concentration (μM, oxy-, deoxy-, and total) blood oxygen saturation (%) and water concentration (M) for a pre-menopausal subject at Day 14 and Day 25 of a 28 day menstrual cycle.

Figure 1

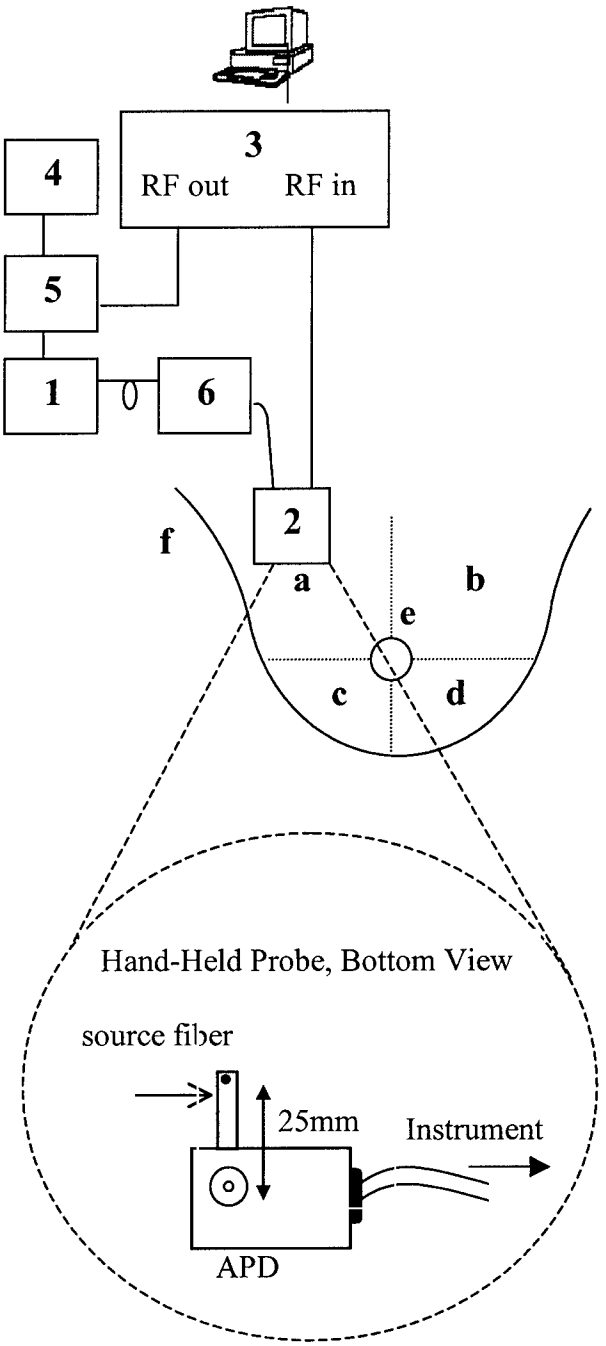
3
RF out
RF in
4
5
1
6
2
f
a
b
e
c
d
Hand-Held Probe, Bottom View
source fiber
25mm
Instrument
APD

Figure 2:

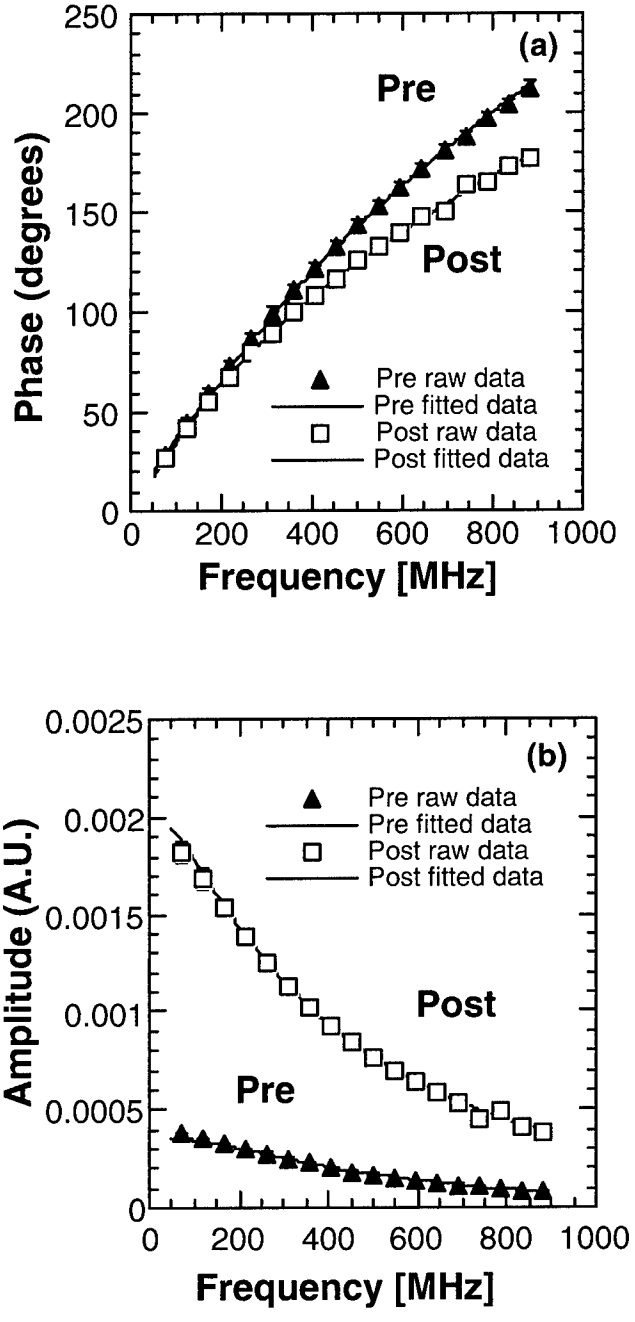
(a)
Pre
Post
Pre raw data
Pre fitted data
Post raw data
Post fitted data
Phase (degrees)
Frequency [MHz]
0
50
100
150
200
250
0
200
400
600
800
1000
(b)
Pre raw data
Pre fitted data
Post raw data
Post fitted data
Post
Pre
Amplitude (A.U.)
Frequency [MHz]
0
0.0005
0.001
0.0015
0.002
0.0025
0
200
400
600
800
1000

Figure 3:

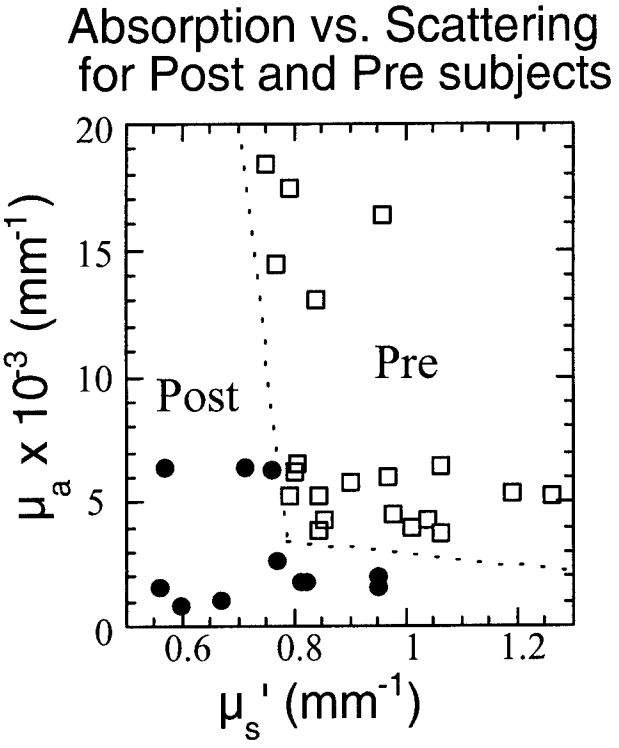

Figure 4:

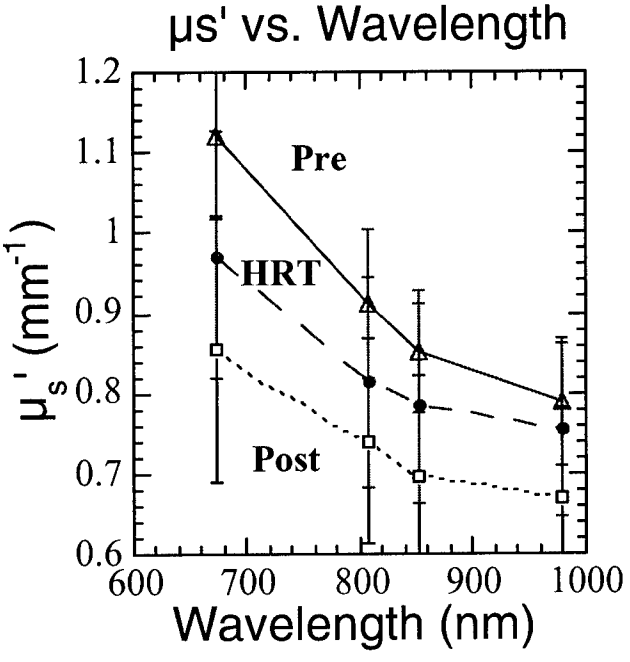

FIGURE 5

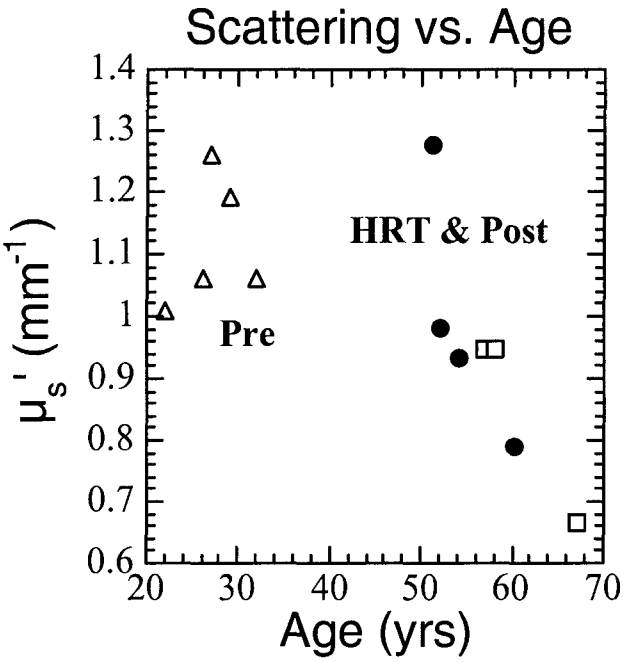

Figure 6:

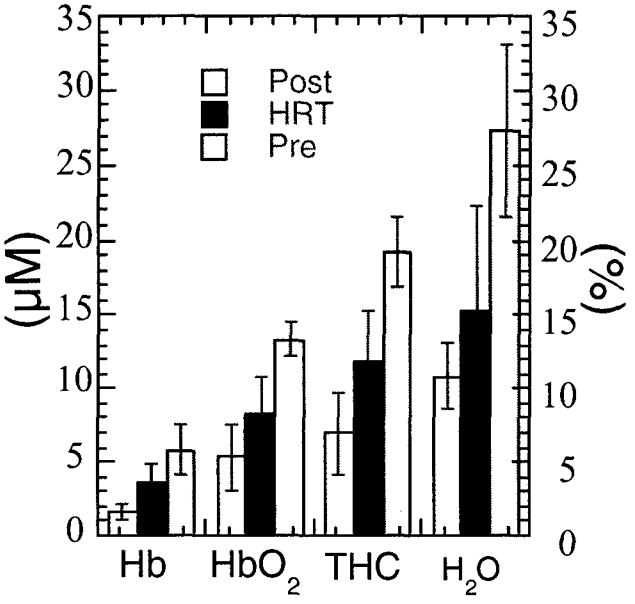

FIGURE 7

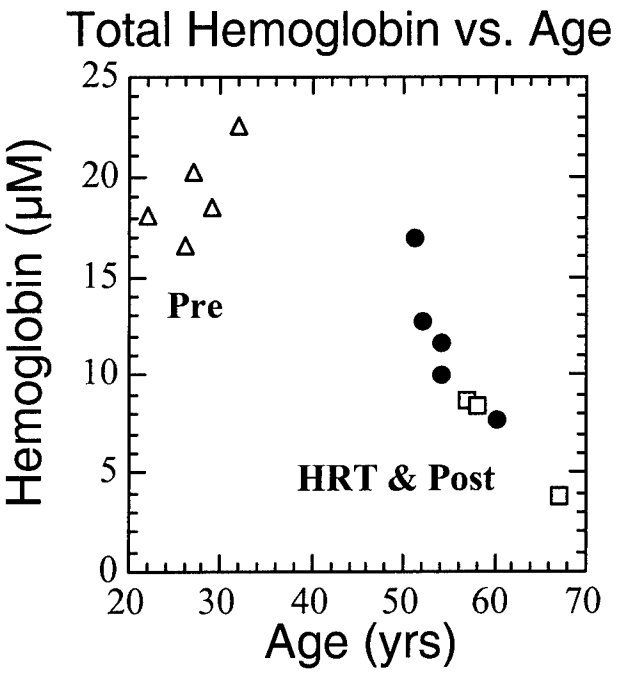

Table 1: Variation in physiological properties during the menstrual cycle.

Parameter	Day 14	Day 25
Hb (μM)	3.07 ± 0.04	4.72 ± 0.05
HbO_2 (μM)	7.56 ± 0.04	11.04 ± 0.06
Total Hb (μM)	10.63 ± 0.05	15.76 ± 0.08
$O_2 Sat_2$ (%)	71.12 ± 0.53	70.06 ± 0.53
Water (%)	16.49 ± 0.11	21.12 ± 0.15

DEPARTMENT OF THE ARMY
US ARMY MEDICAL RESEARCH AND MATERIEL COMMAND
504 SCOTT STREET
FORT DETRICK, MARYLAND 21702-5012

REPLY TO
ATTENTION OF

MCMR-RMI-S (70-1y) 30 Sep 02

MEMORANDUM FOR Administrator, Defense Technical Information Center (DTIC-OCA), 8725 John J. Kingman Road, Fort Belvoir, VA 22060-6218

SUBJECT: Request Change in Distribution Statement

1. The U.S. Army Medical Research and Materiel Command has reexamined the need for the limitation assigned to technical reports written for Grant DAMD17-98-1-8186. Request the limited distribution statement for Accession Document Numbers ADB265247 and ADB281574 be changed to "Approved for public release; distribution unlimited." This report should be released to the National Technical Information Service.

2. Point of contact for this request is Ms. Judy Pawlus at DSN 343-7322 or by e-mail at judy.pawlus@det.amedd.army.mil.

FOR THE COMMANDER:

PHYLIS M. RINEHART
Deputy Chief of Staff for
Information Management